Development and Optimization of Synthetic High-Density Lipoprotein Vaccine Nanodiscs for Immune Modulation

by

Sayed Alireza Hassani Najafabadi

A dissertation submitted in partial fulfillment
of the requirements for the degree of
Doctor of Philosophy
(Pharmaceutical Sciences)
in the University of Michigan
2020

Doctoral Committee:

Associate Professor James Moon, Chair
Associate Professor Wei Cheng
Professor Joerg Lahann
Research Associate Professor Qiao Li
Associate Professor Anna Schwendeman
Professor Steven P. Schwendeman

Sayed Alireza Hassani Najafabadi

Hassania@med.umich.edu

ORCID iD: 0000-0002-8215-4374

Dedication

To my parents Mahbobeh Izadi, Ahmad Hassani.

To my wife Zeynab Izadi Najaf Abadi.

In memory of Abdolkarim Izadi.

To Iran Hamledari.

Acknowledgments

This thesis shows five years of my long Ph.D. journey. Fortunately, I was aided by numerous contributions and the help of others. I had a chance to meet many friendly people during the past five years, and they provided me with countless support, without which I would not have been able to finish my long journey.

Firstly, I would like to express my sincere appreciation to my advisor and doctoral committee chair, Prof. James Moon, for taking me on as a student, the continuous support of my study and research, for his patience and motivation. His guidance helped me throughout my research and writing this thesis. I cannot imagine having a better advisor and mentor for my Ph.D. study.

In addition to my advisor, I would also like to acknowledge my doctoral committee consisting of Prof. Wei Cheng, Prof. Joerg Lahann, Prof. Qiao Li, Prof. Anna Schwendeman, and Prof. Steven Schwendeman, for their insightful comments and encouragement, but also for the hard questions which incentivized me to view my research from various perspectives. Your great suggestions, advice, and help over the years have helped me pursue my research as well as my life.

I want to acknowledge the faculty at the University of Michigan and, in particular, the College of Pharmacy. I would like to thank all of the Moon Lab members who have assisted me with their feedback, time, and labor. Marisa Aikins has generously provided scientific input, troubleshooting ideas, critical review, editing, and aided in several experiments over the five years that would not have been possible without her help. Dr.

Rui Kuai, Dr. Jutaek Nam, Dr. Lukasz Ochyl, and Dr. Emeka Okeke have provided feedback and insight into my work as well. Yao Xu has generously helped with the cell culture, tissue processing, and ELISPOT, which dramatically improved the efficiency of my research.

Flow cytometry core, and specifically Dr. Dave Adams and Ann Marie Deslauriers-Cox, have been invaluable with their feedback and help. Unit for Laboratory Animal care (ULAM), and specifically Dr. Patrick Lester, Taryn Hetrick, have been invaluable with their help as well. Biointerfaces Institute allowed me to established connections and created possibilities with scientists of various backgrounds generating unique perspectives. Nadine Wong and Karl Olsen have worked tirelessly in ensuring that the lab operates smoothly during this hard pandemic. I would also like to thank Dr. Priyan Weerappuli, Dr. Chitra Subramanian, Prof. Lonnie Shea, Dr. Aaron Morris, Ashley Munie, Prof. Benjamin Segal, Dr. Jing Zhang, Prof. Qiao Li, and Prof. Robert Seder for outstanding collaboration.

Thank you to all of the friends that help me. In particular, I would like to mention Dr. Katie Cavanagh, Dr. Jenna Walker, and Alexander Benet for all the kind words and the good times. Marisa Aikins has been a good friend inside and outside of the lab, along with Nahal Habibi, and Mark Nelson.

Finally, I would never have accomplished anything without support and help from my family. I want to give a special thanks to my parents and parents-in-law. Thank you for giving me tremendous support during my graduate study. My parents always supported me when I needed help and pushed me to better. Most importantly, I would like to thank my wonderful wife, Zeynab, for all of her support, patience, help, and confidence in me.

Table of Contents

List of Tables

List of Figures

Abstract

Cancer immunotherapy is a novel, attractive approach for cancer treatment. Cancer immunotherapy based on vaccines has shown promising results but suffers from poor immunogenicity. This lack of efficacy can be attributed to the inefficient delivery of antigens and adjuvants to immune activation sites, resulting in weak cytotoxic T lymphocyte (CTL) responses. With profound advances in nanotechnology and biomaterials in recent years, researchers have shown the promise of nanoparticles designed to co-deliver antigens and adjuvants to antigen-presenting cells (APCs) for improving immunogenic responses of cancer vaccines.

Cancer stem cells (CSC) are a subpopulation of cancer cells that can proliferate extensively and drive tumor metastasis and recurrence. Despite intensive research, it remains challenging to specifically target and eliminate CSCs. In the first project, I report a novel approach to target CSCs by vaccination against aldehyde dehydrogenase (ALDH), which is highly up-regulated in CSCs. I have developed synthetic high-density lipoprotein (sHDL) nanodiscs co-loaded with ALDH peptide antigen and CpG (a Toll-like receptor (TLR)-9 agonist) adjuvant. Nanodisc vaccination combined with αPD-L1 immune checkpoint blocker led to significant induction of CTL responses against ALDH, leading to inhibition of D5 melanoma and 4T1 breast cancer. Overall, we have shown that nanodisc vaccination against ALDH, in combination with αPD-L1 immunotherapy, can exert strong anti-tumor efficacy.

In the second part of my project, we have optimized sHDL nanodiscs that can efficiently deliver cancer antigens to lymph nodes and elicit strong anti-tumor T-cell responses against colorectal cancer. Overall, we have shown that polyICLC (a potent TLR3 agonist) admixed with sHDL can form a powerful adjuvant system (sHDL+polyICLC) that can be readily combined with an antigen. sHDL+polyICLC induced robust activation of dendritic cells, and sHDL+polyICLC generated strong anti-tumor immune responses, exerting strong anti-tumor efficacy in the MC-38 colon cancer model. Furthermore, we have shown that non-human primates vaccinated with sHDL+polyICLC elicited potent T-cell responses. Overall, these results show that immunotherapy based on sHDL+polyICLC can generate potent anti-tumor T-cell responses.

In the third project, we have developed sHDL-based immunotherapy for inducing antigen-specific immune tolerance. Multiple sclerosis (MS) is an autoimmune disease caused by autoreactive lymphocytes against axons and myelin sheaths of the central nervous system (CNS), leading to axonal loss and demyelination. Current treatments for MS are mainly based on immunosuppressive therapies that have unintended side effects on global immune responses and cause significant toxicity. To address these issues, we have developed synthetic high-density lipoproteins (sHDL) designed for the delivery of tolerogenic MS antigens and tested them in a murine model of experimental autoimmune encephalomyelitis (EAE), a widely accepted pre-clinical model of MS. sHDL-MOG considerably inhibited the symptoms of EAE, whereas treatments with blank sHDL, sHDL-M30, PBS, or free MOG peptide had no significant impact. Overall, inverse vaccination with sHDL carrying tolerogenic peptide antigens is effective against EAE and warrants

further research as the basis for immunotherapy against MS and other autoimmune diseases.

Chapter 1 Introduction

1.1 Cancer Immunotherapy

Despite recent advances in cancer treatment, cancer remains the second leading cause of death worldwide. Treatments, such as surgical resection, chemotherapy, and radiation, improve the survival rates of cancer patients. Yet, the world cancer burden and death is expected to increase from 18.9 million new cases and 9.6 million deaths in 2018 to 27.5 million new cases and 17.3 million deaths, respectively, by 2040 [1]. Additionally, these treatments have severe side effects that negatively affect the overall health and quality of life for cancer patients [2].

Since its discovery in 1991, immunotherapy has revolutionized cancer treatment [3]. Immunotherapy is a treatment strategy that relies on and activates the immune system to fight cancer. After recognition of the cancer cells, the immune system either triggers a mechanism that can eliminate cancer cells and generate antigen-specific immune cells to provide long-lasting immunity or initiates infiltration of immune cells to the tumor leading to immune escape of tumor cells and down-modulation of the immune system (**Figure 1-1**) [4, 5].

Several mechanisms have been proposed for the immune escape of tumor cells [6]. One such mechanism involves the expression of FasL (ligand for Fas receptor) on cytotoxic T lymphocytes (CTLs). Fas operates as a death receptor by binding to the ligand found on the CTL to induce apoptosis. FasL expression by tumor cells also provides

resistance to Fas-induced apoptosis of tumor cells [7]. Another mechanism of cancer cell immune escape is through downregulation of the antigen processing machinery, mainly diminishing HLA type 1 expression levels in the MHC class I pathway, thus preventing antigen presentation [8]. Activation of T cells requires co-stimulatory signals, and the absence of these signals leads to T cell anergy and generation of regulatory T cells (Treg). The FoxP3 transcription factor present in Treg cells inhibits the activation of effector T cells, resulting in diminished immune responses during the immune escape of tumor cells [8].

In addition to tumor cells, the tumor microenvironment has several immunologic checkpoints that play an important role in the attenuation of both innate and adaptive anti-tumor immunity. In response to Stat3 or Braf activation, tumors release factors, such as IL10, that cause Stat3 signaling in NK cells and granulocytes, resulting in the prevention of their tumorigenic activity. Furthermore, activation of Stat3 also converts conventional dendritic cells (CDC) to tolerogenic DCs, which in turn induces Tregs and T cell anergy [9-11]. Additionally, co-inhibitory B7 family members, such as B7-H1 and B7-H4 present in the tumor microenvironment can also downregulate T cell activation and/or cytolytic activity [8].

A recent approach for overcoming immune evasion by tumors involves targeting the interaction between programmed death 1 (PD-1) receptor expressed on T cells and programmed death 1 ligand (PD-1L) expressed in the tumor microenvironment to block the inhibitory signals [12]. Pembrolizumab (anti-PD-1) and nivolumab (anti-PD-1L) are promising monoclonal antibodies that are currently investigated as agents for cancer immunotherapy. The clinical results of these two monoclonal antibodies demonstrated a

decrease in toxicity compared to conventional therapies, an increase in response rate (between 17% and 44%), and comparable frequencies of durable responses [13-15]. Despite promising results with these checkpoint inhibitors, not all patients respond to immunotherapies, and some develop resistance [14, 16]. Therefore, novel, innovative options such as cancer vaccination are needed for improving these responses and to overcome therapy resistance.

1.2 Cancer vaccines

Cancer vaccines are a type of immunotherapy that use a vaccine to boost the body's natural immune system to fight and eliminate cancer cells. The immune system has two interconnected arms, namely innate and adaptive immune system that can protect the human body from bacteria, viruses, and infected cells. Innate immunity initiated by the pathogen recognition receptors (PRRs) is the first branch of the immune system that protects the host against infectious pathogens [17]. Adaptive immunity is triggered after activation of the innate immune responses by antigen-presenting cells (APCs), which process pathogens and present their antigenic portions to T cells (effector cells) to initiate an antigen-specific response [18]. In addition to bacteria and viruses, cancer cells with tumorigenic properties express different antigens that initiate immune response [19, 20].

APCs, which connect the innate and adaptive immune systems, capture pathogens and present antigens to the T and B cells. Dendritic cells (DCs) act as professional APCs as they play a major role in the process of pathogen uptake and presentation of antigen to T cells. DCs and macrophages use their pathogen recognition

receptors to capture proteins in their surroundings and recognize pathogens. Unlike macrophages that transfer captured proteins to their lysosomes and degrade them, DCs convert pathogens to antigens and deliver said antigens to the local lymph nodes [21, 22]. In the lymph nodes, the delivered antigens by APC present to T cells and initiate antigen-specific T cells responses [23].

During this antigen presentation process, immunostimulatory molecules, such as CD80/86, are required to stimulate antigen-specific T cells. Healthy cells are unable to express these immunostimulatory molecules, and thus, the immune system uses cross-presentation in which APCs take up antigens from the extracellular environment and present them on MHC-I. During the proteasome-mediated transfer of cytosolic proteins from cells, the proteins inside the cells are cleaved to short amino acid chains or peptides [24]. These peptides are either transported into the endoplasmic reticulum (ER) by TAP1/2 or they bind to major histocompatibility complex class I (MHC-I) (**Figure 1-1**) [23]. The MHC-I complex expressed on the cell surface then presents the antigenic peptides for CTL recognition.

Although the efficacy of the vaccine depends on various factors, such as the site of injection, timing of the first injection, and booster immunizations, the vaccine composition is also an essential factor that can affect the strength of the immunity. In addition to antigens, vaccines should have strong adjuvants, which trigger immune action against that antigen (Figure 1-1) [3].

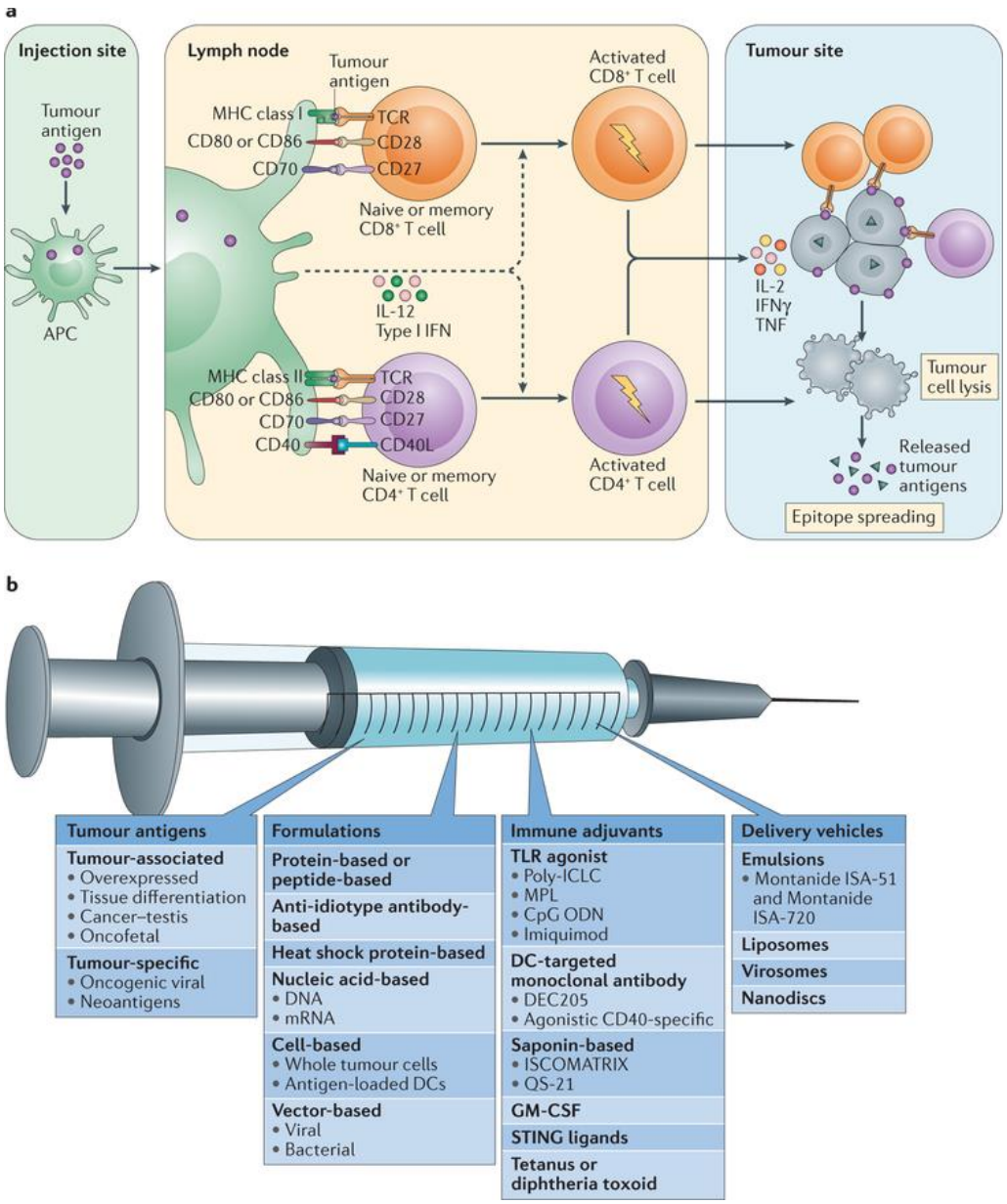

Figure 1-1. Schematic of mechanisms and components of an effective cancer vaccine [25].

1.2.1 Tumor antigens

Tumor antigens expressed in tumor cells should be absent or expressed at low levels in healthy adult tissue. Also, tumor antigen should be broadly categorized based on the specificity for certain tumors. Overall, tumor antigens can be categorized as tumor-associated or tumor-specific antigens.

Tumor-associated antigens (TAAs) include antigens that are overexpressed, involved in tissue differentiation, or preferentially expressed by cancer cells but not normal tissues. Notable examples of overexpressed tumor antigens include human epidermal growth factor receptor 2 (HER2, also known as ERBB2), human telomerase reverse transcriptase (TERT), and antiapoptotic proteins (such as survivin (also known as BIRC5)) [26]. On the other hand, tissue differentiation antigens are encoded genes that are only expressed by the specific cell lineages from which a tumor and its corresponding normal tissue arise but that are not expressed more widely. Examples of tissue differentiation antigens include mammaglobin-A overexpressed in breast cancer as well as prostate-specific antigen (PSA).

However, the use of TAAs in cancer vaccines carries the risk of autoimmunity against the corresponding normal tissues and is subject to some degree of central tolerance and lack of complete specificity to the tumor [27]. Furthermore, as these antigens are also expressed in healthy tissue, natural T cell recognition is often of low affinity as a result of the negative selection of high-affinity T cells in the thymus [28]. Thus, choosing an appropriate antigen peptide against the cancer cells is one of the most important steps in vaccine therapy.

Tumor-specific antigens (neoantigens) are another group of antigens that are foreign to the body (and therefore not subject to central tolerance) and expressed only by cancer cells (and therefore specific to the tumor), which makes them highly suitable for use in a cancer vaccine. Accumulating experimental evidence in human cancer studies show that vaccines using neoantigens are efficacious in both preventive and therapeutic settings for cancer vaccines [29]. However, to determine appropriate, immunogenic neoantigens, researchers should sequence the whole genome of primary as well as metastatic tumors, which is not feasible for some tumors to date and requires tremendous effort and resources [30].

1.2.2 Adjuvants

It is crucial to select an appropriate adjuvant for cancer vaccines, as adjuvants play key roles in generation of an adaptive immune response of sufficient scale, quality, breadth, and persistence necessary for efficacy (**Figure 1-2**). Currently, there are only a few adjuvants approved in the USA and Europe for human use. Aluminum salts (alum) were approved in the mid-1920s and have been used widely as an adjuvant for producing strong Th2 responses [31]. Preclinical studies have shown that after intramuscular and intraperitoneal injection of alum, strong immune responses encompassing an influx of neutrophils, eosinophils, NK cells, CD11b+ monocytes, and dendritic cells (DCs) were observed at the site of injection [32]. This has been attributed due to the fact that alum forms a depot at the injection site for slow release of antigens after administration [33].

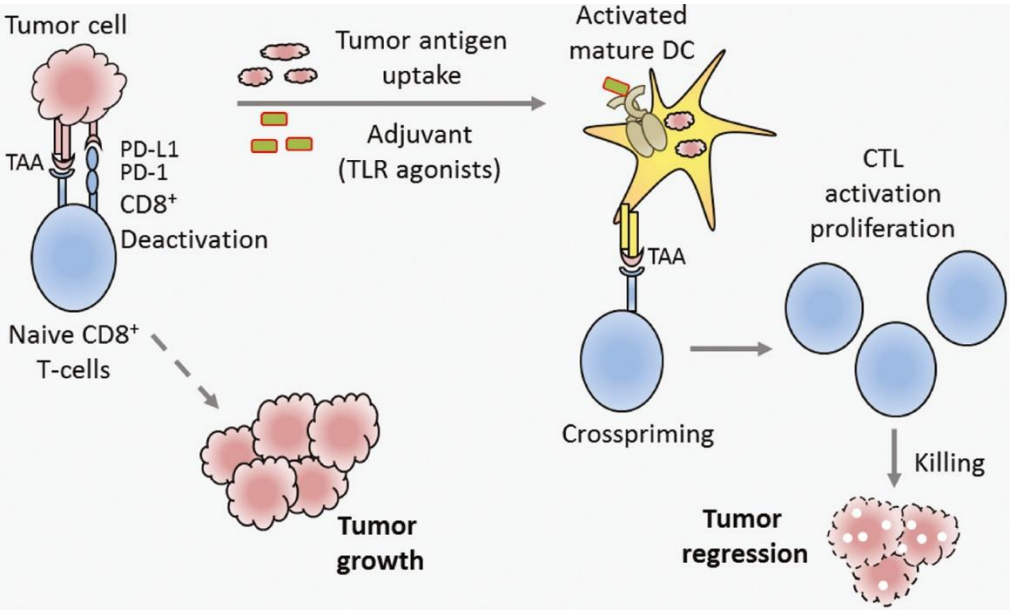

Figure 1-2. Role of Adjuvant in immune activation against tumor cells [34].

Double-stranded RNA (dsRNA) related to viral infections activates Toll-like receptor (TLR) 3 in the endosomal compartment and helps skew Th1 responses, which favor the involvement of CTLs [23]. Furthermore, dsRNA molecules, such as synthetic polyinosinic:cytidylic acid (Poly I:C), can increase IL-12 and type I interferon (IFN) secretion and activate cytosolic receptors, such as retinoic acid-inducible gene-1(RIG-I). In addition, Poly I:C can be administered in complex with poly-L-lysine to increase its stability. In recent clinical trials, topical administration of the complex against glioblastoma showed the safety and efficacy of the adjuvant [35].

Another interesting adjuvant is monophosphoryl lipid A (MPLA), which is a derivative of lipopolysaccharides (LPS) and is a TLR4 agonist [36]. Vaccine studies using MPLA have indicated that MPLA induces strong Th1 responses, but when incorporated into the particles, it shows more balanced Th1 and Th2 responses [37]. TLR4 has been identified for its role in recognition of LPS and activation of adaptive immunity [38]. MPLA

is found in FDA-approved vaccines against human papillomavirus (HPV) and hepatitis B virus (HBV) [39].

Recently, TLR 7/8 agonists have shown potential as vaccine adjuvants. They can directly activate APCs and improve both humoral and cellular immune responses, particularly the Th1 response. Although ssRNAs are the natural ligands for TLR7 and TLR8, the majority of vaccine experiments have been performed with synthetic small molecule imidazoquinolines, such as imiquimod and resiquimod as TLR7/8 agonists. These agonists show low efficacy as a soluble vaccine, which can be attributed to high hydrophobicity that strongly affects their colocalization with the antigen [40]. Therefore, researchers are investigating different ways to improve the efficacy of TLR7/8 agonists, such as conjugation of TLR7/8 agonists to antigens and nanoparticle formulations. Imiquimod (TLR7) has been used as a 5% cream (Aldara® Imiquimod 5% cream; 3M, MN, USA) in clinics for external genital warts, superficial basal cell carcinoma, and actinic keratosis [23]. Experimental clinical studies have shown that imiquimod administered with CpG increased T cell activation and induced antigen-specific central memory phenotype CTL responses [41, 42].

CpG, a TLR9 agonist, is widely used as it can promote antigen cross-presentation efficiency and activation of TLR9 in plasmacytoid DCs produces a high level of IFNγ. IFNγ expression leads to antibody responses, elevated T cell proliferation, survival and memory phenotype, and intense polarization of the T helper cell phenotype to CTL-supportive Th1. CpG has been tested in various therapeutic cancer vaccines and recent clinical trials, where it has shown encouraging results when mixed with another adjuvant with an immunogenic peptide from melanoma-specific protein [43, 44].

Despite the identification of appropriate antigens and an effective adjuvant increasing the efficacy of the cancer vaccine, a remaining challenge is delivering it to the site of immune activation [45].

1.2.3 Nanoparticle cancer vaccine

To have an effective vaccine, an antigen should be delivered to sites that can produce an adequate response, and an adjuvant should be delivered to the same sites as the antigen. Significant improvement in inducing immune responses is seen when antigen and adjuvant are co-delivered to the location of responses [46], leading in enhanced cross-presentation and activation of the immune system. For soluble vaccines, the simultaneous delivery of antigens and adjuvants are not guaranteed due to differences in pharmacokinetic parameters, permeability, distribution properties, and biodistribution of antigen and adjuvants, which significantly affects where and to what degree vaccine components are delivered to the host. To address these issues, researchers have employed nanoparticles to encapsulate both antigens and adjuvants and improve the immunogenic responses of cancer vaccines [47].

Various nanoparticles have been studied for cancer vaccines. Among a number of nanoparticle systems for cancer vaccines, polymeric nanoparticles are one of the most widely studied vaccine platforms. In addition to PLGA [48-51], liposomes, micelles, dendrimers, inorganic nanoparticles such as gold nanoparticles, iron oxide nanoparticles, carbon nanoparticles, and quantum dots are also successfully used as carriers for antigens and adjuvants to the desired target sites, such as lymph nodes or other intracellular locations, for the activation of the immune response [52-54].

High-density lipoprotein (HDL), known as good cholesterol, is a lipid-based nanoparticle involved in the transport and metabolism of cholesterol and triglyceride. HDL has anti-inflammatory and anti-oxidation properties and can carry various endogenous proteins, vitamins, hormones, and microRNA to different organs [55]. The small size of HDL, high tolerability, long blood circulation half-life, and special ability to target different recipient cells make HDL a promising nanocarrier for the delivery of peptide to APCs. In addition to the properties mentioned above, HDL is degraded in endosomal compartments of APCs, resulting in high levels of cross-presentation. Therefore, HDL is a promising candidate for cancer vaccine studies. Additionally, HDL can load both hydrophobic as well as hydrophilic compounds, allowing for incorporation of a wide range of antigens and adjuvants [55]. Previous Phase I clinical trial of synthetic high-density lipoprotein (sHDL) nanodiscs for cardiovascular application has indicated clinical safety of sHDL [55]. In our previous work, we investigated the preparation of sHDL nanodiscs using apolipoprotein A1 (ApoA1)-mimetic peptides (22A) and showed that sHDL could successfully load antigen and adjuvant (TLR9 agonist, CpG), co-deliver them to lymph nodes, increasing the uptake of antigen to APCs, and trigger the CTL response against cancer cells, leading to an effective response against tumors [56]. However, the antigen-lipid anchor and in vitro and in vivo stability of the sHDL formulation have not been fully optimized. In terms of selecting an effective adjuvant to induce cross-presentation and strong CTL responses, our sHDL formulation should be optimized for a strong adjuvant to achieve potent anti-tumor efficacy.

1.3 Cancer stem cells as a target of vaccination

Cancer stem cells (CSCs) were first reported in myeloid leukemia and then further characterized in breast cancer in a seminal study by Al-Hajj, et al., who identified the CD44+CD24-/LowLineage− population of cells for their tumor-initiating properties [57, 58]. Unlike the majority of cancer cells, CSCs, like regular stem cells, exist in a mostly inactive state regarding cell cycle activity, making them resistant to standard cytotoxic anti-cancer drug treatments designed to kill rapidly dividing cells. As a result, CSCs are a key factor in both tumor relapse and chemo-resistance [59, 60]. Thus, it has been suggested that targeting and killing CSCs may be crucial to eliminate cancer metastases and prevent tumor recurrence. Despite advances in the field of CSC-targeted therapies, it remains very challenging to kill CSCs in vivo. New anti-CSC therapeutics should have minimal toxicity to healthy stem cells or progenitor cells, while achieving selectivity against CSCs and overcoming chemo-resistance of CSC [61]. To address these challenges, strategies incorporating selective, cell cycle-independent treatments should be developed to increase the efficacy of CSC treatments with minimal toxicity [8-14].

In recent years, ALDEFLUOR/ALDH (aldehyde dehydrogenase) expression has been identified as a functional biomarker for CSCs. ALDH detoxifies intracellular aldehydes through oxidation and thus may play a role in the differentiation of stem cells [62-64]. ALDH activity is a crucial biomarker for breast and colon CSCs as well as CSCs from more than 20 types of cancer [65-68]. Li, et al. have demonstrated the feasibility of immunological targeting of CSCs using $ALDH^{high}$ CSC lysate-pulsed dendritic cell (DC) vaccines. Therefore, ALDH may serve as a basis for vaccination against CSCs [69]. Ning, et al. showed that inoculation of as few as 500 cells of ALDH+ D5 could result in tumor

formation, compared to the injection of 50,000 ALDH- cells [70]. Furthermore, cancer vaccines made from ALDH+ D5 cells showed a 2- and a 3-fold decrease in the number of lung metastases generated by D5 cells, compared with unsorted tumor cells. Also, prophylactic vaccination with CSC lysate from SCC7 cell line (murine squamous cell cancer) showed a decrease in the growth of tumors in a subcutaneous model. Collectively, these studies have indicated that ALDH may serve as a promising antigen for immunological targeting of CSCs. In chapter 2, we will discuss nanodisc-based vaccination against ALDH for activating the immune system against CSCs.

1.4 Colon cancer: current therapies and challenges

Among the different types of cancers, colorectal cancer (CRC) is one of the deadliest cancers worldwide, accounting for approximately 700,000 deaths per year. Patients diagnosed with metastatic CRC cancer have a low 5-year survival rate. Although the origin of colon cancer is not well established, research has shown that error-prone DNA leading to uncontrollable growth is responsible for colon cancer development and metastasis [71]. Untreated CRC cancer spreads to the local lymph nodes and various tissues, finally establishing metastases in the brain, lungs, and liver [12]. Current treatment for CRC includes 1) surgery (such as laparoscopic surgery, colostomy for rectal cancer, and radiofrequency ablation (RFA) or cryoablation), 2) radiation therapy (such as external-beam radiation therapy, intraoperative radiation therapy, and brachytherapy), 3) chemotherapy using capecitabine, fluorouracil, irinotecan, oxaliplatin, and trifluridine/tiprail, and 4) targeted therapies, such as angiogenic inhibitors, epidermal

growth factor receptor (EGFR) inhibitors, and checkpoint inhibitors (immunotherapy) [72].

Surgery is the most common treatment for CRC at all stages. In addition to surgical resection, some patients may be able to have another type of surgery such as laparoscopic surgery, colostomy for rectal cancer, and radiofrequency ablation (RFA) or cryoablation [73]. Radiation therapy is another method for cancer therapy that utilizes high-energy X-rays to eliminate cancer cells. Radiation therapy is commonly used for treating rectal cancer because CRC tumors tend to recur near the initial location [74]. External-beam radiation therapy is one of the common types of radiation therapy that uses the delivery of X-rays to the cancer location. It is usually administered five days a week for several weeks. The delivery of such large and precise radiation doses to a small area eliminate all the cancer cells efficiently. For rectal cancer, radiation therapy may be used before or after surgery to shrink or kill cancer cells [75]. The main advantages of radiation therapy include a lower rate of cancer recurrence and fewer patients who need permanent colostomies [75]. Radiation therapy may include some side effects such as fatigue, mild skin reactions, upset stomach, loose bowel movements, bloody stools from bleeding through the rectum or blockage of the bowel, and sexual problems (the failure to have a child) [76, 77]. Chemotherapy, a common treatment against many cancers, is used to kill cancer cells by inhibiting the ability of cancer cells to divide.

Anti-angiogenesis therapy is a targeted therapy that focuses on stopping angiogenesis, which is a process of making new blood vessels [78]. Since tumor cells need more nutrients than healthy cells to grow and spread, anti-angiogenesis therapy targets and blocks blood vessel formation by tumors, thereby starving the tumor cells.

Bevacizumab (Avastin), an anti-angiogenesis treatment, in combination with chemotherapy, increased the survival rate of patients with advanced colorectal cancer [79]. Therefore, in 2004, the FDA approved bevacizumab as the first-line therapy for advanced colorectal cancer, and recent research has shown that it is also effective as second-line therapy [80]. Regorafenib (Stivarga) is another FDA approved drug for target therapy [81]. It was approved in 2012 by the FDA for patients with metastatic colorectal cancer who have already been treated with certain types of chemotherapy and other targeted therapies [81]. Ziv-aflibercept (Zaltrap) and ramucirumab (Cyramza) are other target therapies for CRC, which can be combined with FOLFIRI chemotherapy as a second-line action against metastatic colorectal cancer [82].

Epidermal growth factor receptor (EGFR) inhibitors block the EGF receptors and slow or stop the growth of cancer cells. EGFRs are a member of the ErbB family of receptors that play an important role in colorectal cancer, as it is highly expressed in CRC. An EGFR inhibitor Cetuximab (Erbitux), is an antibody made from mouse cells. A Phase 2 clinical study in 121 patients with colorectal cancer showed a 17% better response rate, compared with fluorouracil after weekly treatment with Cetuximab [83].

Overall, the currently available therapeutics against CRC are not sufficiently effective and cause harsh side effects or low responses. Despite advancement in CRC therapy, chemotherapy is still the most commonly used treatment against CRC, which is associated with low-level responses and severe side effects, especially toward healthy cells. EGFR inhibitors show some successful results because of their high level of precision but were only effective in a small portion of CRC patients. Thus, novel approaches are needed for the treatment of CRC.

Cancer vaccines, as described above, can activate the immune system to target cancer cells. This is a promising immunotherapeutic strategy for cancer, and in chapter 3, we will discuss how nanodisc-based vaccines can be used to elicit T-cell responses against CRC.

1.5 Immune tolerance

In addition to cancer, vaccines can also be utilized to treat other diseases. In this next section, we will discuss other applications of vaccines to reverse misdirected activation or over activation of the immune system, which is classified as an autoimmune disease.

The primary responsibility of the immune system is to protect the host from a broad range of pathogens as well as abnormal or excessive immune reactions that would be harmful to the host. Immune tolerance is selective in that the immune system disregards molecules native to the host and responds aggressively to remove foreign molecules. A breakdown in immune tolerance may lead to tissue and organ damage, resulting in autoimmunity (**Figure 1-3**) [84].

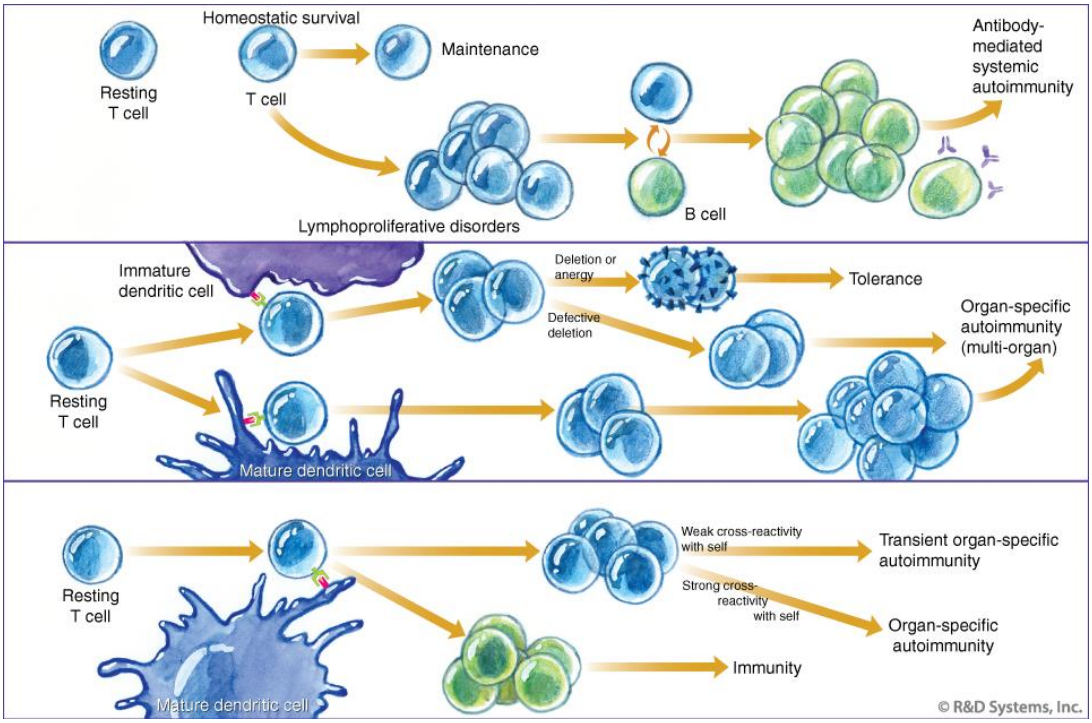

Figure 1-3. Breakdowns in immune tolerance may lead to autoimmunity [84].

Immune tolerance is classified as central tolerance or peripheral tolerance based on the site of origin. If tolerance happens during T and B cell maturation in the thymus or bone marrow, it is classified as central tolerance. If it occurs in other tissues and lymph nodes, it is known as peripheral tolerance. Central tolerance is the primary way by which the immune system discriminates self from non-self-antigens. However, peripheral tolerance is critical to protect and prevent the over-reactivity of the immune system in various environments [84-86].

Autoimmune diseases occur when abnormal B cell or T cell recognition of self-antigens occurs and triggers an immune reaction. This type of unconventional T cell is usually eliminated from the immune system by central or peripheral tolerance. Autoimmune diseases occur when abnormal B and T cells escape from central or

peripheral tolerance [87-89]. On the other hand, regulatory T cells (Tregs) can induce immune suppression. Emerging evidence indicates that every adaptive immune response involves recruitment and activation of not only effector T and B cells but also Tregs [90]. Additionally, the balance between the two populations is critical for the control of quality and magnitude of adaptive immune responses as well as establishing or breaching tolerance to self- and non-self-antigens (**Figure 1-4**) [84, 89]. Overall, autoimmune diseases, such as multiple sclerosis, psoriasis, rheumatoid arthritis, and type 1 diabetes, are the third-ranked cause of human morbidity and mortality in the United States [91].

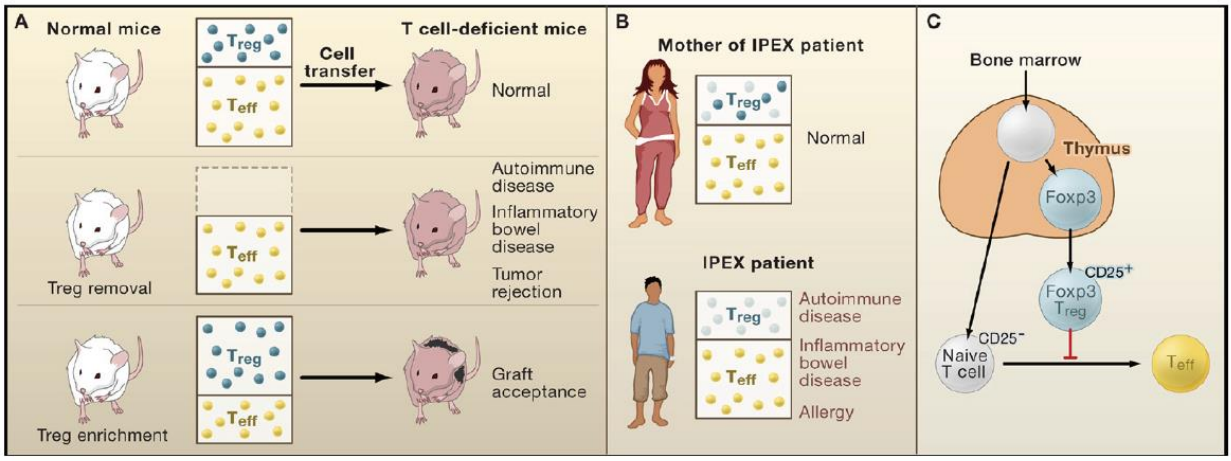

Figure 1-4. Effects of Treg Deficiency in Mice and Humans [85].

Multiple sclerosis (MS), in particular, is an unpredictable disease, characterized by an autoimmune response against the axons and myelin sheath proteins of the central nervous system (CNS), resulting in axonal loss and demyelination. It affects one million people in the United States and nearly 2.5 million people globally [92, 93]. The majority

of MS patients first present with relapsing and remitting neurological symptoms. MS diagnosis is confirmed by the presence of multiple inflammatory lesions with temporospatial dissemination in the brain, spinal cord, and/or optic nerves [94, 95]. The lesions are comprised of inflammatory infiltrates, including myeloid cells, which contribute to disease pathogenesis by releasing cytotoxic factors that damage myelin and myelin-producing oligodendrocytes and induce aberrant immune responses [77, 96]. Research on the immune system and CNS lesions of MS patients, as well as studies in murine models of MS, have shown that CD4+ T cells (Th) cells polarized to Th1 (IFN-γ-producing) and/or Th17 (IL-17-producing) phenotypes are the drivers of CNS autoimmunity [77, 97, 98].

Current MS treatments can be categorized into two groups: (1) those that mitigate symptoms and (2) those that aim to alter the progression of the disease (disease-modifying therapies, or DMTs). DMTs aim to reduce circulating immune cells or to prevent them from crossing the blood-brain barrier (BBB), thereby decreasing the local inflammatory response. There are currently ten DMTs approved for relapsed multiple sclerosis [99]. These DMTs can be organized according to their route of administration as self-injectable, oral, or intravenously-administered formulations [100]. Most of the MS therapies are administered systemically, whether in oral or injectable formulations [101]. Hence, a considerable amount of the drug circulating in the bloodstream can interact with off-target cells and decrease the dose to the intended target. At the forefront of these treatments are TNFa blockers, which sequester TNFa cytokines, a primary inducer of inflammation in common autoimmune diseases such as rheumatoid arthritis (RA). TNFα blockers are becoming the standard of care for patients with autoimmune diseases due

to their effectiveness in controlling diseases with lower risk profiles [102]. However, anti-TNF therapies have limitations as they are ineffective in patients with the refractory disease [103]. Thus, the next wave of transformative therapeutics should aspire to provide a cure by selectively suppressing autoantigen-specific immune responses without sacrificing the immune system's normal function.

Inverse vaccination is a process defined by antigen-specific tolerogenic immunization, which returns the effector T cell/Treg balance resulting in inhibition of autoimmune responses. Inverse vaccination can be achieved by prolonged treatment with high doses of the specific tolerogenic antigen. The introduction of antigen-specific tolerance is considered a promising approach for the treatment of MS and other autoimmune disorders. Several myelin proteins, such as myelin basic protein (MBP), proteolipid protein (PLP), and myelin oligodendrocyte glycoprotein (MOG), have been identified as targets of autoreactive T cells in MS as well as in experimental autoimmune encephalomyelitis (EAE), a widely investigated murine model of MS [104]. EAE is a complex condition in which the interaction between a variety of immunopathological and neuropathological mechanisms leads to an approximation of the key pathological features of MS: inflammation, demyelination, axonal loss, and gliosis [105]. Active-EAE can be induced by immunizing mice with CNS tissue of myelin peptides, such as myelin basic protein (MBP), proteolipid protein (PLP), and myelin oligodendrocyte glycoprotein (MOG) in CFA [106].

Oral delivery of myelin-oligodendrocyte glycoprotein 35-55 (MOG35-55) peptide is known to reduce disease severity in MOG35-55-induced EAE in C57Bl/6 mice [107]. Mechanisms for this treatment include suppression and deletion of autoreactive T cells,

induction of tolerogenic DCs, and stimulation of Tregs [108-112]. However, similar treatment with soluble peptides for MS carries the risk of an anaphylactic reaction due to the repeated delivery of high doses necessary to obtain optimum therapeutic effect in MS. Nanoparticle mediated delivery of antigens in tolerogenic dose is one way to overcome this problem [91, 113, 114].

Among the various types of nanoparticles examined by researchers for treatment of autoimmune diseases, lipid nanocarriers such as liposomes, solid lipid nanoparticles (SLNs), nanostructured lipid carriers (NLCs), and nanoemulsions are considered an ideal platform for effective delivery of therapeutics against MS. This type of nanoparticle possesses the ability to cross the brain-blood barrier (BBB) by entering the brain capillary endothelial cells and reducing peripheral side effects. In addition, lipid nanocarriers with appropriate decoration (such as ligand and peptide surface-modification) can efficiently interact with cell receptors presented in the BBB and deliver drugs or peptides cross the BBB [115].

1.6 Summary

This introduction provides an overview of the current state of cancer immunotherapy, different components of a cancer vaccine, and challenges facing the field of cancer vaccines. It has also highlighted autoimmune diseases and mechanisms of immune tolerance. In both instances, nanoparticles have been discussed as a promising carrier for the delivery of antigens and adjuvants for immune activation and oppositely, tolerogenic application.

In my dissertation, we have developed sHDL incorporated with a CSC antigen as a model antigen for cancer immunotherapy, investigated the role of different adjuvants to activate the immune system, and finally, applied the sHDL technology to induce antigen-specific immune tolerance as a new form of immunotherapy against autoimmune diseases. The overall goal of Chapter 2 and Chapter 3 of my dissertation was to develop a clinically translatable and scalable platform for the delivery of antigen and adjuvants to APCs for increasing the efficacy of cancer vaccines and reducing off-target side effects.

To achieve this goal, in Chapter 2, we have developed sHDL nanodiscs co-loaded with CSC antigen and adjuvant to generate strong antigen-specific CD8+ T response against CSCs. In chapter 3, we have studied the role of adjuvants in the sHDL vaccine formulations to further augment anti-tumor T cell immune responses. Finally, in Chapter 4, we have studied autoimmune disorders as a new application for our sHDL nanodiscs. we have evaluated the therapeutic and preventive application of tolerogenic antigen delivery by sHDL nanodiscs. we have assessed the sHDL formulation in the murine EAE model of MS. In Chapter 5, we have summarized the major findings from my dissertation and provided perspectives and directions for future studies.

1.7 References

[1] https://www.cancer.org/research/cancer-facts-statistics/global.html.

[2] P.R. Holt, P. Kozuch, S. Mewar, Colon cancer and the elderly: from screening to treatment in management of GI disease in the elderly, Best Practice & Research Clinical Gastroenterology, 23 (2009) 889-907.

[3] P. van der Bruggen, C. Traversari, P. Chomez, C. Lurquin, E. De Plaen, B. Van den Eynde, A. Knuth, T. Boon, A gene encoding an antigen recognized by cytolytic T lymphocytes on a human melanoma, Science, 254 (1991) 1643-1647.

[4] C.G. Clemente, M.C. Mihm, R. Bufalino, S. Zurrida, P. Collini, N. Cascinelli, Prognostic value of tumor infiltrating lymphocytes in the vertical growth phase of primary cutaneous melanoma, Cancer, 77 (1996) 1303-1310.

[5] M.C. Mihm Jr, C.G. Clemente, N. Cascinelli, Tumor infiltrating lymphocytes in lymph node melanoma metastases: a histopathologic prognostic indicator and an expression of local immune response, Laboratory investigation; a journal of technical methods and pathology, 74 (1996) 43-47.

[6] L. Rivoltini, M. Carrabba, V. Huber, C. Castelli, L. Novellino, P. Dalerba, R. Mortarini, G. Arancia, A. Anichini, S. Fais, Immunity to cancer: attack and escape in T lymphocyte–tumor cell interaction, Immunological reviews, 188 (2002) 97-113.

[7] M.M. Keane, S.A. Ettenberg, G.A. Lowrey, E.K. Russell, S. Lipkowitz, Fas expression and function in normal and malignant breast cell lines, Cancer research, 56 (1996) 4791-4798.

[8] C.G. Drake, E. Jaffee, D.M. Pardoll, Mechanisms of immune evasion by tumors, Advances in immunology, 90 (2006) 51-81.

[9] S. Jang, M.B. Atkins, Which drug, and when, for patients with BRAF-mutant melanoma?, The lancet oncology, 14 (2013) e60-e69.

[10] S. Moreau, P. Saiag, P. Aegerter, D. Bosset, C. Longvert, Z. Hélias-Rodzewicz, C. Marin, F. Peschaud, S. Chagnon, U. Zimmermann, Prognostic value of BRAF V600

mutations in melanoma patients after resection of metastatic lymph nodes, Annals of surgical oncology, 19 (2012) 4314-4321.

[11] R.J. Sullivan, K.T. Flaherty, New strategies in melanoma: entering the era of combinatorial therapy, Clinical Cancer Research, 21 (2015) 2424-2435.

[12] A.M.M. Eggermont, A. Spatz, C. Robert, Cutaneous melanoma, Lancet, 383 (2014) 816-827.

[13] J.R. Brahmer, S.S. Tykodi, L.Q.M. Chow, W.J. Hwu, S.L. Topalian, P. Hwu, C.G. Drake, L.H. Camacho, J. Kauh, K. Odunsi, H.C. Pitot, O. Hamid, S. Bhatia, R. Martins, K. Eaton, S.M. Chen, T.M. Salay, S. Alaparthy, J.F. Grosso, A.J. Korman, S.M. Parker, S. Agrawal, S.M. Goldberg, D.M. Pardoll, A. Gupta, J.M. Wigginton, Safety and Activity of Anti-PD-L1 Antibody in Patients with Advanced Cancer, N. Engl. J. Med., 366 (2012) 2455-2465.

[14] O. Hamid, C. Robert, A. Daud, F.S. Hodi, W.J. Hwu, R. Kefford, J.D. Wolchok, P. Hersey, R.W. Joseph, J.S. Weber, R. Dronca, T.C. Gangadhar, A. Patnaik, H. Zarour, A.M. Joshua, K. Gergich, J. Elassaiss-Schaap, A. Algazi, C. Mateus, P. Boasberg, P.C. Tumeh, B. Chmielowski, S.W. Ebbinghaus, X.N. Li, S.P. Kang, A. Ribas, Safety and Tumor Responses with Lambrolizumab (Anti-PD-1) in Melanoma, N. Engl. J. Med., 369 (2013) 134-144.

[15] S.L. Topalian, F.S. Hodi, J.R. Brahmer, S.N. Gettinger, D.C. Smith, D.F. McDermott, J.D. Powderly, R.D. Carvajal, J.A. Sosman, M.B. Atkins, P.D. Leming, D.R. Spigel, S.J. Antonia, L. Horn, C.G. Drake, D.M. Pardoll, L.P. Chen, W.H. Sharfman, R.A. Anders, J.M. Taube, T.L. McMiller, H.Y. Xu, A.J. Korman, M. Jure-Kunkel, S. Agrawal, D. McDonald, G.D. Kollia, A. Gupta, J.M. Wigginton, M. Sznol, Safety, Activity,

and Immune Correlates of Anti-PD-1 Antibody in Cancer, N. Engl. J. Med., 366 (2012) 2443-2454.

[16] J.D. Wolchok, H. Kluger, M.K. Callahan, M.A. Postow, N.A. Rizvi, A.M. Lesokhin, N.H. Segal, C.E. Ariyan, R.A. Gordon, K. Reed, M.M. Burke, A. Caldwell, S.A. Kronenberg, B.U. Agunwamba, X.L. Zhang, I. Lowy, H.D. Inzunza, W. Feely, C.E. Horak, Q. Hong, A.J. Korman, J.M. Wigginton, A. Gupta, M. Sznol, Nivolumab plus Ipilimumab in Advanced Melanoma, N. Engl. J. Med., 369 (2013) 122-133.

[17] H. Kumar, T. Kawai, S. Akira, Pathogen Recognition by the Innate Immune System, Int. Rev. Immunol., 30 (2011) 16-34.

[18] U. Aickelin, J. Greensmith, J. Twycross, Immune system approaches to intrusion detection–a review, International Conference on Artificial Immune Systems, Springer, 2004, pp. 316-329.

[19] A.E. Grulich, M.T. van Leeuwen, M. Falster, C.M. Vajdic, Incidence of cancers in people with HIV/AIDS compared with immunosuppressed transplant recipients: a meta-analysis, Lancet, 370 (2007) 59-67.

[20] S.A. Rosenberg, J.C. Yang, N.P. Restifo, Cancer immunotherapy: moving beyond current vaccines, Nature medicine, 10 (2004) 909.

[21] A.E. Grulich, M.T. Van Leeuwen, M.O. Falster, C.M. Vajdic, Incidence of cancers in people with HIV/AIDS compared with immunosuppressed transplant recipients: a meta-analysis, The Lancet, 370 (2007) 59-67.

[22] C.J. Melief, Cancer immunotherapy by dendritic cells, Immunity, 29 (2008) 372-383.

[23] R.L. Coffman, A. Sher, R.A. Seder, Vaccine Adjuvants: Putting Innate Immunity to Work, Immunity, 33 (2010) 492-503.

[24] O.P. Joffre, E. Segura, A. Savina, S. Amigorena, Cross-presentation by dendritic cells, Nature Reviews Immunology, 12 (2012) 557-569.
[25] Z. Hu, P.A. Ott, C.J. Wu, Towards personalized, tumour-specific, therapeutic vaccines for cancer, Nature Reviews Immunology, 18 (2018) 168.
[26] L. Novellino, C. Castelli, G. Parmiani, A listing of human tumor antigens recognized by T cells: March 2004 update, Cancer Immunology, Immunotherapy, 54 (2005) 187-207.
[27] M.E. Dudley, J.R. Wunderlich, P.F. Robbins, J.C. Yang, P. Hwu, D.J. Schwartzentruber, S.L. Topalian, R. Sherry, N.P. Restifo, A.M. Hubicki, Cancer regression and autoimmunity in patients after clonal repopulation with antitumor lymphocytes, Science, 298 (2002) 850-854.
[28] J.E. Thaxton, Z. Li, To affinity and beyond: harnessing the T cell receptor for cancer immunotherapy, Human vaccines & immunotherapeutics, 10 (2014) 3313-3321.
[29] N. Renkvist, C. Castelli, P.F. Robbins, G. Parmiani, A listing of human tumor antigens recognized by T cells, Cancer Immunology, Immunotherapy, 50 (2001) 3-15.
[30] V. Karanikas, D. Colau, J.-F. Baurain, R. Chiari, J. Thonnard, I. Gutierrez-Roelens, C. Goffinet, E. Van Schaftingen, P. Weynants, T. Boon, High frequency of cytolytic T lymphocytes directed against a tumor-specific mutated antigen detectable with HLA tetramers in the blood of a lung carcinoma patient with long survival, Cancer research, 61 (2001) 3718-3724.
[31] M. Singh, M. Ugozzoli, J. Kazzaz, J. Chesko, E. Soenawan, D. Mannucci, F. Titta, M. Contorni, G. Volpini, G. Del Guidice, A preliminary evaluation of alternative adjuvants

to alum using a range of established and new generation vaccine antigens, Vaccine, 24 (2006) 1680-1686.

[32] M. Kool, K. Fierens, B.N. Lambrecht, Alum adjuvant: some of the tricks of the oldest adjuvant, Journal of medical microbiology, 61 (2012) 927-934.

[33] J.C. Cox, A.R. Coulter, Adjuvants—a classification and review of their modes of action, Vaccine, 15 (1997) 248-256.

[34] S. Santos-Sierra, Developments in anticancer vaccination: budding new adjuvants, Biological Chemistry, 401 (2020) 435-446.

[35] M.R. Rosenfeld, M.C. Chamberlain, S.A. Grossman, D.M. Peereboom, G.J. Lesser, T.T. Batchelor, S. Desideri, A.M. Salazar, X.B. Ye, A multi-institution phase II study of poly-ICLC and radiotherapy with concurrent and adjuvant temozolomide in adults with newly diagnosed glioblastoma(dagger), Neuro-Oncology, 12 (2010) 1071-1077.

[36] P.M. Moyle, I. Toth, Modern subunit vaccines: development, components, and research opportunities, ChemMedChem, 8 (2013) 360-376.

[37] J.J. Moon, H. Suh, A.V. Li, C.F. Ockenhouse, A. Yadava, D.J. Irvine, Enhancing humoral responses to a malaria antigen with nanoparticle vaccines that expand Tfh cells and promote germinal center induction, Proceedings of the National Academy of Sciences, 109 (2012) 1080-1085.

[38] K. Hoebe, E. Janssen, B. Beutler, The interface between innate and adaptive immunity, Nature Immunology, 5 (2004) 971-974.

[39] A. Mount, S. Koernig, A. Silva, D. Drane, E. Maraskovsky, A.B. Morelli, Combination of adjuvants: the future of vaccine design, Expert Rev. Vaccines, 12 (2013) 733-746.

[40] S.M. Goldinger, R. Dummer, P. Baumgaertner, D. Mihic-Probst, K. Schwarz, A. Hammann-Haenni, J. Willers, C. Geldhof, J.O. Prior, T.M. Kündig, Nano-particle vaccination combined with TLR-7 and-9 ligands triggers memory and effector CD 8+ T-cell responses in melanoma patients, European journal of immunology, 42 (2012) 3049-3061.

[41] S.M. Goldinger, R. Dummer, P. Baumgaertner, D. Mihic-Probst, K. Schwarz, A. Hammann-Haenni, J. Willers, C. Geldhof, J.O. Prior, T.M. Kündig, Nano-particle vaccination combined with TLR-7 and-9 ligands triggers memory and effector CD8+ T-cell responses in melanoma patients, European journal of immunology, 42 (2012) 3049-3061.

[42] R. Narayan, H. Nguyen, J.J. Bentow, L. Moy, D.K. Lee, S. Greger, J. Haskell, V. Vanchinathan, P.-L. Chang, S. Tsui, Immunomodulation by imiquimod in patients with high-risk primary melanoma, Journal of Investigative Dermatology, 132 (2012) 163-169.

[43] A. Iwasaki, R. Medzhitov, Toll-like receptor control of the adaptive immune responses, Nature immunology, 5 (2004) 987.

[44] D.E. Speiser, D. Liénard, N. Rufer, V. Rubio-Godoy, D. Rimoldi, F. Lejeune, A.M. Krieg, J.-C. Cerottini, P. Romero, Rapid and strong human CD8+ T cell responses to vaccination with peptide, IFA, and CpG oligodeoxynucleotide 7909, Journal of Clinical Investigation, 115 (2005) 739.

[45] E.A. Vasievich, L. Huang, The suppressive tumor microenvironment: a challenge in cancer immunotherapy, Molecular pharmaceutics, 8 (2011) 635-641.

[46] S.L. Demento, W. Cui, J.M. Criscione, E. Stern, J. Tulipan, S.M. Kaech, T.M. Fahmy, Role of sustained antigen release from nanoparticle vaccines in shaping the T cell memory phenotype, Biomaterials, 33 (2012) 4957-4964.

[47] V.P. Torchilin, Recent advances with liposomes as pharmaceutical carriers, Nature reviews Drug discovery, 4 (2005) 145-160.

[48] H. Zhang, J. Chen, Current status and future directions of cancer immunotherapy, Journal of Cancer, 9 (2018) 1773.

[49] M.S. Singh, S. Bhaskar, Nanocarrier-based immunotherapy in cancer management and research, ImmunoTargets and Therapy, 3 (2014) 121.

[50] M.L. Bookstaver, S.J. Tsai, J.S. Bromberg, C.M. Jewell, Improving vaccine and immunotherapy design using biomaterials, Trends in immunology, 39 (2018) 135-150.

[51] E. Vranić, O. Rahić, J. Hadžiabdić, A. Elezović, D. Bošković, Opportunities and challenges for utilization of nanoparticles as bioactive drug carriers for the targeted treatment of cancer, Folia Medica Facultatis Medicinae Universitatis Saraeviensis, 50 (2015).

[52] Y. Jia, A. Omri, L. Krishnan, M.J. McCluskie, Potential applications of nanoparticles in cancer immunotherapy, Human vaccines & immunotherapeutics, 13 (2017) 63-74.

[53] S. Fogli, C. Montis, S. Paccosi, A. Silvano, E. Michelucci, D. Berti, A. Bosi, A. Parenti, P. Romagnoli, Inorganic nanoparticles as potential regulators of immune response in dendritic cells, Nanomedicine, 12 (2017) 1647-1660.

[54] J. Conniot, J.M. Silva, J.G. Fernandes, L.C. Silva, R. Gaspar, S. Brocchini, H.F. Florindo, T.S. Barata, Cancer immunotherapy: nanodelivery approaches for immune cell targeting and tracking, Frontiers in chemistry, 2 (2014) 105.

[55] R. Kuai, D. Li, Y.E. Chen, J.J. Moon, A. Schwendeman, High-density lipoproteins: nature's multifunctional nanoparticles, ACS nano, 10 (2016) 3015-3041.

[56] R. Kuai, L.J. Ochyl, K.S. Bahjat, A. Schwendeman, J.J. Moon, Designer vaccine nanodiscs for personalized cancer immunotherapy, Nature materials, 16 (2017) 489-496.

[57] T. Lapidot, C. Sirard, J. Vormoor, B. Murdoch, T. Hoang, J. Caceres-cortes, M. Minden, B. Paterson, M.A. Caligiuri, J.E. Dick, A cell initiating human acute myeloid leukaemia after transplantation into SCID mice, Nature, 367 (1994) 645-648.

[58] M. Al-Hajj, M.S. Wicha, A. Benito-Hernandez, S.J. Morrison, M.F. Clarke, Prospective identification of tumorigenic breast cancer cells, Proc. Natl. Acad. Sci. U. S. A., 100 (2003) 3983-3988.

[59] K.M. Sales, M.C. Winslet, A.M. Seifalian, Stem cells and cancer: an overview, Stem cell reviews, 3 (2007) 249-255.

[60] D.R. Pattabiraman, R.A. Weinberg, Tackling the cancer stem cells—what challenges do they pose?, Nature reviews Drug discovery, 13 (2014) 497.

[61] E. Batlle, H. Clevers, Cancer stem cells revisited, Nature medicine, 23 (2017) 1124.

[62] B. Sahu, A. Maeda, Retinol dehydrogenases regulate vitamin a metabolism for visual function, Nutrients, 8 (2016) 746.

[63] N.A. Sophos, V. Vasiliou, Aldehyde dehydrogenase gene superfamily: the 2002 update, Chemico-biological interactions, 143 (2003) 5-22.

[64] J.P. Chute, G.G. Muramoto, J. Whitesides, M. Colvin, R. Safi, N.J. Chao, D.P. McDonnell, Inhibition of aldehyde dehydrogenase and retinoid signaling induces the

expansion of human hematopoietic stem cells, Proceedings of the National Academy of Sciences, 103 (2006) 11707-11712.

[65] C. Ginestier, M.H. Hur, E. Charafe-Jauffret, F. Monville, J. Dutcher, M. Brown, J. Jacquemier, P. Viens, C.G. Kleer, S. Liu, ALDH1 is a marker of normal and malignant human mammary stem cells and a predictor of poor clinical outcome, Cell stem cell, 1 (2007) 555-567.

[66] Y. Luo, K. Dallaglio, Y. Chen, W.A. Robinson, S.E. Robinson, M.D. McCarter, J. Wang, R. Gonzalez, D.C. Thompson, D.A. Norris, ALDH1A isozymes are markers of human melanoma stem cells and potential therapeutic targets, Stem cells, 30 (2012) 2100-2113.

[67] D.J. Pearce, D. Taussig, C. Simpson, K. Allen, A.Z. Rohatiner, T.A. Lister, D. Bonnet, Characterization of cells with a high aldehyde dehydrogenase activity from cord blood and acute myeloid leukemia samples, Stem cells, 23 (2005) 752-760.

[68] W. Matsui, C.A. Huff, Q. Wang, M.T. Malehorn, J. Barber, Y. Tanhehco, B.D. Smith, C.I. Civin, R.J. Jones, Characterization of clonogenic multiple myeloma cells, Blood, 103 (2004) 2332-2336.

[69] L. Lu, H. Tao, A.E. Chang, Y. Hu, G. Shu, Q. Chen, M. Egenti, J. Owen, J.S. Moyer, M.E. Prince, Cancer stem cell vaccine inhibits metastases of primary tumors and induces humoral immune responses against cancer stem cells, Oncoimmunology, 4 (2015) e990767.

[70] N. Ning, Q. Pan, F. Zheng, S. Teitz-Tennenbaum, M. Egenti, J. Yet, M. Li, C. Ginestier, M.S. Wicha, J.S. Moyer, M.E.P. Prince, Y.X. Xu, X.L. Zhang, S. Huang, A.E.

Chang, Q. Li, Cancer Stem Cell Vaccination Confers Significant Antitumor Immunity, Cancer research, 72 (2012) 1853-1864.

[71] D. Trichopoulos, F.P. Li, D.J. Hunter, What causes cancer?, Scientific American, 275 (1996) 80-84.

[72] M.J. Koppe, O.C. Boerman, W.J. Oyen, R.P. Bleichrodt, Peritoneal carcinomatosis of colorectal origin: incidence and current treatment strategies, Annals of surgery, 243 (2006) 212.

[73] B. Gustavsson, G. Carlsson, D. Machover, N. Petrelli, A. Roth, H.-J. Schmoll, K.-M. Tveit, F. Gibson, A review of the evolution of systemic chemotherapy in the management of colorectal cancer, Clinical colorectal cancer, 14 (2015) 1-10.

[74] S. Haraldsdottir, H.M. Einarsdottir, A. Smaradottir, A. Gunnlaugsson, T.R. Halfdanarson, Colorectal cancer-review, Laeknabladid, 100 (2014) 75-82.

[75] M.G. Haddock, Intraoperative radiation therapy for colon and rectal cancers: a clinical review, Radiation Oncology, 12 (2017) 11.

[76] B.M. Wolpin, R.J. Mayer, Systemic treatment of colorectal cancer, Gastroenterology, 134 (2008) 1296-1310. e1291.

[77] R. Sobel, B. Blanchette, A. Bhan, R. Colvin, The immunopathology of experimental allergic encephalomyelitis. I. Quantitative analysis of inflammatory cells in situ, The Journal of Immunology, 132 (1984) 2393-2401.

[78] F. Shojaei, Anti-angiogenesis therapy in cancer: current challenges and future perspectives, Cancer letters, 320 (2012) 130-137.

[79] S. Rafii, D. Lyden, R. Benezra, K. Hattori, B. Heissig, Vascular and haematopoietic stem cells: novel targets for anti-angiogenesis therapy?, Nature Reviews Cancer, 2 (2002) 826-835.

[80] G.M. Keating, Bevacizumab: a review of its use in advanced cancer, Drugs, 74 (2014) 1891-1925.

[81] S. Dhillon, Regorafenib: a review in metastatic colorectal cancer, Drugs, 78 (2018) 1133-1144.

[82] A.C.S.C.F.F.A.C. Society, 2016.

[83] D. Cunningham, Y. Humblet, S. Siena, D. Khayat, H. Bleiberg, A. Santoro, D. Bets, M. Mueser, A. Harstrick, C. Verslype, Cetuximab monotherapy and cetuximab plus irinotecan in irinotecan-refractory metastatic colorectal cancer, New England journal of medicine, 351 (2004) 337-345.

[84] https://www.rndsystems.com/resources/articles/immune-tolerance.

[85] F. Ferrera, A.L. CAVA, M. Rizzi, B.H. Hahn, F. Indiveri, G. Filaci, Gene vaccination for the induction of immune tolerance, Annals of the New York Academy of Sciences, 1110 (2007) 99-111.

[86] A.M. Bilate, J.J. Lafaille, Induced CD4+ Foxp3+ regulatory T cells in immune tolerance, Annual review of immunology, 30 (2012) 733-758.

[87] A. Liston, Immunological tolerance 50 years after the Burnet Nobel Prize, Immunology and cell biology, 89 (2011) 14.

[88] W.D. Billington, The immunological problem of pregnancy: 50 years with the hope of progress. A tribute to Peter Medawar, Elsevier, 2003.

[89] K. Murphy, C. Weaver, Janeway's immunobiology, Garland science2016.

[90] M. Kleinewietfeld, D.A. Hafler, Regulatory T cells in autoimmune neuroinflammation, Immunological reviews, 259 (2014) 231-244.
[91] D.R. Getts, A.J. Martin, D.P. McCarthy, R.L. Terry, Z.N. Hunter, W.T. Yap, M.T. Getts, M. Pleiss, X. Luo, N.J. King, Microparticles bearing encephalitogenic peptides induce T-cell tolerance and ameliorate experimental autoimmune encephalomyelitis, Nature biotechnology, 30 (2012) 1217-1224.
[92] M.T. Wallin, W.J. Culpepper, J.D. Campbell, L.M. Nelson, A. Langer-Gould, R.A. Marrie, G.R. Cutter, W.E. Kaye, L. Wagner, H. Tremlett, The prevalence of MS in the United States: a population-based estimate using health claims data, Neurology, 92 (2019) e1029-e1040.
[93] M.T. Wallin, W.J. Culpepper, E. Nichols, Z.A. Bhutta, T.T. Gebrehiwot, S.I. Hay, I.A. Khalil, K.J. Krohn, X. Liang, M. Naghavi, Global, regional, and national burden of multiple sclerosis 1990–2016: a systematic analysis for the Global Burden of Disease Study 2016, The Lancet Neurology, 18 (2019) 269-285.
[94] D. Karussis, The diagnosis of multiple sclerosis and the various related demyelinating syndromes: a critical review, Journal of autoimmunity, 48 (2014) 134-142.
[95] J. Oh, A. Vidal-Jordana, X. Montalban, Multiple sclerosis: clinical aspects, Current Opinion in Neurology, 31 (2018) 752-759.
[96] W. Brück, N. Sommermeier, M. Bergmann, U. Zettl, H.H. Goebel, H.A. Kretzschmar, H. Lassmann, Macrophages in multiple sclerosis, Immunobiology, 195 (1996) 588-600.

[97] J.M. Fletcher, S. Lalor, C. Sweeney, N. Tubridy, K. Mills, T cells in multiple sclerosis and experimental autoimmune encephalomyelitis, Clinical & Experimental Immunology, 162 (2010) 1-11.

[98] A. Compston, A. Coles, Multiple sclerosis. Lancet (Lond, Engl) 372: 1502–1517, 2008.

[99] D.M. Wingerchuk, B.G. Weinshenker, Disease modifying therapies for relapsing multiple sclerosis, Bmj, 354 (2016) i3518.

[100] D.L. Vargas, W.R. Tyor, Update on disease-modifying therapies for multiple sclerosis, Journal of Investigative Medicine, 65 (2017) 883-891.

[101] M.M. Goldenberg, Multiple sclerosis review, Pharmacy and Therapeutics, 37 (2012) 175.

[102] N. Scheinfeld, Adalimumab: a review of side effects, Expert opinion on drug safety, 4 (2005) 637-641.

[103] M. Feldmann, R.N. Maini, TNF defined as a therapeutic target for rheumatoid arthritis and other autoimmune diseases, Nature medicine, 9 (2003) 1245-1250.

[104] L. Steinman, Inverse vaccination, the opposite of Jenner’s concept, for therapy of autoimmunity, Journal of internal medicine, 267 (2010) 441-451.

[105] S. Sriram, I. Steiner, Experimental allergic encephalomyelitis: a misleading model of multiple sclerosis, Annals of Neurology: Official Journal of the American Neurological Association and the Child Neurology Society, 58 (2005) 939-945.

[106] C.S. Constantinescu, N. Farooqi, K. O'Brien, B. Gran, Experimental autoimmune encephalomyelitis (EAE) as a model for multiple sclerosis (MS), British journal of pharmacology, 164 (2011) 1079-1106.

[107] J.P.S. Peron, K. Yang, M.-L. Chen, W.N. Brandao, A.S. Basso, A.G. Commodaro, H.L. Weiner, L.V. Rizzo, Oral tolerance reduces Th17 cells as well as the overall inflammation in the central nervous system of EAE mice, Journal of neuroimmunology, 227 (2010) 10-17.

[108] H. Li, G.-X. Zhang, Y. Chen, H. Xu, D.C. Fitzgerald, Z. Zhao, A. Rostami, CD11c+ CD11b+ dendritic cells play an important role in intravenous tolerance and the suppression of experimental autoimmune encephalomyelitis, The Journal of Immunology, 181 (2008) 2483-2493.

[109] H. Li, B. Ciric, J. Yang, H. Xu, D.C. Fitzgerald, M. Elbehi, Z. Fonseca-Kelly, S. Yu, G.-X. Zhang, A. Rostami, Intravenous tolerance modulates macrophage classical activation and antigen presentation in experimental autoimmune encephalomyelitis, Journal of neuroimmunology, 208 (2009) 54-60.

[110] J.M. Critchfield, M.K. Racke, J.C. Zuniga-Pflucker, B. Cannella, C.S. Raine, J. Goverman, M.J. Lenardo, T cell deletion in high antigen dose therapy of autoimmune encephalomyelitis, Science, 263 (1994) 1139-1143.

[111] S.Y. Min, K.S. Park, M.L. Cho, J.W. Kang, Y.G. Cho, S.Y. Hwang, M.J. Park, C.H. Yoon, J.K. Min, S.H. Lee, Antigen-induced, tolerogenic CD11c+, CD11b+ dendritic cells are abundant in Peyer's patches during the induction of oral tolerance to type II collagen and suppress experimental collagen-induced arthritis, Arthritis & Rheumatism, 54 (2006) 887-898.

[112] D.C. Fitzgerald, G.-X. Zhang, S. Yu, M.L. Cullimore, Z. Zhao, A. Rostami, Intravenous tolerance effectively overcomes enhanced pro-inflammatory responses and

experimental autoimmune encephalomyelitis severity in the absence of IL-12 receptor signaling, Journal of neuroimmunology, 247 (2012) 32-37.

[113] M. Mahmoudi, M.A. Sahraian, M.A. Shokrgozar, S. Laurent, Superparamagnetic iron oxide nanoparticles: promises for diagnosis and treatment of multiple sclerosis, ACS chemical neuroscience, 2 (2011) 118-140.

[114] A. Carambia, B. Freund, D. Schwinge, O.T. Bruns, S.C. Salmen, H. Ittrich, R. Reimer, M. Heine, S. Huber, C. Waurisch, Nanoparticle-based autoantigen delivery to Treg-inducing liver sinusoidal endothelial cells enables control of autoimmunity in mice, Journal of hepatology, 62 (2015) 1349-1356.

[115] M. Chountoulesi, C. Demetzos, Promising Nanotechnology Approaches in Treatment of Autoimmune Diseases of Central Nervous System, Brain Sciences, 10 (2020) 338.

Chapter 2 Combination Immunotherapy Against Cancer Stem Cells Using Synthetic High-Density Lipoprotein Nanodiscs

2.1 Abstract

Despite recent advances in cancer therapies, cancer is still one of the major causes of death worldwide. Standard procedures for cancer treatments include surgical resection and chemotherapy, but their limited efficacy leads to tumor relapse and metastasis. Cancer stem cells (CSC) are a subpopulation of cancer cells that can proliferate extensively and drive tumor metastasis and recurrence. Despite intensive research, it remains challenging to specifically target and eliminate CSCs. Aldehyde dehydrogenase (ALDH) is one of the markers that have been used extensively for isolating CSCs. Here, I report a novel approach to target CSCs by vaccination against ALDH. We have developed synthetic high-density lipoprotein nanodiscs co-loaded with ALDH peptide antigen and CpG (TLR-9 agonist) adjuvant. Nanodiscs increased antigen trafficking to lymph nodes and generated T cell responses against ALDH expressed in CSCs. Nanodisc vaccination combined with αPD-L1 immune checkpoint blocker led to significant inhibition of tumor growth in murine models of D5 melanoma and 4T1 breast cancer. Overall, we have shown that nanodisc vaccination against ALDH in combination with αPD-L1 immunotherapy can exert strong anti-tumor efficacy.

2.2 Introduction

Cancer is one of the most significant causes of death worldwide despite decades of research [1]. Standard treatments for patients with solid malignancies are surgical resection, chemotherapy, and radiation therapy. Each of these can be used as a stand-alone or complementary treatment, but their efficacy is limited by tumor recurrence and metastasis [2, 3]. One possible explanation for tumor recurrence is cancer stem cells (CSC), which are a small fraction of cancer cells that self-renews, mediates tumor growth, and contributes to tumor metastasis [4]. Unlike the majority of cancer cells, CSCs exist in a mostly inactive cell cycle, making them resistant to standard cytotoxic drugs designed to target rapidly dividing cells. Thus, CSCs are considered one of the key culprits that drive chemo-resistance, leading to tumor relapse and metastasis [2, 3, 5]. Cancer immunotherapy based on immune checkpoint blockade (ICB) is now established as one of the most promising cancer therapies [6]. However, current ICB therapy only benefits a small group of cancer patients, with 10-30% response rates [7, 8]. Recent studies have suggested that CSCs may contribute to immune resistance by employing multiple mechanisms to evade immune surveillance, including expression of immunosuppressive genes and cytokines [9-11]. These challenges highlight the need to develop new approaches for selectively targeting and eliminating CSCs.

Aldehyde dehydrogenase (ALDH) is a promising target detoxifies intracellular aldehydes through oxidation expression and has been extensively used as a functional biomarker to isolate CSCs from more than 20 cancer types [12-18]. We have previously shown that dendritic cells (DCs) pulsed with cell lysate from $ALDH^{high}$ CSCs generated CSC-specific T cell and humoral immune responses, which were augmented by co-

administration of αPD-L1 IgG [19-21]. Despite these promising results, this approach is limited by the requirement for isolation of a sufficient number of patient-specific CSCs as well as the suboptimal clinical efficacy of DC vaccines [22, 23].

To overcome such limitations, we have developed a nanoparticle vaccine platform that can deliver ALDH epitope peptides to antigen-presenting cells (APCs) in the lymph nodes and elicit robust T cell responses against ALDH expressed in CSCs. Our approach is based on synthetic high-density lipoprotein nanodiscs (ND) composed of apolipoprotein A1 mimetic peptide (22A) and phospholipids [24]. In particular, these ND have four key attributes for cancer vaccination: (1) 10 nm diameter of ND allows direct access to draining lymph nodes (dLNs) after subcutaneous (SC) administration; (2) ND mediates co-delivery of antigen and adjuvant to dendritic cells (DCs) in dLNs; (3) ND promotes antigen processing and presentation on DCs; and (4) ND is safe, well-characterized, and amenable for scalable manufacturing [25].

In this chapter, we report that ND co-loaded with ALDH and immunostimulatory molecules induces robust T cell responses against CSCs. In particular, while ALDH constitutes a family of over 30 members, we have previously shown that ALDH1-A1 and ALDH1-A3 as the primary isoforms regulating CSC functions [26]. Hence, we focused on antigenic sequences predicted to be immunogenic from human ALDH1-A1 and ALDH1-A3 and have identified ALDH1-A1$_{88\text{-}96}$ and ALDH1-A3$_{98\text{-}106}$ with sequence homology in mice. Using these epitopes (termed as ALDH-A1 and ALDH-A3 peptides), we have demonstrated that ND vaccination elicit strong T cell responses against ALDH-A1 and ALDH-A3, reduces the frequency of ALDH^{high} CSCs from residual tumor masses, and

exert potent anti-tumor efficacy in murine models D5 melanoma and 4T1 mammary carcinoma (**Figure 2-1.**).

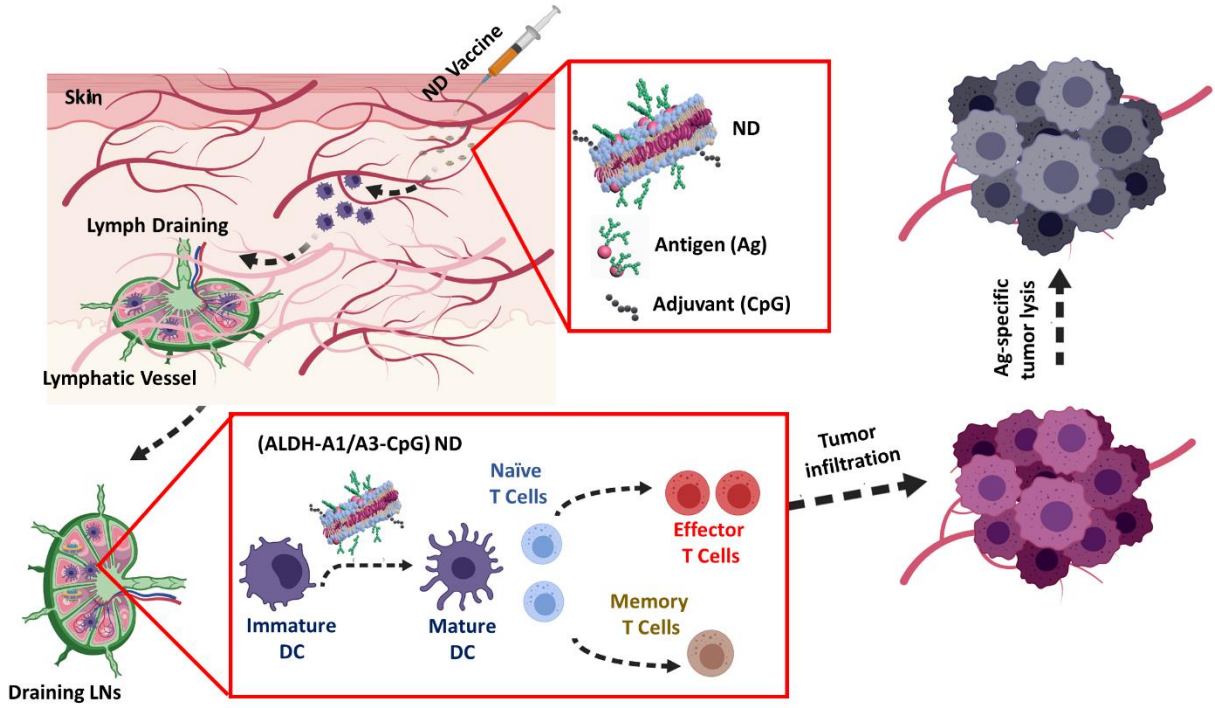

Figure 2-1. Illustration of nanodisc (ND) vaccination against cancer stem cells (CSCs).

2.3 Experimental section

2.3.1 Materials and reagents

CA1 and CA3 neoantigen peptides were synthesized by RS Synthesis (Louisville, KY). Female C57BL/6 mice aged 6-8 weeks were purchased from Jackson Laboratories (Bar Harbor, ME). Antibody against mouse PD-L1 was purchased from BioXCell (West Lebanon, NH). 1,2-dimyristoyl-sn-glycerol-3-phosphocholine (DMPC) was purchased from NOF America (White Plains, NY). 22A Apolipoprotein-A1 mimetic peptide was

synthesized by GenScript (Piscataway,NJ). 1,2-dioleoyl-sn-glycero-3-phosphoethanolamine-N-[3-(2-pyridyldithio)propionate] (DOPE-PDP) was purchased from Avanti Polar Lipids (Alabaster, AL). Both cholesterol-modified CpG1826 and unmodified CpG1826 were synthesized by Integrated DNA Technologies (Coralville, IA). Interferon-γ (IFN-γ) ELISPOT kits were purchased from Fisher Scientific (Hampton, NH). Cell media was purchased from Invitrogen (Carlsbad, CA). The following antibodies for flow cytometry were purchased from BioLegend: anti-mouse CD8a-APC; anti-mouse CD45R (B220)-PE/Cy7; rat anti-mouse CD4-Brilliant Violet 605; anti-mouse CD3-FITC; rat anti-mouse F4/80-APC-CY7; anti-mouse CD11c-FITC. MHC tetramer kit was purchased from MBL international corporation (Woburn, MA). TMR-NHS was purchased from Thermo Fisher Scientific (Waltham, MA).

2.3.2 Synthesis and characterization of nanodiscs (ND) carrying ALDH peptides

Lipid-peptide conjugates were prepared as previously reported [27]. To incorporate ALDH peptides into ND, the peptides were modified with a cysteine at the N-terminus. Then, the cysteine-terminated peptides were reacted with DOPE-PDP (antigen peptide:DOPE-PDP = 2:1, molar ratio) for 4 h on an orbital shaker in dimethylformamide (DMF) (**Figure 2-2.**). The conjugation efficiency of the reaction was calculated based on the reduction in absorbance signal associated with DOPE-PDP as measured by HPLC/MS. Nanodiscs were prepared as previously reported [24, 27]. To incorporate ALD peptides into ND, lipid-peptide dissolved in dimethylsulfoxide (DMSO) was added to ND solution, followed by incubation at RT for 1 h. After incubation, unincorporated lipid-peptide was separated by using ultracentrifuge filtration (MilliporeSigma™ Amicon™ Ultra Centrifugal Filter, 10KD).

Incorporation of lipid-peptide into ND was measured by reverse-phase HPLC/MS. In some studies, peptides tagged with tetramethylrhodamine (TMR, excitation/emission ~540/560 nm) were used to prepare ND carrying TMR-tagged peptide. To load CpG into ND, a cholesterol-modified CpG 1826 (Cho-CpG, Integrated DNA Technologies) was added dropwise to antigen-loaded ND, followed by incubation at RT for 1 h. The amount of CpG loaded into ND was quantified by gel permeation chromatography (GPC) equipped with TSKgel G3000SWxl column (7.8 mm ID × 30 cm, Tosoh Bioscience LLC). The hydrodynamic size and zeta potential of ND were measured by dynamic light scattering (DLS, Zetasizer Nano ZSP). The morphology of ND was investigated by transmission electron microscopy (TEM) after 10X dilution with Osmium tetroxide solution used as negative staining. All TEM images were obtained by a JEM 1200EX electron microscope (JEOL USA) equipped with an AMT XR-60 digital camera (Advanced Microscopy Techniques).

2.3.3 Lymph node draining and antigen presentation mediated by nanodiscs

Animals were cared for following the federal, state, and local guidelines. All work conducted on animals was in accordance with and approved by the University Committee on Use and Care of Animals (UCUCA) at the University of Michigan, Ann Arbor. For lymph node draining studies, female C57BL/6 mice of age 6–8 weeks (Jackson Laboratories) were immunized with free ALDH-A1-TMR or (ALDH-A1-TMR) ND containing antigen peptide (15.5 nmol per mouse) in 100 µl volume by subcutaneous injection at the tail base. At the 24 h time point after injection, animals were euthanized, different organs were harvested, and the TMR signal was measured with an IVIS optical imaging system

(Caliper Life Sciences). Afterward, inguinal lymph nodes were cut into small pieces and passed through a 70-μm cell strainer, washed two times with FACS buffer, and stained with the indicated antibodies, followed by flow cytometry analysis.

2.3.4 In vivo immunization study

For the D5 vaccination study, C57BL/6 female mice of age 6–8 weeks (Jackson laboratory) were inoculated s.c. in the right flank with 5×10^4 D5 cells on day 0. For the therapeutic studies in 4T1 tumor-bearing animals, Balb/c mice (6-8 weeks old, Jackson Laboratories) were inoculated s.c. with 1.0×10^4 4T1 cells in mammary fat pad on day 0. Tumor-bearing animals were then immunized s.c. at the tail base on days 1 and 8 with 15.5 nmol/dose of each ALDH peptides (A1 and A3) and 15 μg/dose of CpG in either soluble or ND form. In some studies, anti-mouse αPD-L1 antibody (100 μg per mouse) was administered intraperitoneally on days 2, 4, and 6 after each vaccination. Tumor growth was observed every other day, and the tumor volume was reported using the following equation: tumor volume = length × $(\text{width})^2$ × 0.5. Animals were euthanized when the tumor mass reached 1.5 cm in any dimension or when animals became moribund with > 20% weight loss or ulceration.

2.3.5 Immunological analyses

Blood samples were collected from the submandibular vein of mice, and red blood cells were lysed with Ammonium-Chloride-Potassium (ACK) lysis buffer. Tetramer staining assay was used to quantify the percentage of tumor antigen-specific $CD8a^+$ T cells among PBMCs, as described previously [28]. Briefly, the peptide-MHC tetramer was made

according to the manufacturer's instructions. PBMCs were isolated, washed with FACS buffer, and incubated with anti-CD16/32 blocking antibody. Cells were then incubated with tetramer for 1 h on ice, then incubated with anti-mouse CD8a-APC for 20 min on ice. Cells were then washed 2× with FACS buffer, resuspended in DAPI solution (2 µg/ml), and analyzed by flow cytometry. For IFN-γ ELISPOT analysis, 0.2×10^6 PBMCs were added on anti-IFN-γ-coated 96-well immunospot plate. PBMCs were restimulated with ALDH peptides (A1 and A3) for 18 hours at 37ºC, followed by washing and development of plates according to the manufacturer's instructions. For intracellular cytokine staining (ICS) assay, PBMCs were cultured at 2 million cells/ml on 96-well U-bottom plate and restimulated with 10 µg/ml of antigen peptides for 18 hours in the presence of a protein transport inhibitor, brefeldin A (BD Biosciences). Subsequently, cells were washed with ice-cold FACS buffer (1% BSA in PBS), incubated with anti-CD16/32 for 10 min, followed by anti-CD8a, Anti-CD4, and DAPI for 20 min on ice. Cells were then fixed/permeabilized and stained with anti–IFN-γ for 30 min on the ice. After 2× washing with FACS buffer, cells were resuspended in FACS buffer and analyzed by flow cytometry. Cytotoxic T lymphocytes (CTLs) were generated from splenocytes as reported previously [29]. Splenocytes stimulated with anti-CD3/CD28 and IL-2 consistently resulted in > 90% of $CD3^+$ T cells. CTL-mediated cell killing of CSCs or non-CSCs was performed using the LDH-release assay (CytoTox 96 non-radioactive cytotoxicity assay, Promega, Madison, WI) according to the manufacturer's instructions. In some studies, tumors were excised and cut into small pieces, followed by digestion using collagenase/hyaluronidase for 30-40 minutes. Single-cell suspension was produced and used to detect the percentage of ALDHhigh D5 CSCs by flow cytometry.

2.3.6 Statistical analysis

Sample sizes were selected according to pilot experiments and previously published results in the literature. All animal studies were performed after randomization. Data were analyzed by one-way or two-way ANOVA, followed by Tukey's multiple comparisons post-test or log-rank (Mantel-Cox) test with Prism 8.0 (GraphPad Software). Statistical significance is indicated as *P < 0. 5, **P < 0.01, ***P < 0.001 and ****P < 0.0001. All values are reported as means ± SEM.

2.4 Results and discussion

2.4.1 Synthesis and characterization of ND carrying ALDH peptide

We synthesized ND co-loaded with ALHD antigen peptides and CpG (a TLR-9 agonist) (**Figure 2-2.A**). Briefly, ND was synthesized by mixing 1,2-dimyristoyl-sn-glycerol-3-phosphocholine (DMPC) and apolipoprotein-A1 mimetic peptide, 22A, followed by lyophilization, rehydration, and heating and cooling cycles. Afterward, ALDH antigen peptides (ALDH-A1 and ALDH-A3) conjugated with 1,2-dioleoyl-sn-glycero-3-phosphoethanolamine-N-[3-(2-pyridyldithio)propionate] (DOPE-PDP) was added to pre-formed ND to produce antigen-loaded ND (**Figure 2-2.B**). Quantification with HPLC/MS showed a highly efficient conjugation of ALDH antigen peptides to DOPE lipid and subsequent incorporation of lipid-peptide into ND (> 90% efficiency for both) (**Figure 2-2.C-E**). HPLC chromatograms showed a reduction in area under the curve (AUC) for the DOPE-PDP peak after mixing with cysteine-modified ALDH-A1 or ALDH-A3 peptides,

indicating a successful conjugation. This reduction in AUC was accompanied by the appearance of the lipid-peptide peak at 21.9 min. Subsequently, cholesterol-modified CpG1826 (cho-CpG) was incubated with antigen-loaded ND by simple mixing at a weight ratio of 50:1 DMPC:cho-CpG. GPC analysis showed > 90% cho-CpG loading into ND, resulting in nanodiscs co-loaded with CpG and either ALDH-A1 or ALDH-A3 peptide, termed as (ALDH-A1-CpG)-ND and (ALDH-A3-CpG)-ND, respectively (**Figure 2-3.A-B**). Dynamic light scattering (DLS) revealed that the addition of antigen and cho-CpG to blank ND did not significantly increase the size of the resulting ND (**Figure 2-3.C**). Both (ALDH-A1-CpG)-ND and (ALDH-A3-CpG)-ND had comparable particle sizes ranging from 9-13 nm, a polydispersity index of 0.20 ± 0.02, and slightly positive charges of 2.8 ± 0.1 mV and 3.4 ±.3 mV, respectively. The transmission electron microscopy (TEM) images showed that ND had an average diameter of 10 ± 3 nm (**Figure 2-3.D**) in line with the DLS results.

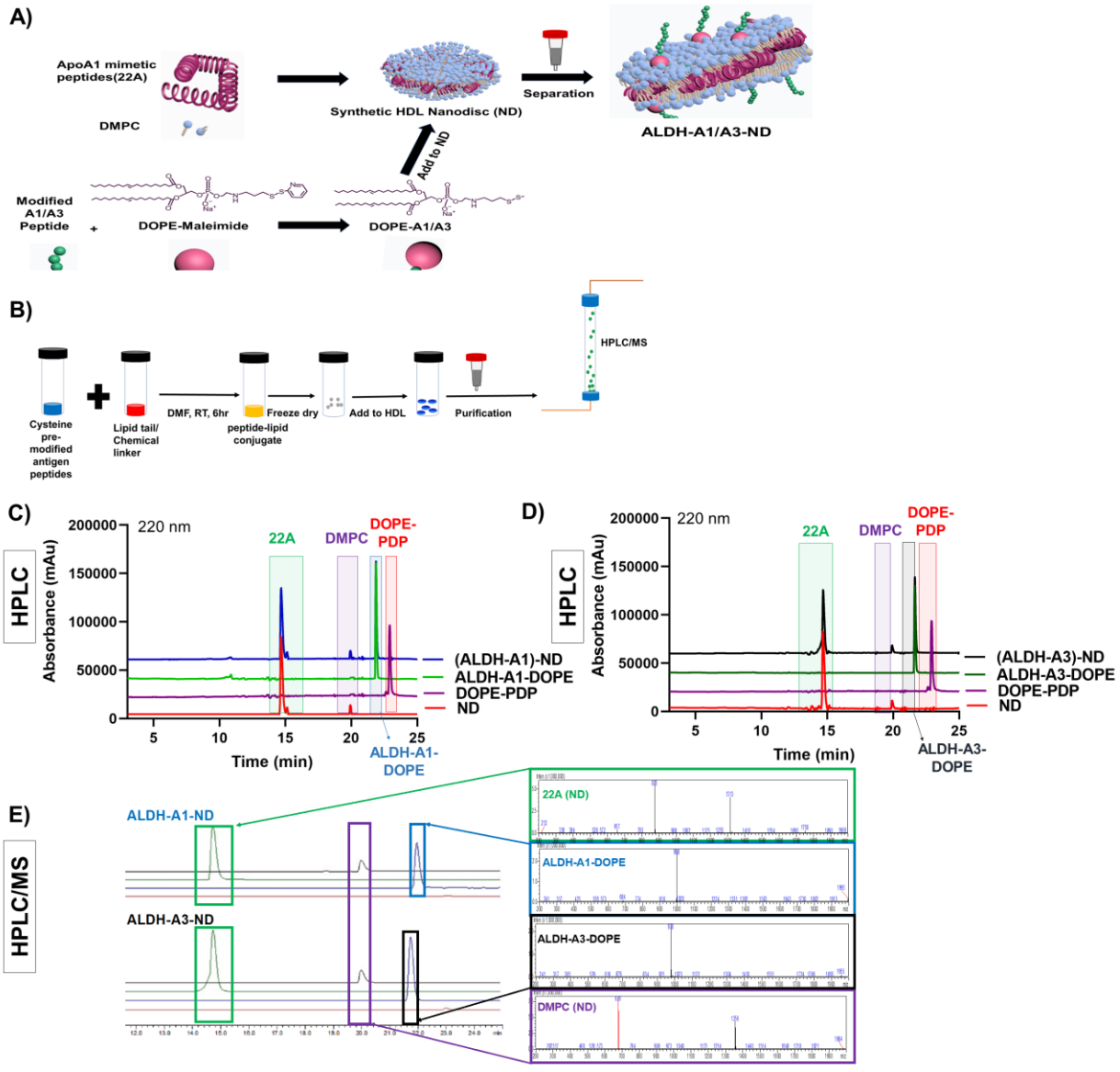

Figure 2-2. Synthesis and characterization of nanodiscs (ND) carrying ALDH peptides. A. Schematic illustration of the preparation, purification, and characterization of ND vaccine as well as B. incorporation of lipid-peptide conjugates in ND. Shown are HPLC chromatograms of C. (ALDH-A1)-ND, D. (ALDH-A3)-ND, and their individual components. E. HPLC/MS chromatograms indicated the conjugation of ALDH-A1 and ALDH-A3 peptides to DOPE-PDP and the subsequent incorporation of lipid-peptides into ND.

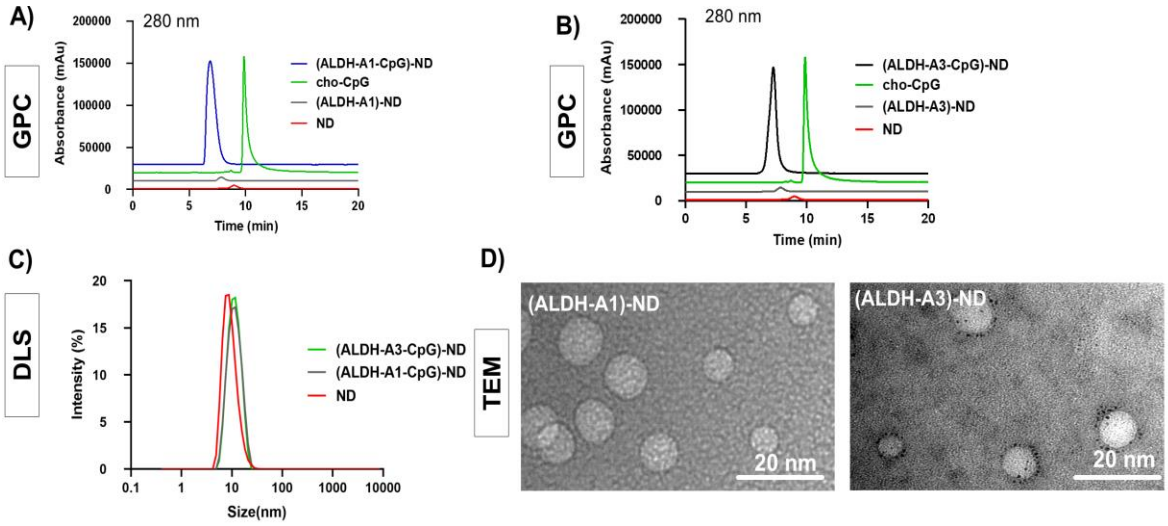

Figure 2-3. Characterization of ND co-loaded with ALDH peptides and cho-CpG. Shown are GPC chromatograms of A. (ALDH-A1-CpG)-ND, and B. (ALDH-A3-CpG)-ND, and their individual components. C. DLS analyses of blank ND, (ALDH-A1-CpG)-ND, and (ALDH-A3-CpG)-ND. D. TEM images of (ALDH-A1 or A3)-ND.

2.4.2 ND-mediated delivery of ALDH peptides to APCs in lymph nodes

To study the lymphatic delivery of antigen *in vivo*, C57BL/6 mice were immunized s.c. at the tail base with ALDH-A1 peptide fluorescently tagged with TMR in a soluble form or ND form (**Figure 2-4.A**). Administration of soluble ALDH-A1-TMR peptide resulted in minimal TMR signal in inguinal dLNs after 24 h (**Figure 2-4.B-C**). This is consistent with the literature reporting limited lymphatic delivery of short soluble peptides after s.c. administration due to systemic dissemination of small-molecular-weight peptides and direct antigen binding to non-APCs at the injection site [30]. In contrast, administration of (ALDH-A1-TMR)-ND led to significantly higher TMR signal in inguinal dLNs, compared with soluble ALDH-A1-TMR group ($p < 0.0001$, **Figure 2-4.B-C**). Next, we examined antigen uptake by APCs in dLNs by flow cytometry analysis. Consistent with the above results, (ALDH-A1-TMR)-ND promoted cellular uptake of ND, significantly increasing the

mean fluorescence intensity (MFI) of TMR among CD11c$^+$ DCs (5.9-fold, $p < 0.01$), B220$^+$ B cells (7.9-fold, $p < 0.001$), and F4/80$^+$ macrophages (6.3-fold, $p < 0.001$), compared with soluble ALDH-A1-TMR group (**Figure 2-4.D-F**). Taken together, these results showed that ND efficiently delivered ALDH peptide to dLNs and promoted antigen uptake by APCs in dLNs, which are prerequisite for induction of T cell responses.

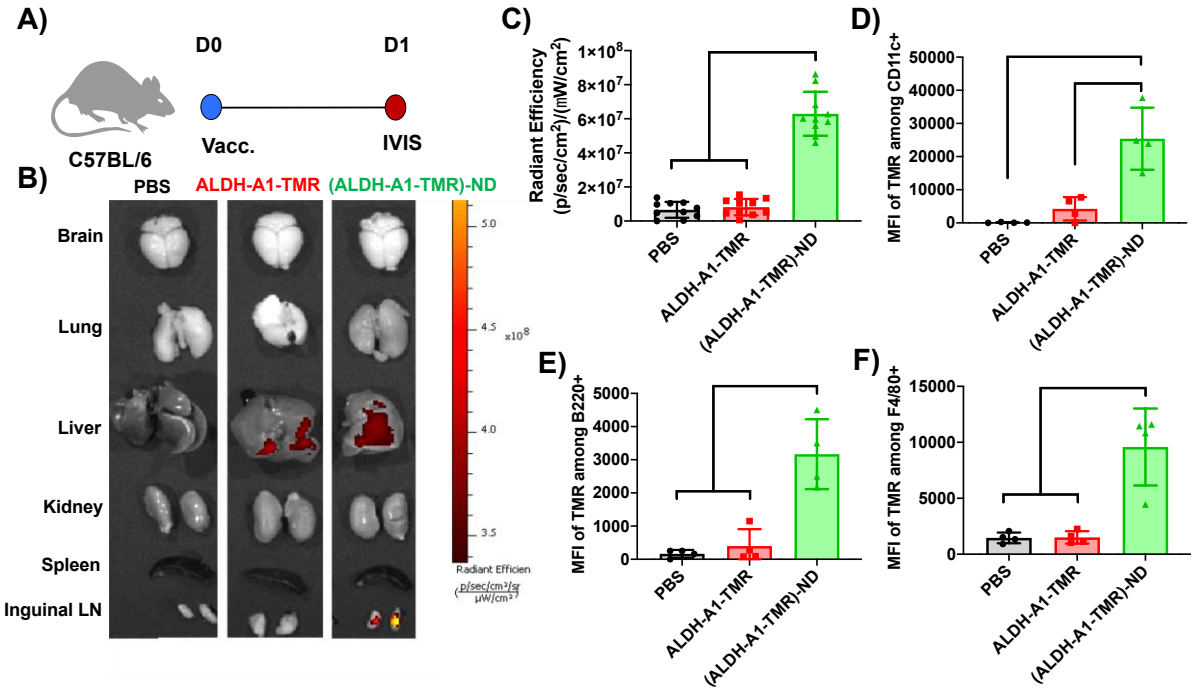

Figure 2-4. ND promotes the delivery of ALDH peptide to antigen-presenting cells in draining lymph nodes. A. C57BL/6 mice were administered s.c. with 15.5 nmol TMR-tagged ALDH-A1 peptides as a soluble or ND form. After 24 h, various organs were isolated, and TMR signal was quantified. B. Fluorescence image of major organs. C. Quantification of TMR signal in inguinal LNs. Data are represented as mean ± SEM (n = 10). D-F. Antigen uptake by APCs in dLNs was quantified by flow cytometry analysis. Shown are MFI TMR signal among D. CD11c+ DCs, E. B220+ B cells, and F. F4/80+ macrophages in inguinal dLNs at 24 h after s.c. administration of (ALDH-A1-TMR)-ND or ALDH-A1-TMR. The data show mean ± SEM from a representative experiment (n = 4) from 2 independent experiments.

2.4.3 Therapeutic efficacy of ND vaccination against D5 melanoma

Having shown that ND increases antigen delivery to LNs, we next investigated their efficacy as a therapeutic vaccine in a murine model of D5 melanoma, which is known to harbor $ALDH^{high}$ CSCs [31]. C57BL/6 mice were inoculated at s.c. flank with 5×10^4 D5 melanoma cells. On day 1, mice were immunized s.c. at tail base with ALDH-A1, ALDH-A3, and CpG either as a soluble mixture or (ALDH-A1/A3-CpG)-ND formulations (**Figure 2-5.A**). (ALDH-A1/A3-CpG)-ND denotes a pooled mixture of ND carrying CpG and either ALDH-A1 or ALDH-A3 peptide, each loaded in separate ND. On day 8, a boost vaccination was administered, and mice were monitored for D5 tumor growth. To block the immunosuppressive PD-1/PD-L1 pathway, a subset of animals also received intraperitoneal (i.p.) administration of αPD-L1 IgG. Vaccination with soluble peptide mixture + CpG had no impact on D5 tumor growth or animal survival, compared with the PBS control group (**Figure 2-5.B-D**). In contrast, ND vaccination significantly slowed tumor growth ($p < 0.0001$, **Figure 2-5.B-C**) and extended animal survival ($p < 0.001$, **Figure 2-5.D**), compared with soluble peptide vaccination. We also observed strong synergy when ALDH-targeted vaccines were combined with αPD-L1 IgG therapy. The addition of αPD-L1 IgG therapy further amplified the anti-tumor efficacy of ND, leading to enhanced tumor growth control and extension of animal survival ($p < 0.001$, **Figure 2-5.B-D**). Moreover, αPD-L1 IgG therapy also improved soluble peptide vaccination, enhancing tumor growth inhibition and animal survival to a similar extent as ND vaccine alone group (**Figure 2-5.B-D**).

Next, we examined the impact of ND vaccination on ALDH-specific T cell responses. D5 tumor-bearing mice were treated as in **Figure 2-5.A**, and immunological

assays were performed on day 15. Soluble vaccine with or without αPD-L1 IgG failed to generate a detectable level of ALDH-specific $CD8^+$ T cell responses in peripheral blood. In contrast, mice treated with (ALDH-A1/A3-CpG)-ND plus αPD-L1 IgG elicited robust ALDH-specific $CD8^+$ T cell responses with 62-fold ($p < 0.0001$) and 44-fold ($p < 0.05$) higher frequency of ALDH-A1-tetramer+ and ALDH-A3-tetramer+ $CD8^+$ T cells, compared with soluble vaccine plus αPD-L1 IgG (**Figure 2-6.A-C**). ND vaccination combined with αPD-L1 therapy also induced robust IFN-γ^+ CD8+ and CD4+ T cell responses, as evidenced by intracellular cytokine staining of PBMCs re-stimulated with ALDH-A1/A3 peptides (**Figure 2-6.D-E**). To further delineate the magnitude of T cell responses against ALDH-A1 and ALDH-A3, we performed IFN-γ ELISPOT assay using splenocytes re-stimulated with individual epitopes. Compared with soluble vaccine plus αPD-L1 IgG, ND vaccination plus αPD-L1 IgG generated 3.9-fold, 4.2-fold, and 7.5-fold higher IFN-γ^+ T cell responses against ALDH-A1, ALDH-A3, and the mixture of two peptides, respectively ($p < 0.0001$, **Figure 2-6.F**). Residual tumor tissues excised on day 23 revealed that ND vaccination significantly reduced the frequency of $ALDH^{high}$ D5 CSCs, compared with PBS control or soluble peptide vaccination ($p < 0.05$, **Figure 2-6.G**). ND vaccine plus αPD-L1 IgG group had a similar level of $ALDH^{high}$ D5 CSCs, as in the ND vaccine alone group (**Figure 2-6.G**). We also tested whether ND treatment generated T cells capable of killing target CSCs *in vitro*. We isolated T cells from splenocytes on day 23 and incubated with $ALDH^{high}$ CSCs, followed by lactate dehydrogenase assay to measure cell killing. Splenocytes isolated from mice vaccination with ND produced T cells with significantly enhanced *in vitro* killing potential against the target $ALDH^{high}$ D5 CSCs, compared with free peptide vaccination with or without αPD-

L1 IgG (p < 0.0001, **Figure 2-6.H**). Notably, we observed slightly reduced the *in vitro* killing potential for T cells obtained from ND vaccine plus αPD-L1 IgG group, potentially due to differences from the physiological *in vivo* condition. Taken together, these results have demonstrated that ND vaccination generated robust ALDH-specific T cell responses capable of killing ALDH^{high} D5 CSCs and that ND vaccination synergizes with αPD-L1 IgG therapy to exert potent anti-tumor efficacy.

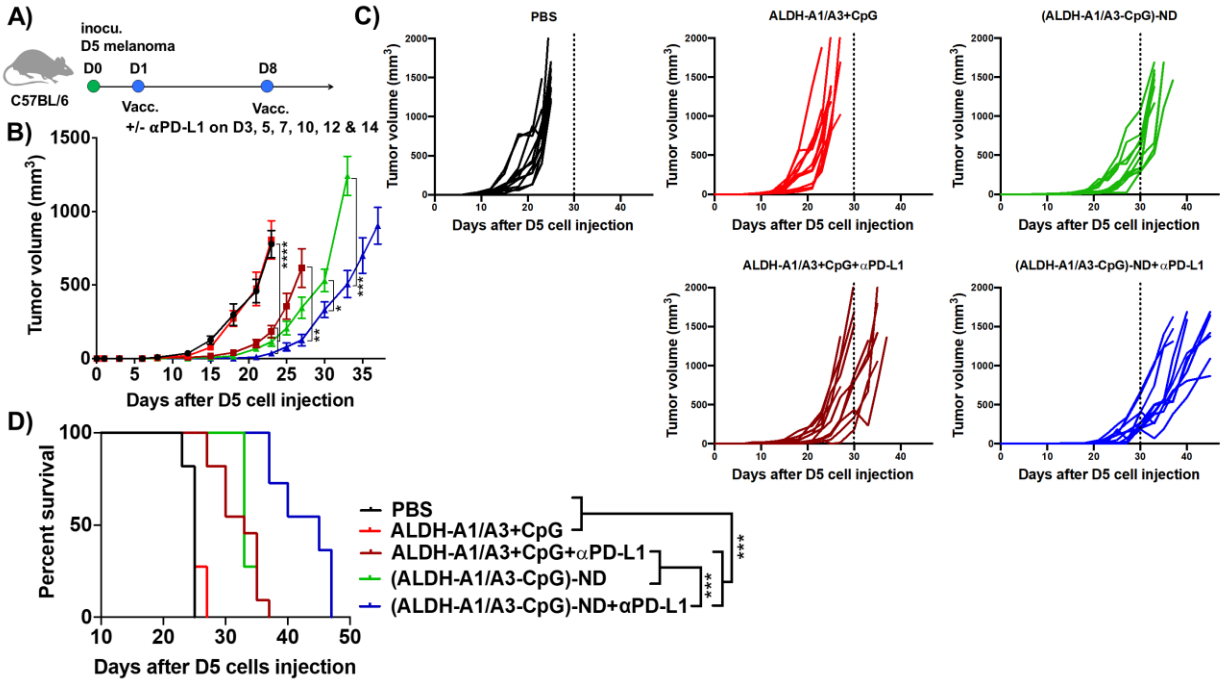

Figure 2-5. Therapeutic efficacy of ALDH-ND vaccination in D5 melanoma model. A. C57BL/6 mice were inoculated at s.c. flank with 5 × 10^4 D5 tumor cells and immunized with (ALDH-A1/A3-CpG)-ND or a soluble mixture of ALDH-A1/A3 and CpG (15.5 nmol/dose each Ag peptide and 15 μg/dose CpG) on days 1 and 8. A subset of mice also received i.p. administration of αPDL-1 (100 μg per dose) on the indicated days. Shown are the B. average tumor growth, C. individual tumor growth, and D. the overall animal survival. The data show mean ± SEM from a representative experiment (n = 11) from 2 independent experiments.

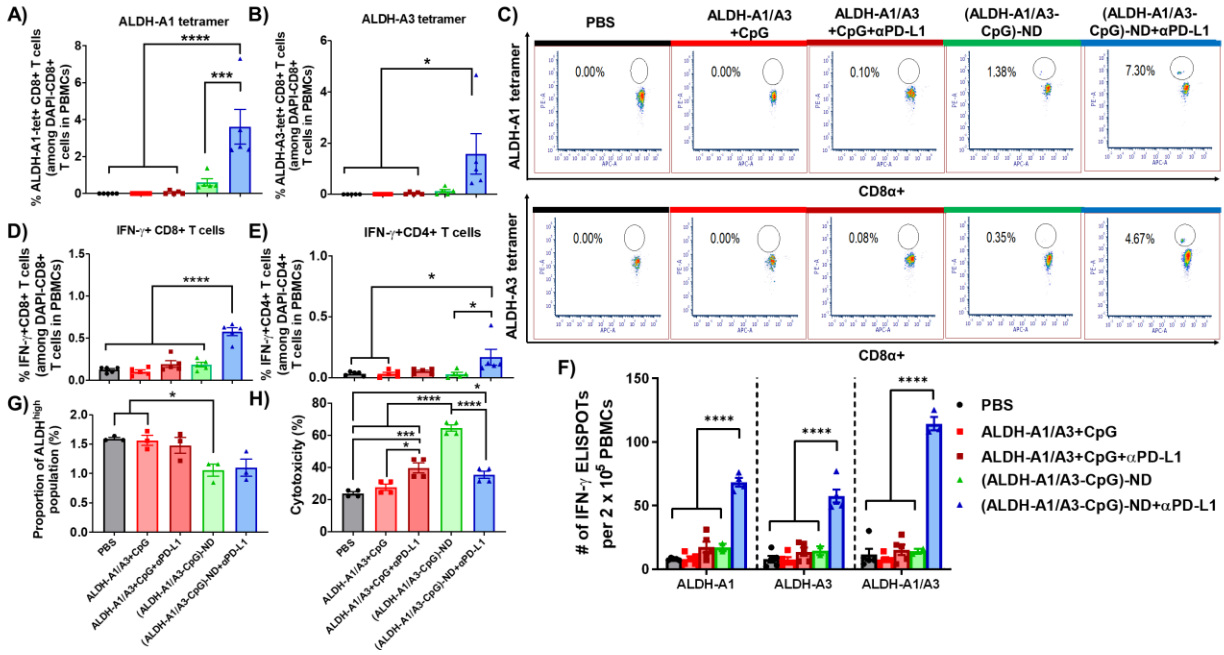

Figure 2-6. ALDH-ND vaccination elicits potent T cell responses against ALDHhigh CSCs. Mice bearing D5 tumors were treated as in Figure 4A, and the frequency of A. ALDH-A1-specific and B. ALDH-A3-specific CD8+ T cells were quantified among PBMCs obtained on day 15. C. Shown are the representative scatter plots of ALDH-A1 and ALDH-A3 tetramer+ CD8+ T cells. D-F. The frequencies of D. IFN-γ+ CD8+ T cells and E. IFN-γ+ CD4+ T cells were quantified by intracellular staining. F. IFN-γ ELISPOT was performed using splenocytes obtained on day 15, followed by ex vivo re-stimulation with the indicated peptides. G. The frequencies of ALDHhigh CSCs were quantified within the residual tumor masses on day 23. H. Cytotoxic potential of T cells isolated from spleens was evaluated by incubating effector cells with the target ALDHhigh D5 cells in 10:1 ratio for 3 days, followed by LDH assay. The data show mean ± SEM from a representative experiment (n = 4) from 2 independent experiments.

Moreover, mice immunized with (ALDH-A1/A3-CpG)-ND or soluble ALDH-A1/A3+CpG did not exhibit any signs of toxicity. Mice had normal numbers of hematopoietic stem cells (HSC, Lin-c-Kit+Sca-1+) and long-term HSCs (LT-HSC, Lin-c-Kit+Sca-1+CD34-) in bone marrow as well as normal animal bodyweight, blood chemistry, and complete blood cell counts (**Figure 2-6.A and B and Table 2-1. and 2-2.**). Taken together, these results show that ND vaccination generates robust ALDH-specific T cell responses in a safe and

effective manner, exerts potent anti-tumor efficacy, and synergizes in combination with anti-PD-L1 IgG.

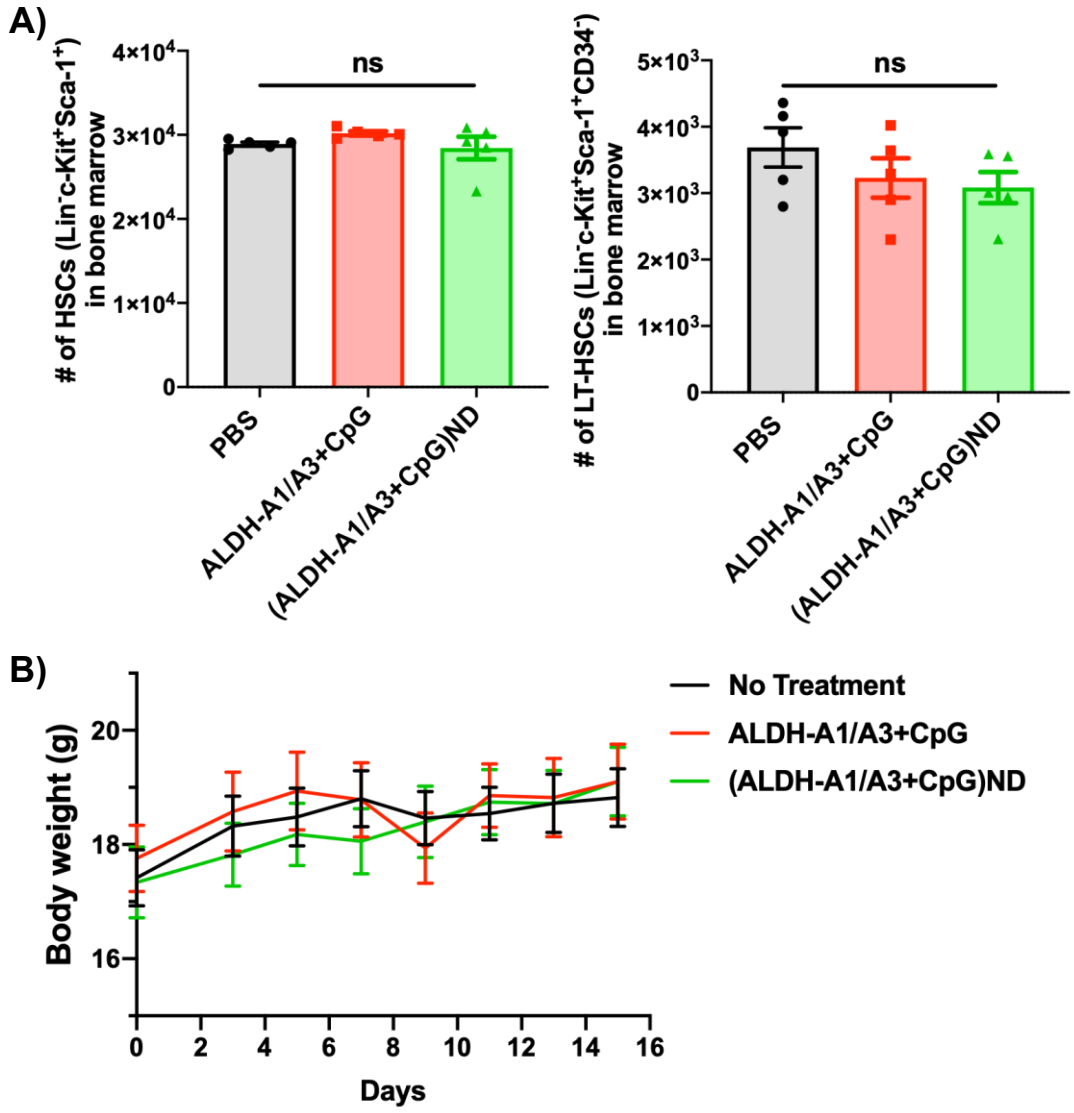

Figure 2-7. Impact of ALDH vaccines on hematopoietic stem cells and animal body weight. C57BL/6 mice were immunized with (ALDH-A1/A3-CpG)-ND or a soluble mixture of ALDH-A1/A3 and CpG (15.5 nmol/dose each Ag peptide and 15 µg/dose CpG) on days 0 and 7. Shown are the A. numbers of hematopoietic stem cells (HSC, Lin-c-Kit+Sca-1+) and long-term HSCs (LT-HSC, Lin-c-Kit+Sca-1+CD34-) in bone marrow on day 15 and B. changes in animal body weight over time. The data show mean ± SEM. Statistical significance was calculated by A) one-way ANOVA, or B) two-

away ANOVA, followed by the Tukey's multiple comparisons post-test. ns = not statistically significant.

Table 2-1. C57BL/6 mice were immunized as in Figure 2-6. Shown are the complete blood counts.

	No Treatment	ALDH-A1/A3+CpG	(ALDH-A1/A3+CpG)ND	Normal Range
White blood cells (WBC, K/uL)	7.608 ± 1.940	10.624 ± 1.102	6.872 ± 1.249	1.8 - 10.7
Neutrophils (NE, K/uL)	0.922 ± 0.266	1.068 ± 0.222	1.306 ± 0.285	0.1 - 2.4
Lymphocytes (LY, K/uL)	6.528 ± 1.755	5.674 ± 1.023	9.092 ± 1.013	0.9 - 9.3
Monocytes (MO, K/uL)	0.14 ± 0.04	0.12 ± 0.06	0.22 ± 0.11	0 - 0.4
Eosinophil (EO, K/uL)	0.012 ± 0.008	0.008 ± 0.013	0.006 ± 0.005	0 - 0.2
Basophil (BA, K/uL)	0.004 ± 0.008944	0 ± 0	0 ± 0	0 - 0.2
Neutrophils (NE, %)	12.1 ± 1.8	15.6 ± 2.3	12.3 ± 2.6	6.6 - 38.9
Lymphocytes (LY, %)	85.578 ± 2.115	82.588 ± 1.954	85.536 ± 1.875	55.8 -91.6
Monocytes (MO, %)	1.986 ± 0.926	1.708 ± 0.723	2.084 ± 1.084	1.10 - 7.5
Eosinophil (EO, %)	0.2 ± 0.1	0.12 ± 0.14	0.05 ± 0.03	0.0 -3.9
Basophil (BA, %)	0.082 ± 0.103	0.018 ±0.026	0.028 ± 0.019	0.0 -2.0
Red blood cells (RBC, M/uL)	9.40 ± 0.53	8.13 ± 3.41	9.08 ± 0.41	6.36 – 9.42
Hemoglobin (HB, g/dL)	13.4 ± 0.8	11.5 ± 4.7	13.3 ± 0.4	11.0 – 15.1
Hematocrit (HCT, %)	40.86 ± 2.49	42.42 ± 1.48	40.16 ± 1.15	35.1 – 45.4
Mean Corpuscular Volume (MCV, fL)	43.44 ± 0.43	43.34 ± 0.38	44.24 ± 1.35	45.4 – 60.3
Mean corpuscular hemoglobin (MCH, Pg)	14.24 ± 0.20	14.16 ± 0.33	14.66 ± 0.50	14.1 -19.3
Mean corpuscular hemoglobin concentration (MCHC, g/dL)	32.82 ± 0.47	32.68 ± 0.94	33.14 ± 0.69	30.2 -34.2
Red cell distribution (RDW, %)	15.88 ± 0.53	17.72 ± 0.40	18.84 ± 1.66	12.4 – 27.0
Platelets (PLT, K/uL)	714.4 ± 69.0	923.8 ± 53.5	716.4 ± 130.0	592 – 2972
Mean platelet volume (MPV, fL)	4.5 ± 0.1	4.4 ± 0.0	4.8 ± 0.1	5.0 – 20

Table 2-2.C57BL/6 mice were immunized as in Figure 2-6. Shown are the blood chemistry.

	No Treatment	ALDH-A1/A3+CpG	(ALDH-A1/A3+CpG) ND	Normal Range
Creatinine (CREA, mg/dl)	0.35 ± 0.01	0.39 ± 0.08	0.36 ± 0.03	0.09 - 0.4
Glucose (GLUC, mg/dl)	247.6 ± 34.9	298.6 ± 33.7	241.2 ± 30.0	79.35 - 354.73
Albumin (ALB, g/dl)	3.36 ± 0.09	2.98 ± 0.16	3.34 ± 0.11	2.72 - 4.2
TRPO, g/dl	5.0 ± 0.2	5.6 ± 0.2	5.5 ± 0.2	4.63 - 7.2
Calcium arsenazo (CALA, mg/dl)	9.8 ± 0.2	8.9 ± 0.4	9.8 ± 0.6	9.03 - 12.4
Alanine transaminase (ALT, U/L)	47.4 ± 7	71.4 ±37.1	47.4 ± 6.4	24.30 - 115.25
Total bilirubin (TBIL, mg/dl)	0.255 ± 0.104	0.282 ± 0.091	0.244 ± 0.106	0.12- 0.58
Blood urea nitrogen (BUN, mg/dl)	31.6 ± 5.7	39.2 ± 4.7	32.4 ± 4.4	5.15 - 30.70
Alkaline phosphatase (ALP, U/L)	190.0 ± 20.0	158.6 ± 13.2	164.4 ± 15.7	65.50 - 364.20

2.4.4 Therapeutic efficacy of ND vaccination against 4T1 mammary carcinoma

Next, we sought to confirm our results in a second tumor model. 4T1 cell line is a highly invasive and widely used model of mammary carcinoma. Balb/c mice were inoculated with 10^4 4T1 cells at mammary fat pad, and the animals were immunized on days 1 and 8 at s.c. tail base with ALDH-A1, ALDH-A3, and CpG either as a soluble mixture or (ALDH-A1/A3-CpG)-ND formulations (**Figure 2-8.A**). Compared with the PBS control group, soluble peptide mixture + CpG with or without αPD-L1 IgG therapy had no impact on 4T1 tumor growth or animal survival (**Figure 2-8.B-D**). In stark contrast, ND vaccination alone significantly slowed 4T1 tumor growth and extended animal survival, compared with soluble peptide vaccination ($p < 0.0001$, **Figure 2-8.B-D**). Importantly, αPD-L1 IgG further augmented the anti-tumor efficacy of ND vaccination, resulting in inhibition of tumor growth ($p < 0.0001$, **Figure 2-8.B-C**) and extension of animal survival ($p < 0.05$, **Figure 2-8.D**). We also evaluated whether ND vaccination reduced residual $ALDH^{high}$ CSCs in the 4T1 model. Compared with the PBS control group, ND vaccination combined with αPD-L1 IgG therapy significantly decreased the frequency of $ALDH^{high}$ 4T1 CSCs ($p < 0.05$, **Figure 2-8.E**). Overall, these data indicated that (ALDH-A1/A3-CpG)-ND vaccination combined with αPD-L1 therapy decreased residual 4T1 CSCs and effectively inhibited 4T1 tumor growth.

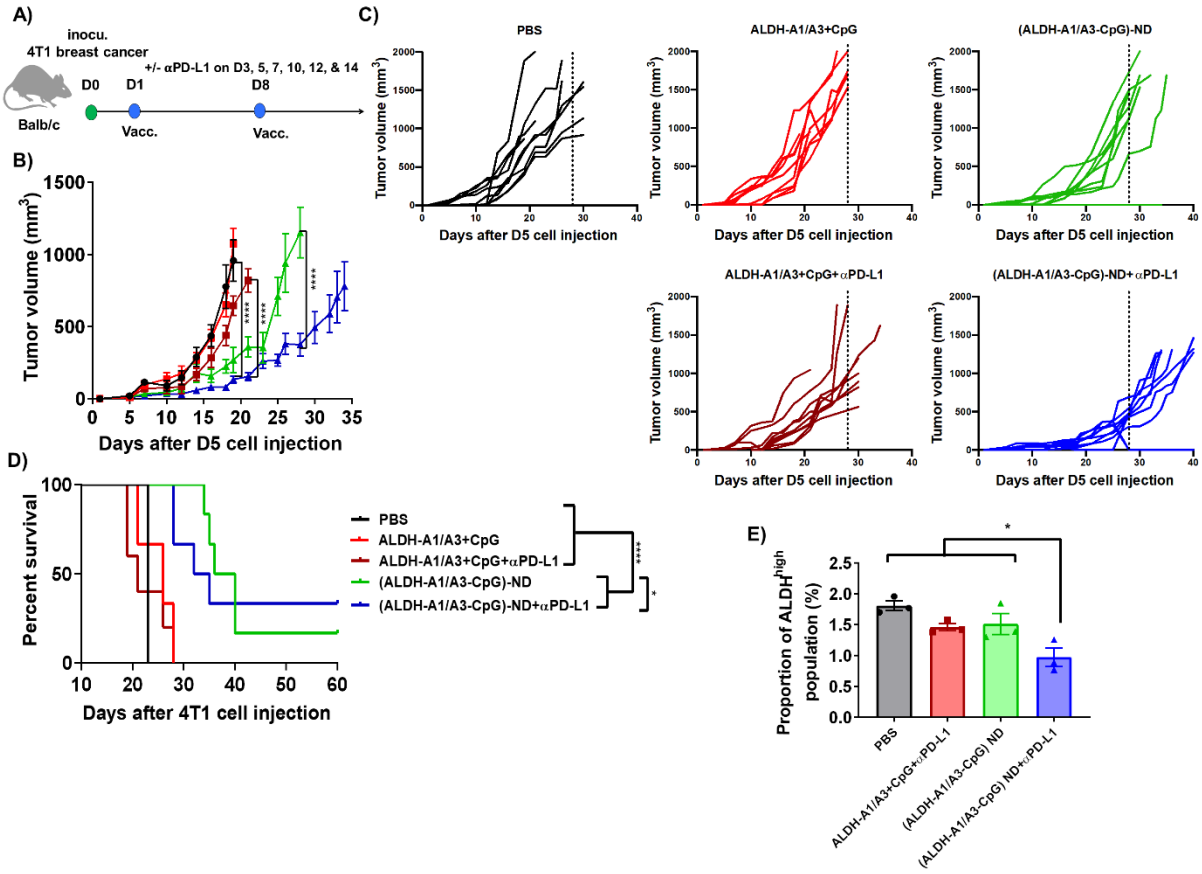

Figure 2-8. Therapeutic efficacy of ALDH-ND vaccination in 4T1 breast cancer model. A. Balb/c mice were inoculated at mammary fat pad with 10^4 4T1 tumor cells and immunized with (ALDH-A1/A3-CpG)-ND or a soluble mixture of ALDH-A1/A3 and CpG (15.5 nmol/dose each Ag peptide and 15 µg/dose CpG) on days 1 and 8. A subset of mice also received i.p. administration of αPDL-1 (100 µg per dose) on the indicated days. Shown are the B. average tumor growth, C. individual tumor growth, and D. the overall animal survival. E. The frequency of ALDHhigh CSCs was quantified within residual 4T1 tumor masses on day 30, and F. the representative flow cytometry scatter plots are shown. The data show mean ± SEM from a representative experiment (n = 9 for A-D and n = 3 for E) from 2 independent experiments.

2.5 Conclusions

In this study, we have developed ND for delivery of ALDH peptide antigens, ALDH-A1 and ALDH-A3, and have demonstrated their potency to elicit $CD8^+$ T cell responses

against CSCs. In particular, ND significantly enhanced the delivery of ALDH peptides to APCs in LNs, increasing antigen uptake among APCs, triggering robust induction of T cell responses against CSCs. ND vaccination combined with αPD-L1 IgG therapy exerted strong anti-tumor efficacy in D5 and 4T1 tumor models, leading to inhibition of tumor growth and extension of animal survival. We have also demonstrated that ND vaccination led to the induction of CD8 T cells capable of killing $ALDH^{high}$ CSCs *in vitro* and reducing their frequency *in vivo*. Overall, these data show the promise of ND vaccination against CSCs. We believe that the ND vaccine technology with an established manufacturing process and clinical safety[25] may serve as a potent vaccine platform for combination cancer immunotherapy.

2.6 References

[1] A. Filipova, M. Seifrtova, J. Mokry, J. Dvorak, M. Rezacova, S. Filip, D. Diaz-Garcia, Breast cancer and cancer stem cells: a mini-review, Tumori Journal 100(4) (2014) 363-369.

[2] K.M. Sales, M.C. Winslet, A.M. Seifalian, Stem cells and cancer: an overview, Stem cell reviews 3(4) (2007) 249-255.

[3] D.R. Pattabiraman, R.A. Weinberg, Tackling the cancer stem cells—what challenges do they pose?, Nature reviews Drug discovery 13(7) (2014) 497-512.

[4] Y. Hu, L. Lu, Y. Xia, X. Chen, A.E. Chang, R.E. Hollingsworth, E. Hurt, J. Owen, J.S. Moyer, M.E. Prince, Therapeutic efficacy of cancer stem cell vaccines in the adjuvant setting, Cancer research 76(16) (2016) 4661-4672.

[5] E. Batlle, H. Clevers, Cancer stem cells revisited, Nature medicine 23(10) (2017) 1124.

[6] P. van der Bruggen, C. Traversari, P. Chomez, C. Lurquin, E. De Plaen, B. Van den Eynde, A. Knuth, T. Boon, A gene encoding an antigen recognized by cytolytic T lymphocytes on a human melanoma, Science 254(5038) (1991) 1643-1647.

[7] S.L. Topalian, F.S. Hodi, J.R. Brahmer, S.N. Gettinger, D.C. Smith, D.F. McDermott, J.D. Powderly, R.D. Carvajal, J.A. Sosman, M.B. Atkins, P.D. Leming, D.R. Spigel, S.J. Antonia, L. Horn, C.G. Drake, D.M. Pardoll, L. Chen, W.H. Sharfman, R.A. Anders, J.M. Taube, T.L. McMiller, H. Xu, A.J. Korman, M. Jure-Kunkel, S. Agrawal, D. McDonald, G.D. Kollia, A. Gupta, J.M. Wigginton, M. Sznol, Safety, activity, and immune correlates of anti-PD-1 antibody in cancer, N Engl J Med 366(26) (2012) 2443-54.

[8] C. Robert, J. Schachter, G.V. Long, A. Arance, J.J. Grob, L. Mortier, A. Daud, M.S. Carlino, C. McNeil, M. Lotem, J. Larkin, P. Lorigan, B. Neyns, C.U. Blank, O. Hamid, C. Mateus, R. Shapira-Frommer, M. Kosh, H. Zhou, N. Ibrahim, S. Ebbinghaus, A. Ribas, K.-. investigators, Pembrolizumab versus ipilimumab in advanced melanoma, N Engl J Med 372(26) (2015) 2521-32.

[9] T. Schatton, M.H. Frank, Antitumor immunity and cancer stem cells, Ann N Y Acad Sci 1176 (2009) 154-69.

[10] Y. Miao, H. Yang, J. Levorse, S. Yuan, L. Polak, M. Sribour, B. Singh, M.D. Rosenblum, E. Fuchs, Adaptive Immune Resistance Emerges from Tumor-Initiating Stem Cells, Cell 177(5) (2019) 1172-1186 e14.

[11] W. Su, H.H. Han, Y. Wang, B. Zhang, B. Zhou, Y. Cheng, A. Rumandla, S. Gurrapu, G. Chakraborty, J. Su, G. Yang, X. Liang, G. Wang, N. Rosen, H.I. Scher, O. Ouerfelli, F.G. Giancotti, The Polycomb Repressor Complex 1 Drives Double-Negative Prostate

Cancer Metastasis by Coordinating Stemness and Immune Suppression, Cancer Cell (2019).

[12] B. Sahu, A. Maeda, Retinol dehydrogenases regulate vitamin a metabolism for visual function, Nutrients 8(11) (2016) 746.

[13] N.A. Sophos, V. Vasiliou, Aldehyde dehydrogenase gene superfamily: the 2002 update, Chemico-biological interactions 143 (2003) 5-22.

[14] J.P. Chute, G.G. Muramoto, J. Whitesides, M. Colvin, R. Safi, N.J. Chao, D.P. McDonnell, Inhibition of aldehyde dehydrogenase and retinoid signaling induces the expansion of human hematopoietic stem cells, Proceedings of the National Academy of Sciences 103(31) (2006) 11707-11712.

[15] C. Ginestier, M.H. Hur, E. Charafe-Jauffret, F. Monville, J. Dutcher, M. Brown, J. Jacquemier, P. Viens, C.G. Kleer, S. Liu, ALDH1 is a marker of normal and malignant human mammary stem cells and a predictor of poor clinical outcome, Cell stem cell 1(5) (2007) 555-567.

[16] Y. Luo, K. Dallaglio, Y. Chen, W.A. Robinson, S.E. Robinson, M.D. McCarter, J. Wang, R. Gonzalez, D.C. Thompson, D.A. Norris, ALDH1A isozymes are markers of human melanoma stem cells and potential therapeutic targets, Stem cells 30(10) (2012) 2100-2113.

[17] D.J. Pearce, D. Taussig, C. Simpson, K. Allen, A.Z. Rohatiner, T.A. Lister, D. Bonnet, Characterization of cells with a high aldehyde dehydrogenase activity from cord blood and acute myeloid leukemia samples, Stem cells 23(6) (2005) 752-760.

[18] W. Matsui, C.A. Huff, Q. Wang, M.T. Malehorn, J. Barber, Y. Tanhehco, B.D. Smith, C.I. Civin, R.J. Jones, Characterization of clonogenic multiple myeloma cells, Blood 103(6) (2004) 2332-2336.

[19] N. Ning, Q. Pan, F. Zheng, S. Teitz-Tennenbaum, M. Egenti, J. Yet, M. Li, C. Ginestier, M.S. Wicha, J.S. Moyer, M.E. Prince, Y. Xu, X.L. Zhang, S. Huang, A.E. Chang, Q. Li, Cancer stem cell vaccination confers significant antitumor immunity, Cancer Res 72(7) (2012) 1853-64.

[20] Y. Hu, L. Lu, Y. Xia, X. Chen, A.E. Chang, R.E. Hollingsworth, E. Hurt, J. Owen, J.S. Moyer, M.E. Prince, F. Dai, Y. Bao, Y. Wang, J. Whitfield, J.C. Xia, S. Huang, M.S. Wicha, Q. Li, Therapeutic Efficacy of Cancer Stem Cell Vaccines in the Adjuvant Setting, Cancer Res 76(16) (2016) 4661-72.

[21] L. Lu, H. Tao, A.E. Chang, Y. Hu, G. Shu, Q. Chen, M. Egenti, J. Owen, J.S. Moyer, M.E. Prince, S. Huang, M.S. Wicha, J.C. Xia, Q. Li, Cancer stem cell vaccine inhibits metastases of primary tumors and induces humoral immune responses against cancer stem cells, Oncoimmunology 4(3) (2015) e990767.

[22] J.C. Yang, Melanoma vaccines, Cancer journal 17(5) (2011) 277-82.

[23] O. Klein, C. Schmidt, A. Knights, I.D. Davis, W. Chen, J. Cebon, Melanoma vaccines: developments over the past 10 years, Expert review of vaccines 10(6) (2011) 853-73.

[24] R. Kuai, X. Sun, W. Yuan, L.J. Ochyl, Y. Xu, A.H. Najafabadi, L. Scheetz, M.-Z. Yu, I. Balwani, A. Schwendeman, Dual TLR agonist nanodiscs as a strong adjuvant system for vaccines and immunotherapy, Journal of Controlled Release 282 (2018) 131-139.

[25] R. Kuai, D. Li, Y.E. Chen, J.J. Moon, A. Schwendeman, High-density lipoproteins: nature's multifunctional nanoparticles, ACS nano 10(3) (2016) 3015-3041.

[26] C. Ginestier, M.H. Hur, E. Charafe-Jauffret, F. Monville, J. Dutcher, M. Brown, J. Jacquemier, P. Viens, C.G. Kleer, S. Liu, A. Schott, D. Hayes, D. Birnbaum, M.S. Wicha, G. Dontu, ALDH1 Is a Marker of Normal and Malignant Human Mammary Stem Cells and a Predictor of Poor Clinical Outcome, Cell Stem Cell 1(5) (2007) 555-567.

[27] R. Kuai, L.J. Ochyl, K.S. Bahjat, A. Schwendeman, J.J. Moon, Designer vaccine nanodiscs for personalized cancer immunotherapy, Nature materials 16(4) (2017) 489-496.

[28] L.J. Ochyl, J.D. Bazzill, C. Park, Y. Xu, R. Kuai, J.J. Moon, PEGylated tumor cell membrane vesicles as a new vaccine platform for cancer immunotherapy, Biomaterials 182 (2018) 157-166.

[29] Q. Li, S. Teitz-Tennenbaum, E.J. Donald, M. Li, A.E. Chang, In vivo sensitized and in vitro activated B cells mediate tumor regression in cancer adoptive immunotherapy, The Journal of Immunology 183(5) (2009) 3195-3203.

[30] C.J. Melief, S.H. Van Der Burg, Immunotherapy of established (pre) malignant disease by synthetic long peptide vaccines, Nature Reviews Cancer 8(5) (2008) 351-360.

[31] L. Lu, H. Tao, A.E. Chang, Y. Hu, G. Shu, Q. Chen, M. Egenti, J. Owen, J.S. Moyer, M.E. Prince, Cancer stem cell vaccine inhibits metastases of primary tumors and induces humoral immune responses against cancer stem cells, Oncoimmunology 4(3) (2015) e990767.

Chapter 3 Optimization of the sHDL Nanodisc-Adjuvant System for Cancer Immunotherapy

3.1 Abstract

Cancer immunotherapy is a novel, attractive approach for cancer treatment with fewer side effects. Also, cancer immunotherapy based on vaccinations shows promising results, but it suffers from the poor immunogenicity. This lack of efficacy can be attributed to the inefficient delivery of antigens to immune activation sites and poorly immunogenic antigens. Hence, adjuvants are needed to induce cross-presentation and elicit strong cytotoxic T lymphocyte (CTL) responses. With profound advances in nanotechnology and biomaterial in recent years, researchers have examined nanoparticles to co-deliver antigen and adjuvant to antigen-presenting cells (APCs) to improve immunogenic responses for cancer vaccination. However, the delivery of the adjuvant to APCs is still a challenge for the field of cancer vaccination.

Previously, we have reported a new synthetic high-density lipoprotein (sHDL) vaccine for co-delivery of antigen peptides and adjuvant. Despite the success of our previous formulation, effective delivery of adjuvants to lymph needs to be optimized to achieve potent immune responses against cancer. Here, we have evaluated various adjuvants for immune activation with sHDL vaccination. For this, we studied two classes of CpG (type B and type C) and modified them with cholesterol lipid tail to enhance their lymphatic delivery and trigger strong immune activation. We have also examined polyICLC, a TLR3 agonist, as a potential adjuvant to improve sHDL vaccines.

Overall, our results show that polyICLC admixed with sHDL (sHDL+polyICLC) forms a powerful adjuvant system for cancer vaccination. sHDL+polyICLC significantly enhanced the activation of dendritic cells, compared with other comparison groups. Importantly, mice immunized with the mixtures of sHDL+polyICLC generated strong anti-tumor immune responses, with strong anti-tumor efficacy in the MC-38 colon cancer model. Furthermore, we investigate the immunogenicity of nanodiscs incorporated with CpG or admixed with polyICLC in non-human primates (NHPs). Vaccination performed in NHPs have shown that sHDL+polyICLC is a potent T-cell vaccine. Overall, these studies have shown that sHDL-Ag+polyICLC immunotherapy can exert strong anti-tumor efficacy and can be used as a potent T-cell vaccine.

3.2 Introduction

Colorectal cancer (CRC) is the third common cause of cancer-related deaths globally. In 2012, around 1.4 million new cases and 700,000 deaths related to CRC were reported, and it is estimated that the number of CRC cases will be increased to 2.2 million with the approximately 1.1 million death by 2030 [1]. Current treatments against CRC improve the survival rates but are associated with side effects that affect the overall health and quality of patients' life [2]. Thus, it is necessary to develop a new, less toxic treatment option for CRC patients. Cancer immunotherapy is a novel, attractive approach for cancer treatment with fewer side effects. Cancer immunotherapy based on vaccinations is intended to elicit a potent CD8+ T cell response by using tumor-associated antigens but are typically not effective due to poor immunogenicity. This lack of efficacy can be attributed to the inefficient delivery of antigens to immune activation sites and poorly

immunogenic antigens, which need adjuvants to induce cross-presentation to elicit strong cytotoxic T lymphocyte (CTL) responses. Selecting an effective adjuvant to induce strong CTL responses is an essential factor for eliciting immune responses against cancer.

Adjuvants can be classified as lipid, protein, nucleic acid, mineral (aluminum salt/alum), and surfactant [3]. Currently, there are only a few adjuvants approved in the USA and Europe for human vaccine applications. Aluminum salts (alum) were approved in the mid-1920s and have been widely used as an adjuvant for producing strong T_h2 responses [4]. However, alum is known to generate weak T-cell responses. CpG oligonucleotides, a TLR9 agonist, has been tested in various therapeutic cancer vaccines, and in recent clinical trials, CpG has produced encouraging results when mixed with another adjuvant (Montanide) with an immunogenic peptide from melanoma-specific protein [5, 6]. CpG adjuvants have been studied in various cancer vaccine clinical trials, such as vaccines against melanoma, sarcoma, glioblastoma, and breast/lung/ovarian cancers [7]. Based on the structure and immunostimulatory activity, CpG can be classified into three classes. CpG-A ODNs are comprised of two poly-G tail regions with phosphorothioate backbones linked by a double-stranded – hairpin-like – region containing a palindromic CpG-motif with a phosphodiester backbone region. These ODNs are potent stimulators of IFN-α production from plasmacytoid dendritic cells (pDCs), but weak inducers of TLR-9 dependent pro-inflammatory cytokine production [8]. CpG-B ODNs are comprised of CpG dinucleotides arranged along a wholly phosphorothioated backbone. These ODNs are potent activators of B-cells, promoters of pDC and monocyte maturation, but weak stimulators of IFN-α production [9]. Finally, CpG-C is a hybrid of CpG-A and CpG-B ODNs [10], composed of a palindromic CpG-motif region and a wholly

phosphorothioated backbone. These ODNs are potent stimulators of IFN-α production from pDCs and activators of B-cells [11-14].

Another nucleic acid-based adjuvant is a synthetic double-stranded RNA analog, referred to as polyinosine-polycytidylic acid (polyIC). PolyIC, like viral double-stranded RNA, is capable of activating DC and macrophages via TLR-3 activation [15] and is currently in clinical trials [16]. PolyIC can increase IL-12 and type I interferon (IFN) secretion as well as activate cytosolic receptors such as retinoic acid-inducible gene-1(RIG-I)[17]. In addition, poly IC can be administered in complex with poly-L-lysine to increase its stability.

Despite the advances that have been made in the identification and development of adjuvants, their delivery to lymphoid tissues needs to be improved. Antigen-specific immune responses require the exposure of antigen-presenting cells (e.g., pDCs) to these adjuvants within lymph nodes, where priming of the adaptive immune response occurs. Efforts to increase targeting of these adjuvants to lymph nodes have included the development of lipid conjugation to adjuvant [18], encapsulation of adjuvant within nanoparticle carriers [19], and stabilization into stable nanoparticles (i.e., polyICLC, also known as Hiltonol [20]).

Previously, we have reported new sHDL vaccines for co-delivery of antigen and cholesterol CpG (CpG-B) [21, 22]. High-density lipoprotein (sHDL), known as good cholesterol, is a lipid-based nanoparticle involved in the transport and metabolism of cholesterol and triglyceride. The small size of sHDL (10 nm), high tolerability, prolonged blood circulation half-life, and unique ability to target different recipient cells make sHDL a promising nanocarrier for delivery of peptide and adjuvant to APCs. In addition, sHDL

is degraded in endosomal compartments of APCs, leading to strong antigen cross-presentation. These properties make Ag-CpG-B-sHDL a promising candidate for cancer vaccines [11]. However, it has been reported that the lipid modification and position of lipid on the CpG sequence can enhance the activities of CpG, reduce toxicity, and enhance immune responses [18]. Although our previous sHDL formulation based on CpG-type-B have shown promising anti-tumor efficacy [23], the adjuvant selection should be optimized to achieve robust anti-tumor T cell responses.

In this study, we have optimized the sHDL formulation in terms of the adjuvant selection. We evaluated the immune-stimulatory activities CpG ODNs and polyICLC. In addition, two classes of CpG (type B and type C) were modified with a cholesterol lipid tail to enhance the LN delivery and trigger a higher level of innate immune activation (Figure 3-1.).

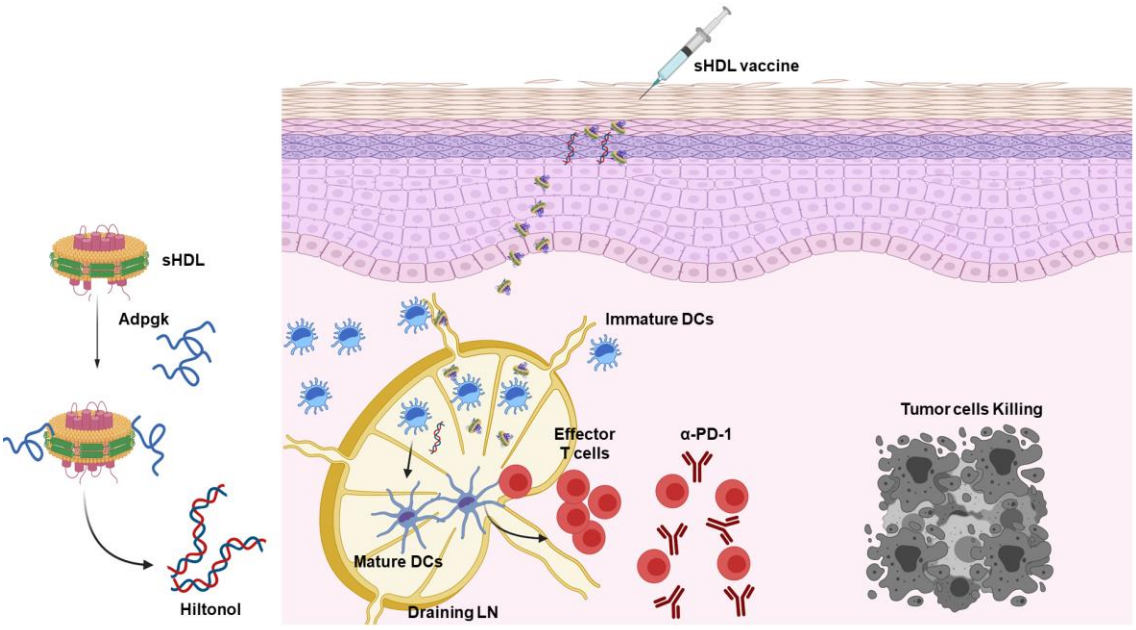

Figure 3-1. Depiction of nanodisc-based (sHDL) vaccine platform for cancer immunotherapy.

3.3 Experimental section

3.3.1 Materials and methods

Adpgk (CSSASMTNMELM) neoantigen or and CM-9 (CTPYDINQM) peptides were synthesized by RS Synthesis (Louisville, KY). Female C57BL/6 mice were purchased from Jackson Laboratories (Bar Harbor, ME). Antibody against mouse PD-1 was purchased from BioXCell (West Lebanon, NH). 1,2-dimyristoyl-sn-glycerol-3-phosphocholine (DMPC) was purchased from NOF America (White Plains, NY). 22A Apolipoprotein-A1 mimetic peptide was synthesized by GenScript (Piscataway, NJ). 1,2-dioleoyl-sn-glycero-3-phosphoethanolamine-N-[3-(2-pyridyldithio)propionate] (DOPE-PDP) was purchased from Avanti Polar Lipids (Alabaster, AL). Cholesterol-modified CpG1826/2395/7907 and unmodified CpG1826/2395 were synthesized by Integrated DNA Technologies (Coralville, IA). Hiltonol® (polyICLC) was kindly provided by Dr. Andres Salazar (Oncovir Inc., Washington DC, USA). Cell media was purchased from Invitrogen (Carlsbad, CA). The following antibodies for flow cytometry were purchased from BioLegend: anti-mouse CD8a-APC; CD11c, CD40, CD80 and CD86; anti-mouse CD11c-FITC.

3.3.2 Synthesis and characterization of Adpgk incorporated sHDL nanodiscs

Lipid-peptide was prepared as previously reported [24]. To incorporate Adpgk neoantigen peptides or CM-9 into sHDL nanodisc, peptides were modified with a cysteine at the N-terminus. This was reacted with DOPE-PDP (antigen peptide/DOPE-PDP = 2:1, molar

ratio) for 4 hr on an orbital shaker in dimethylformamide (Figure 3-1). The conjugation efficiency of the reaction was calculated based on the reduction in absorbance signal associated with DOPE-PDP as measured by HPLC/MS. sHDL was prepared as previously described [22, 24]. Briefly, sHDL was synthesized by dissolving 22A Apo-A1 peptide and DMPC in acetic acid, evaporating acetic acid by freeze dryer to form a desiccated lipid film, and rehydrating this film with 10 mM sodium phosphate buffer. Incorporation of prepared lipid-peptide complex into sHDL to make sHDL-Ag was achieved by dissolving lipid-peptide complexes in DMSO and titrating the mixture into the sHDL solution. The mixture was incubated for 1 hr at room temperature on an orbital shaker at 200 rpm to incorporate the lipid-peptide into the sHDL. Unincorporated lipid-peptide complexes were then separated by ultracentrifuge-driven filtration (MilliporeSigma™ Amicon™ Ultra Centrifugal Filter, 10KD). Reverse-phase HPLC/MS was used to measure the extent of lipid-peptide conjugation and incorporation. To load CpG into sHDL-Ag, aqueous solutions of cholesterol-modified (3'/ 5')-CpG ODNs 1826, 2395, or 7909 (Cho-CpG, Integrated DNA Technologies) were titrated into sHDL-Ag at a DMPC to CpG weight ratio of 50:1 and incubated at room temperature with gentle shaking on an orbital shaker for 1 hr. ODN loading was quantified by gel permeation chromatography (GPC) equipped with TSKgel G3000SWxl column (7.8 mm ID × 30 cm, Tosoh Bioscience LLC). The hydrodynamic sizes and zeta potentials of nanodisc samples were measured by dynamic light scattering (DLS, Zetasizer Nano ZSP). The morphology of sHDL-Ag-CpG-C nanodiscs was visualized by transmission electron microscopy after fixation via osmium tetroxide. All TEM images were obtained by a JEM 1200EX electron microscope (JEOL USA) equipped with an AMT XR-60 digital camera (Advanced

Microscopy Techniques). sHDL-Ag+polyICLC was prepared by mixing sHDL-Ag with polyICLC before immunization.

3.3.3 Stimulation of bone marrow-derived dendritic cells (BMDCs)

Bone marrow-derived dendritic cells (BMDCs) were generated as previously described [18]. Briefly, bone marrow was flushed from femur and tibia bones of 5 to 6 weeks old C57BL/6 mice. Isolated bone marrow cells were plated at 1×10^6 cells per dish in RPMI 1640 supplemented with 10% FBS, 55 μM β-mercaptoethanol, 5ng/ml of GM-CSF, and 100 U ml−1 penicillin. On days three and five, half of the culture media was replaced with fresh media. After eight days, BMDCs were harvested and plated at 1×10^6 cells per well in 12-well- plates. After 24 hrs, BMDCs incubated with 75 nM CpG (3'or 5'-Type B or C) or 60 μg of PolyICLC and 15.5 nmol antigen peptide (multiple formulations in complete media) for 24 hrs at 37 °C with 5% CO_2. Supernatants were then collected, and the levels of different inflammatory cytokines were measured by ELISA (Enzyme-linked immunosorbent assay). BMDCs were, in parallel, washed twice with FACS buffer (1% BSA in PBS), incubated with anti-CD16/32 at room temperature, and then stained on ice with fluorophore-labeled antibodies against CD11c, CD40, CD80, and CD86. Cells were then washed twice by FACS buffer, resuspended in 2 μg/mL DAPI solution, and analyzed by flow cytometry.

3.3.4 In vivo immunization with immunostimulatory compounds and cancer immunotherapy studies

Animals were cared for following all federal, state, and local guidelines. All procedures performed on animals were in accordance with and approved by the University Committee on Use and Care of Animals (UCUCA) at the University of Michigan, Ann Arbor. For preventive vaccine studies, C57BL/6 mice were immunized subcutaneously at the tail base on day 0 (boosted on days 14 and 28) with 15.5 nmol/dose of Adpgk peptide and 15 μg/dose of CpG or 60 μg of polyICLC in either soluble or sHDL forms. Seven days after each immunization, blood samples were collected and analyzed on a flow cytometer. For therapeutic studies in MC-38 tumor-bearing animals, C57BL/6 mice (6-8 weeks old, Jackson Laboratories) were inoculated subcutaneously with 1×10^6 MC-38 cells in the right flank on day 0. Tumor-bearing animals were then immunized subcutaneously at the tail base on day 6 or 10, and boost 7 days after each immunization with 15.5 nmol/dose of Adpgk peptide and 15 μg/dose of CpG/ 60 μg of PolyICLC in either soluble or sHDL form. In a subset of studies, anti-mouse αPD-1 antibody (100 μg per mouse) was administered intraperitoneally on days 1 and 4 after each vaccination. Tumor growth was observed every other day, and the tumor volume was reported using the following equation: tumor volume = length × $(\text{width})^2$ × 0.5. Animals were euthanized when the tumor mass reached 1.5 cm in any dimension or when animals became moribund with > 20% weight loss or ulceration.

Mamu-A1+ rhesus macaques (males and females, 3-8 years old) were obtained from either The Johns Hopkins University or Primgen. They were immunized on weeks 0, 4, 8, and 12 with the sHDL nanodisc samples. CM9 peptide was dosed at 400 μg per

injection. Adjuvants included 1 mg Hiltonol, 60 nmol Cholesterol-CpG-7909 (type B), or 60 nmol Cholesterol-CpG-2395 (type C) per injection dose. Nanodiscs were administered in 2000 µl total volume per animal by subcutaneous injection at four sites (500 µl injection volume per site): subcutaneous L and R behind the knee and subcutaneous L and R inner thigh. These injection sites were selected based on pilot studies in macaques where these sites were shown to provide efficient antigen draining to target lymph nodes and for promoting T-cell immune responses.

On week 24, all animals were boosted with 10^{10} virus particles of recombinant Ad5. SIVmac239-Gag vector by intramuscular vaccination at the left and right quadriceps (500 uL volume each, 1 mL total injection volume). Bronchoalveolar lavage fluid (BAL) was collected on weeks 1, 8, 16, 24, 26, and 28. PBMCs were collected on weeks 1, 6, 10, 14, 16, 24, 26, and 28. BAL and PBMC samples were analyzed by intracellular staining for IFN-γ, IL-2, and TNF-α after restimulation with CM9 peptides at NIAID (Laboratory of Dr. Bob Seder).

3.3.5 Immunological analyses

Blood samples were collected from the submandibular vein of mice. Red blood cells were lysed with Ammonium-Chloride-Potassium (ACK) lysis buffer. Tetramer staining assays were performed to quantify the percentage of tumor antigen-specific CD8a+ T-cells among PBMCs, as described previously [22]. PBMCs were isolated, washed with FACS buffer, and incubated with anti-CD16/32 blocking antibody. Cells were then incubated with tetramer for 1 hr on ice, then incubated with anti-mouse CD8a-APC for 20 min on

ice. Cells were then washed twice with FACS buffer, resuspended in DAPI solution (2 μg/ml), and analyzed by flow cytometry.

3.3.6 Statistical analysis

Sample sizes were selected according to pilot experiments and previous literature. Data were analyzed by one-way or two-way ANOVA, followed by Tukey's multiple comparisons posttest or log-rank (Mantel-Cox) test with Prism 8.0 (GraphPad Software). Statistical significance is indicated as *P < 0.05, **P < 0.01, ***P < 0.001 and ****P < 0.0001. All values are reported as means ± SEM.

3.4 Results and discussion

3.4.1 Synthesis and characterization of sHDL-adjuvant systems

Nanodiscs were generated by mixing 1,2-dimyristoyl-sn-glycerol-3-phosphocholine (DMPC) and 22A apolipoprotein-A1 mimetic peptide in acetic acid, followed by lyophilization to evaporate acetic acid, reconstitution in 10 mM phosphate buffers, and three cycles of heat and cool to form sHDL. Afterward, cysteine pre-modified antigen peptides were reacted with 1,2-dioleoyl-sn-glycero-3-phosphoethanolamine-N-[3-(2-pyridyldithio)propionate] (DOPE-PDP) in DMF (**Figure 3-2. A**). Next, the peptide-lipid conjugate was dissolved in DMSO and added dropwise to sHDL to make (Adpgk or CM-9) Ag-sHDL (**Figure 3-2. A**). Finally, we quantified the amount of peptides conjugated to the DOPE-PDP and incorporation into nanodiscs using HPLC/MS. **Figure 3-2. B** shows the HPLC results that indicate the successful conjugation of antigen peptide to DOPE lipid (> 90% efficiency), and > 90% incorporation efficiency of lipid-peptide into sHDL

(**Figure 3-2. B and C**). HPLC chromatograms show a reduction in DOPE-PDP peak size after mixing with cysteine-Antigen, which indicated the conjugation of the cysteine-modified peptide with DOPE. This reduction in size is followed by the appearance of a new peak at 69.5 min, which can be attributed to the lipid-peptide. Overall, the results show successful conjugation of DOPE lipid tail and peptide with the conjugation efficiency greater than 90%. Additionally, the HPLC and MS chromatograms indicate that more than 90% of added lipid-peptide were incorporated into the sHDL.

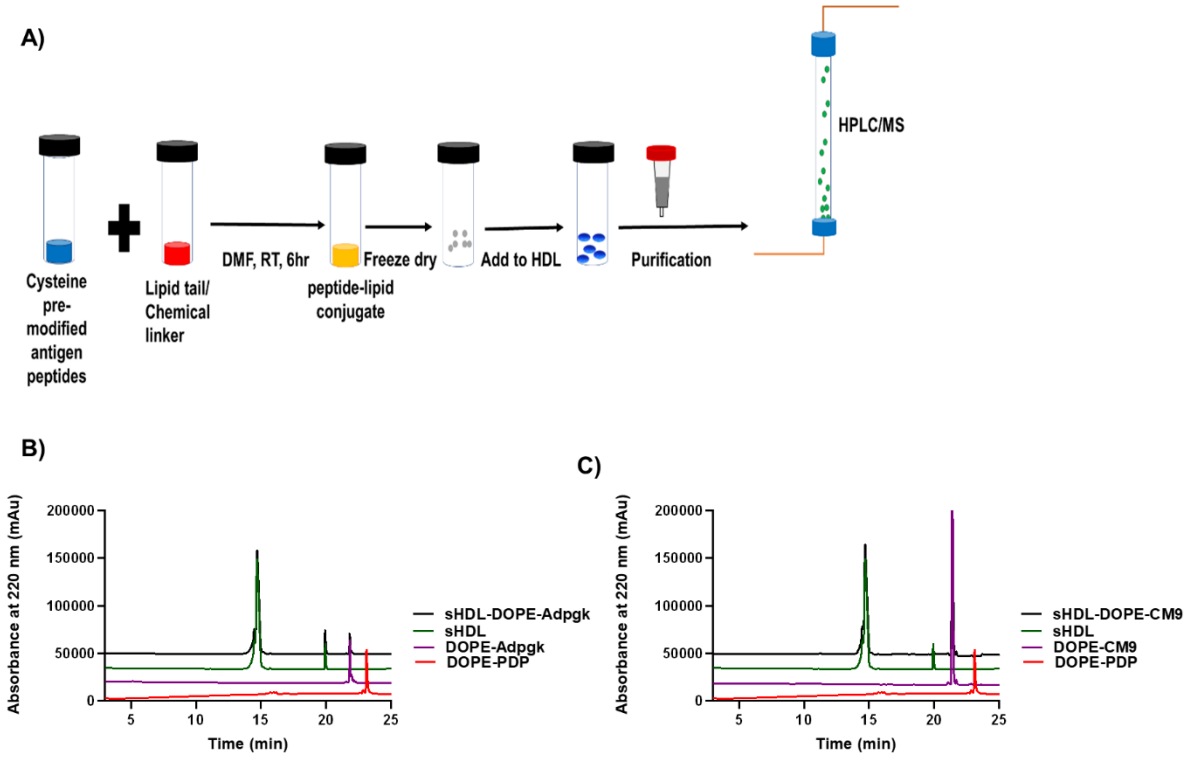

Figure 3-2. Synthesis and characterization of sHDL carrying Adpgk peptides. Shown are HPLC chromatograms of A. Schematic of sHDL synthesis, B. sHDL-Adpgk, C. sHDL-CM9, and their individual components. HPLC/MS chromatograms indicated successful conjugation of Adpgk and CM9 peptides to DOPE-PDP and the subsequent incorporation of lipid-peptides into sHDL.

sHDL-Adpgk- (3’ or 5’ -CpG B and C) were studied by dynamic light scattering (DLS) to reveal the hydrodynamic particle size and zeta potential. No significant variability was observed in the hydrodynamic radius as a function of CpG subtype – with all nanodiscs exhibiting radii ranging from 10-17 nm (**Figure 3-3. A and Table.3-1**). The TEM study of sHDL-Ag-CpG-C show that sHDL-Ag-CpG-C has uniform size and nanodisc-like morphology (10nm ± 3 average diameters. **Figure 3-3. B**), which was consistent with the DLS results. Subsequently, cholesterol-modified CpG1826/2395/7909 (cho-CpG) was incubated with sHDL-Adpgk by simple mixing at a DMPC:cho-CpG weight ratio of 50:1. GPC analysis shows that > 90% of cho-CpG was loaded into the sHDL-Adpgk resulting in nanodiscs co-loaded with peptide and CpG sHDL-Adpgk-CpG (**Figure 3-3. C and D**). Table.1 summarized the incorporation efficacy and hydrodynamic size of various sHDL-Adpgk formulations.

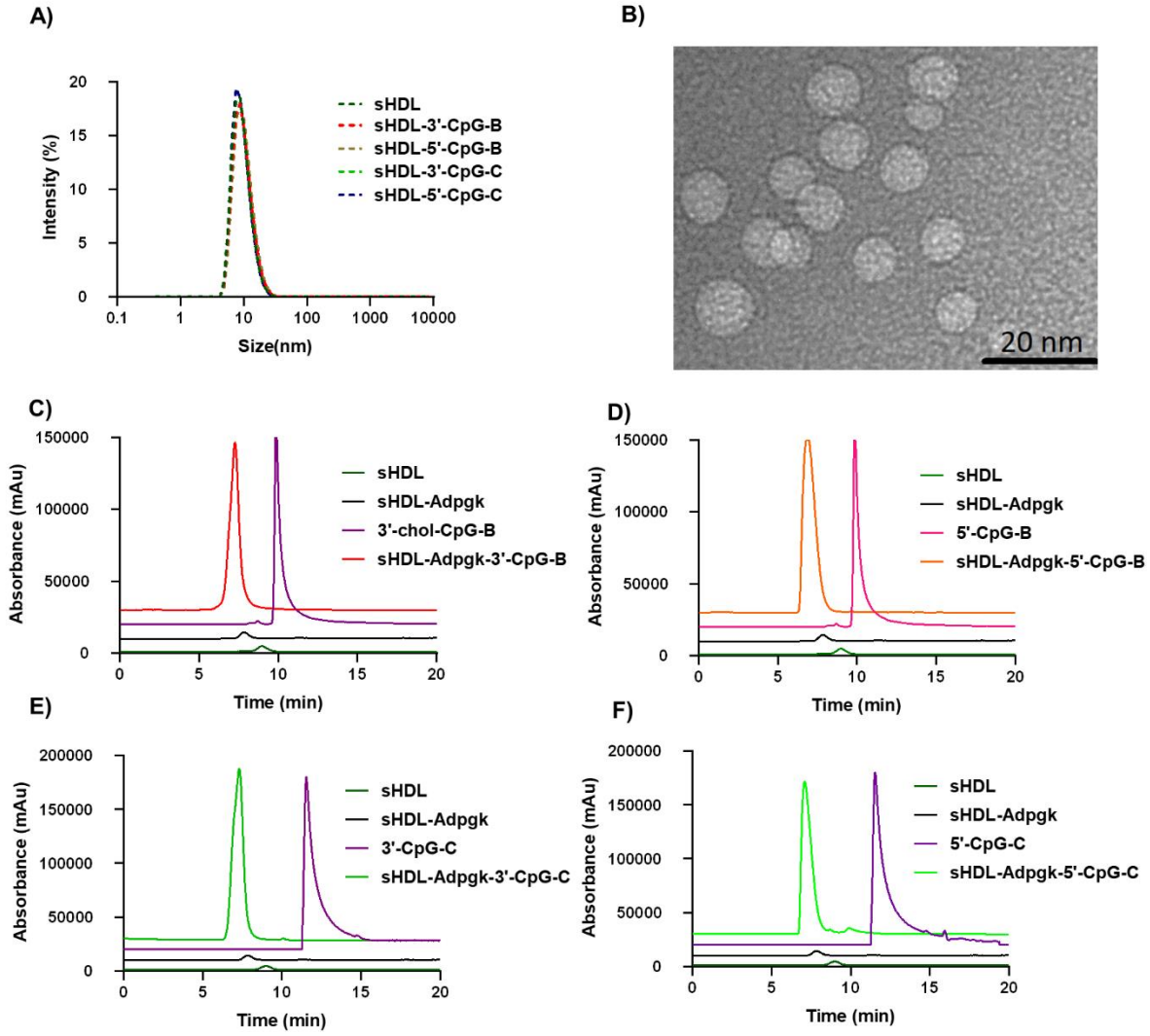

Figure 3-3.Characterization of HDL-DOPE-Adpgk/CpG. A. Dynamic light scattering analysis of HDL-Ag loaded with 3' and 5' CpG types B and C showed the uniform distribution of HDL-Adpgk-CpG, B.- transmission electron microscopy imaging indicated that the nanodisc like morphology of HDL-Adpgk-CpG. GPC showed the efficient incorporation of 3' and 5' chol-CpG type B and C in HDL-DOPE-Adpgk nanodiscs. C. 3'-chol-CpG-TypeB (1826). D. 5'-chol-CpG-TypeB (1826). E. 3'-chol-CpG-TypeC (2395). F. 5'-chol-CpG-TypeC (2395).

Table 3-1. Characterization of HDL-DOPE-Adpgk nanodiscs containing different types of CpG and cholesterol attached to3’ and 5’ of CpG.

	Incorporation of CpG to Ag-sHDL*	Hydrodynamic Size (nm)
Cholesterol-3’-CpG-C (2395)	90 ± 2%	10 ± 6
Cholesterol-5’-CpG-C (2395)	88 ± 4%	12 ± 3
Cholesterol-3’-CpG-B (1826)	90 ± 6%	10 ± 7
Cholesterol-5’-CpG-B (1826)	90 ± 7%	11 ± 7

3.4.2 Activation of dendritic cells (DCs)

Adjuvants play an essential role during immune activation. Our previous data have shown that sHDL can efficiently load CpG-B tethered with cholesterol tail at 3’ end of CpG [22]. Based on the sequences, structural characteristics, and activities, different types of CpG show different levels of T-cell activation. Here, we evaluated the incorporation efficiency and immunostimulatory activities of different CpG classes to achieve the highest efficacy of sHDL nanodiscs. On the other hand, because polyICLC is already a particular adjuvant with an average diameter of 100 nm, polyICLC was admixed with antigen-carrying sHDL. Using both CpG and polyICLC, we sought to identify an ideal adjuvant to use with nanodiscs (either admixed or co-delivered).

To examine immunostimulation of APCs by sHDL-mediated adjuvant, we incubated BMDCs *in vitro* with various adjuvant formulations and investigated the expression levels of costimulatory signals, including CD40, CD80, and CD86, and

secretion of cytokines, including IL-12p70, IL-6, and TNF-α, from BMDCs treated with sHDL-CpG-B/C and sHDL-polyICLC. Our results showed that BMDCs treated with sHDL + polyICLC, sHDL-3'-CpG-B, or sHDL-3'CpG-C significantly up-regulated the expression levels of CD40, CD80, and CD86 (**Figure 3-4. A-C**) and significantly increased secretion of IL-12p70, IL-6, and TNF-α (**Figure 3-4. D-F**), compared with BMDCs treated with free adjuvant controls, sHDL-5'-CpG-B, or sHDL-5'-CpG-C. sHDL + polyICLC was more potent activator of DCs than sHDL + polyIC (**Figure 3-4. A-F**). Overall, these results indicated that sHDL-mediated delivery of CpG increased its potency and that cholesterol tethered at 3' end of CpG was more potent than 5' end-modified CpG. In addition, polyICLC could be readily mixed with sHDL and achieve robust DC activation.

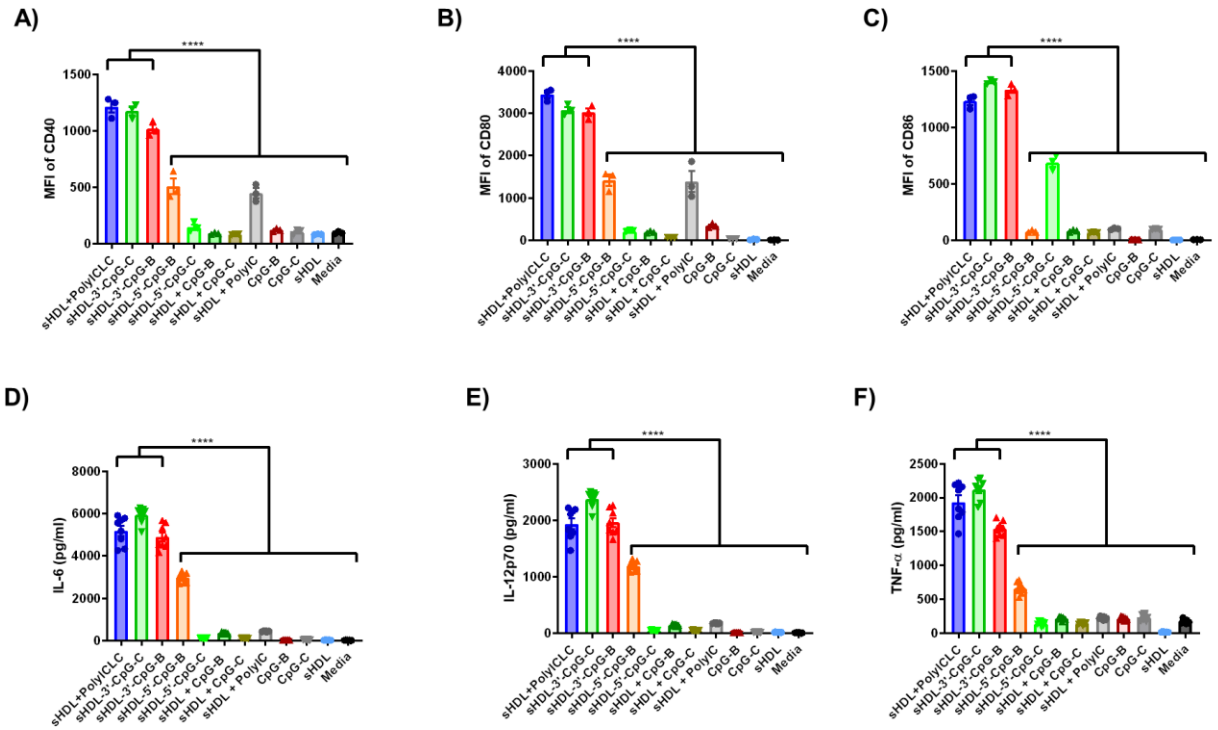

Figure 3-4. Stimulation of bone marrow-derived dendritic cells (BMDCs) with sHDL plus CpG or PolyICLC. BMDCs were incubated 24 hours with 23 nmol/ml CpG CpG, or 60 μg/ml PolyICLC formulations. The expression level of A. CD40, B. CD80, and C. CD86 were measured by flow cytometry. Inflammatory cytokines secreted by BMDCs,

including D- IL-6, E- IL-12p70 F- and TNF-α, were measured by ELISA (enzyme-linked immunosorbent assay). Data show the mean values ± SEM (n = 8).

3.4.3 sHDL vaccine nanodiscs elicit strong CTL responses in mice

We next studied CD8+ cytotoxic T-lymphocyte (CTL) responses generated by various sHDL-adjuvant formulations. Naïve C57BL/6 mice were immunized three times at 2-week intervals with 2.3 nmol CpG (multiple subtypes, tested individually) or 60 μg of polyICLC, with a fixed dose of 1.5 nmol Adpgk neoantigens. On day 7, after each vaccination, we collected blood from mice and quantified the frequency of Adpgk-specific CD8+ T-cells among peripheral blood mononuclear cells (PBMCs) using the tetramer staining assay. Vaccination with the sHDL loaded with 3'chol-CpG-C and sHDL admixed with polyICLC elicited the highest level of Adpgk-tetramer+ CD8+ T-cell responses at 5% and 7%, respectively (**Figure 3-5. A**). Interestingly, three immunizations with sHDL-CpG-C or sHDL+PolyICLC generated robust antigen-specific CD8+ T cell responses among PBMCs, achieving a 7-fold higher frequency of Adpgk-tetramer+ CD8+ T cells than the equivalent dose of soluble Adpgk+CpG-C or Adpgk+PolyICLC vaccine ($P < 0.05$, **Figure 3-5. B and C**). sHDL-CpG-C vaccination also enhanced antigen-specific CD8+ T cell responses, compared with sHDL-CPG-B (a 1.4-fold increase) (**Figure 3-5. B and C**).

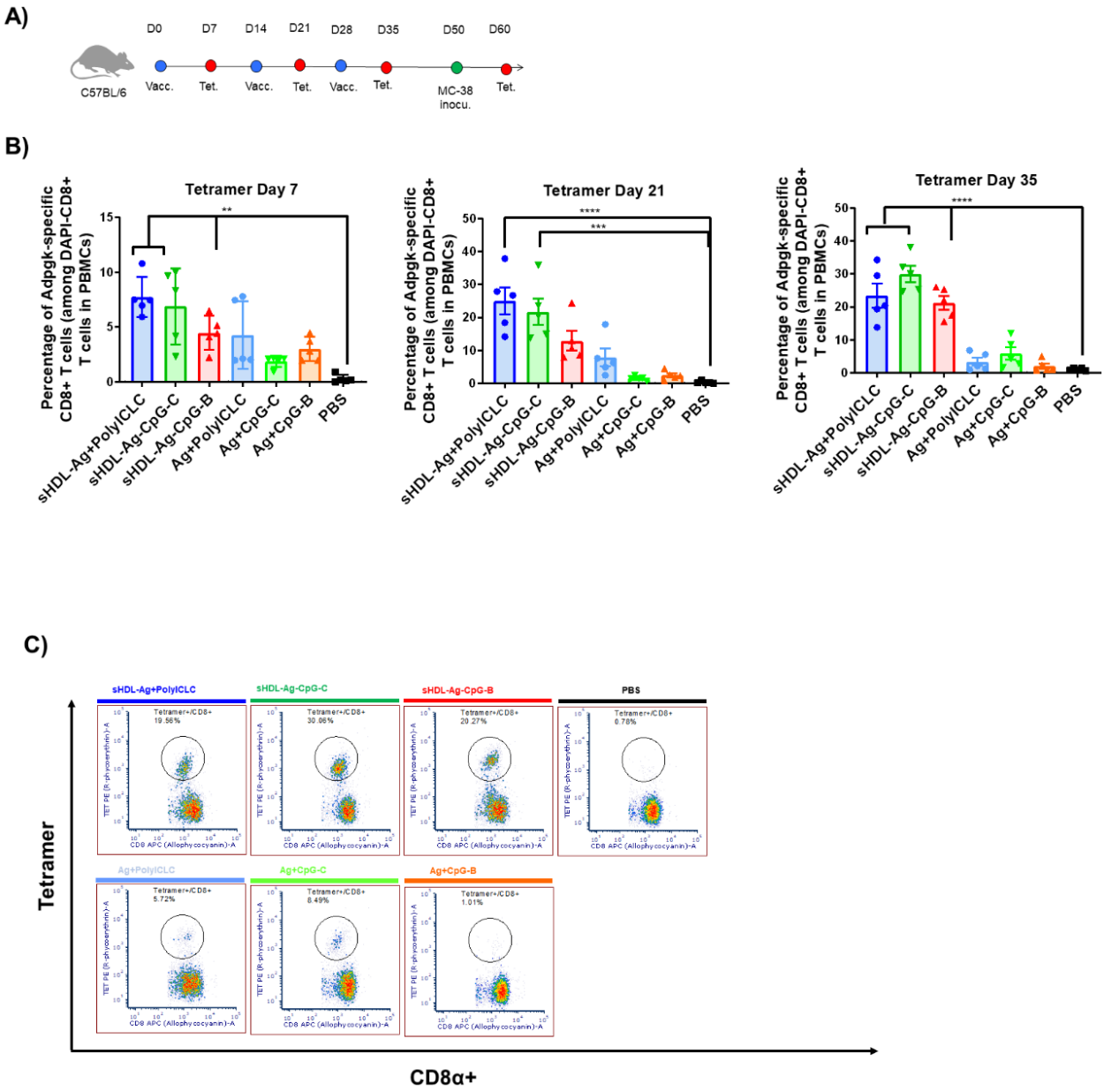

Figure 3-5. sHDL vaccine nanodiscs elicit strong CTL responses. A. C57BL/6 mice were immunized with nanodisc formulations (15.5 nmol Ag peptide, 2.3 nmol CpG, or 60 ug polyICLC) on days 0, 14, and 28. On days 7, 21, and 35, blood was collected from the mice, and the frequency of CD8α+ T-cells among PBMCs was measured. B. Shown is the percentages of Adpgk-specific CD8α+ T-cells among PBMCs one week after each vaccination. C. Shown are representative scatter plots for Adpgk-specific CD8α+ T-cells in peripheral blood at day 35. Data represent mean ± SEM, n=5.

3.4.4 sHDL vaccine nanodiscs exerts strong anti-tumor efficacy in mice

Having shown that sHDL-CpG-C and sHDL+ polyICLC induces potent cellular immune responses, we next examined their efficacy as a therapeutic vaccine in tumor-bearing animals (**Figure 3-6**). C57BL/6 mice were inoculated subcutaneously with $1x10^6$ MC-38 colon cancer cells in their flank. By day 6, tumors were established and exhibited an average volume of 70 mm^3. At this time, animals were immunized subcutaneously at the tail base with 15.5 nmol/dose of Adpgk neoantigen admixed with 2.3 nmol/dose CpG (various classes, tested individually) or 60 μg/dose of PolyICLC in either soluble or sHDL formulations (**Figure 3-6. A**). On days 13 and 20, booster vaccines were administered. Tetramer staining assays were performed to quantify the percentage of antigen-specific CD8+ T cells among PBMCs on days 11 and 18 (**Figure 3-6. B**). Compared with Adpgk admixed with free adjuvant, sHDL-CpG-C significantly enhanced antigen-specific CTL responses with ~8.9% and ~9.8% tetramer+ CD8+ T cells respectively, representing 1.3-fold, 2.11-fold, and 1.94-fold increases relative to sHDL-CpG-B ($P < 0.0001$), CpG-B ($P < 0.001$), and CpG-C ($P < 0.0001$), respectively (**Figure 3-6. B**). Importantly, sHDL+ PolyICLC generated 1.5-fold, 2.1-fold, and 2.1-fold higher antigen-specific CD8+ T cell responses relative to sHDL-CpG-B ($P < 0.001$), CpG-B ($p<0.001$), and CpG-C ($P < 0.05$), respectively (**Figure 3-6. B**). We also monitored tumor growth in these animals. sHDL delivery of CpG-C or polyICLC as an adjuvant improved the therapeutic efficacy of the vaccines (**Figure 3-6. C**). Vaccination with sHDL-CpG-C or sHDL+polyICLC exhibited stronger tumor suppression and extended animal survival, compared with CpG-B or CpG-C ($P < 0.0001$) or sHDL-CpG-B ($P < 0.05$, **Figure 3-6. D-E**).

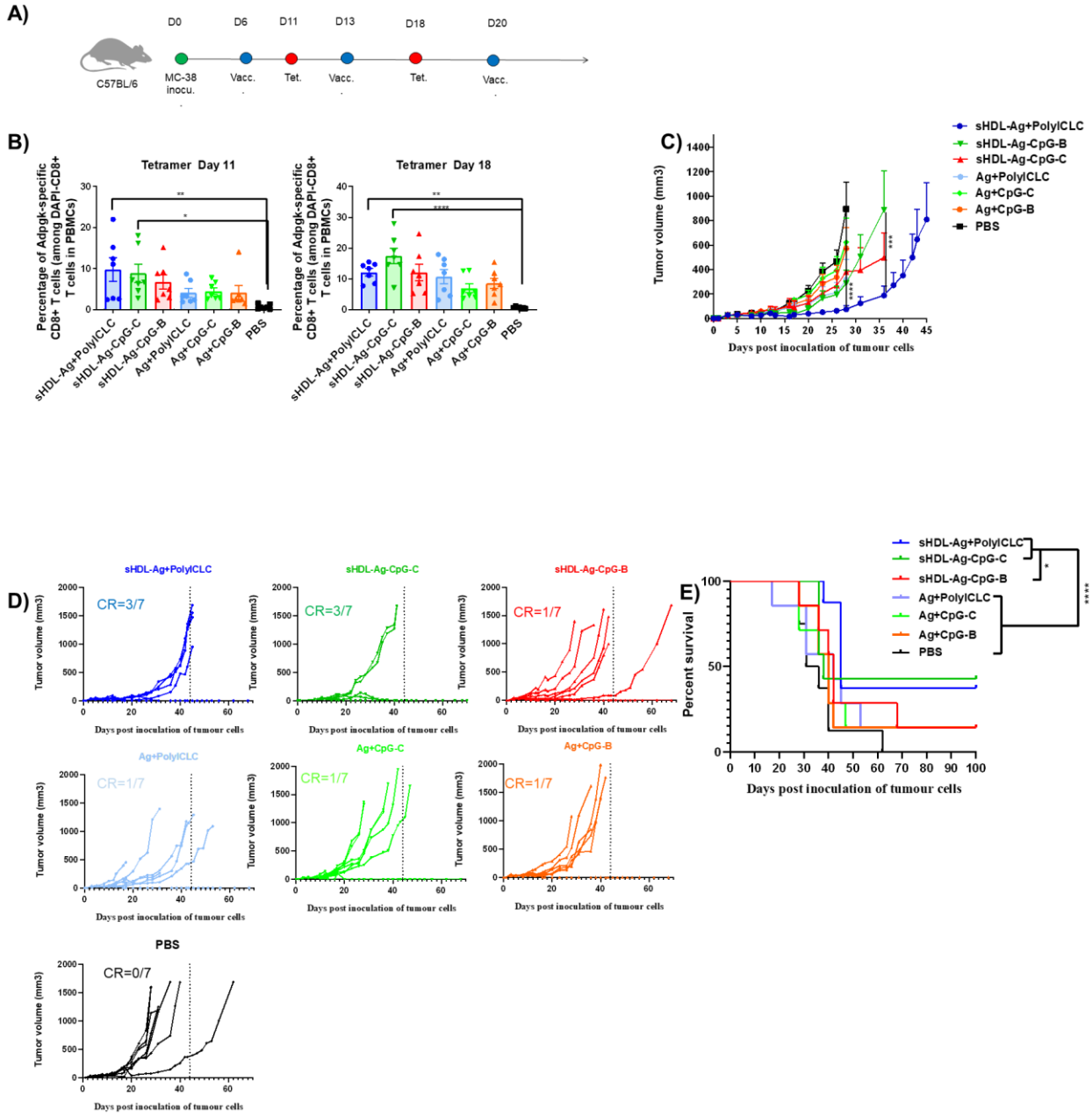

Figure 3-6. sHDL vaccine nanodiscs for vaccination against mutated tumor-specific neo-antigen. A. C57BL/6 mice were inoculated subcutaneously with 1.0 X106 MC-38 tumor cells and immunized with nanodisc formulations (15.5 nmol Ag peptide, 2.3 nmol CpG, or 60ug polyICLC) on day 6, 13, and 20. B. Shown is the percentage of Adpgk-specific CD8α+ T-cells among PBMCs one week after each vaccination. C. Average tumor growth. D. Individual tumor growth of MC-38 tumor masses, and E- animal survival. Data represent mean± SEM, n=7.

We next examined the efficacy of sHDL as a therapeutic vaccine combined with anti-PD-1 immunotherapy in tumor-bearing animals (**Figure 3-7. A**). C57BL/6 mice were inoculated subcutaneously with $1x10^6$ MC-38 colon cancer cells in their flank. By day 10, tumors were established and exhibited an average volume of 100 mm^3. At this time, animals were immunized subcutaneously at the tail base with 15.5 nmol/dose of Adpgk neoantigen admixed with 2.3 nmol/dose CpG (multiple classes, tested individually) or 60 μg/dose of polyICLC in either soluble or sHDL formulations (**Figure 3-7. A**). On day 17, a booster dose was given, and mice were monitored for tumor growth. Notably, compared with all other soluble or sHDL formulations, sHDL+polyICLC vaccination led to robust regression of established tumors. It exerted significantly enhanced anti-tumor efficacy, compared with soluble polyICLC or the CpG control ($P < 0.0001$, **Figure 3-7. B-D**). In contrast, treatments with sHDL-CpG-B or soluble CpG/polyICLC admixture did not show significantly enhanced anti-tumor efficacy (**Figure 3-7. B-D**). ELISPOT assay performed on splenocytes indicated that sHDL+PolyICLC+α-PD-1 therapy (as well as sHDL+CpG-C+α-PD-1) elicited potent IFN-γ+ T-cell responses against Adpgk peptide (**Figure 3-7. E-F**). Overall, these results indicated that sHDL admixed with PolyICLC elicited strong anti-tumor immune responses with potent therapeutic efficacy against established tumors.

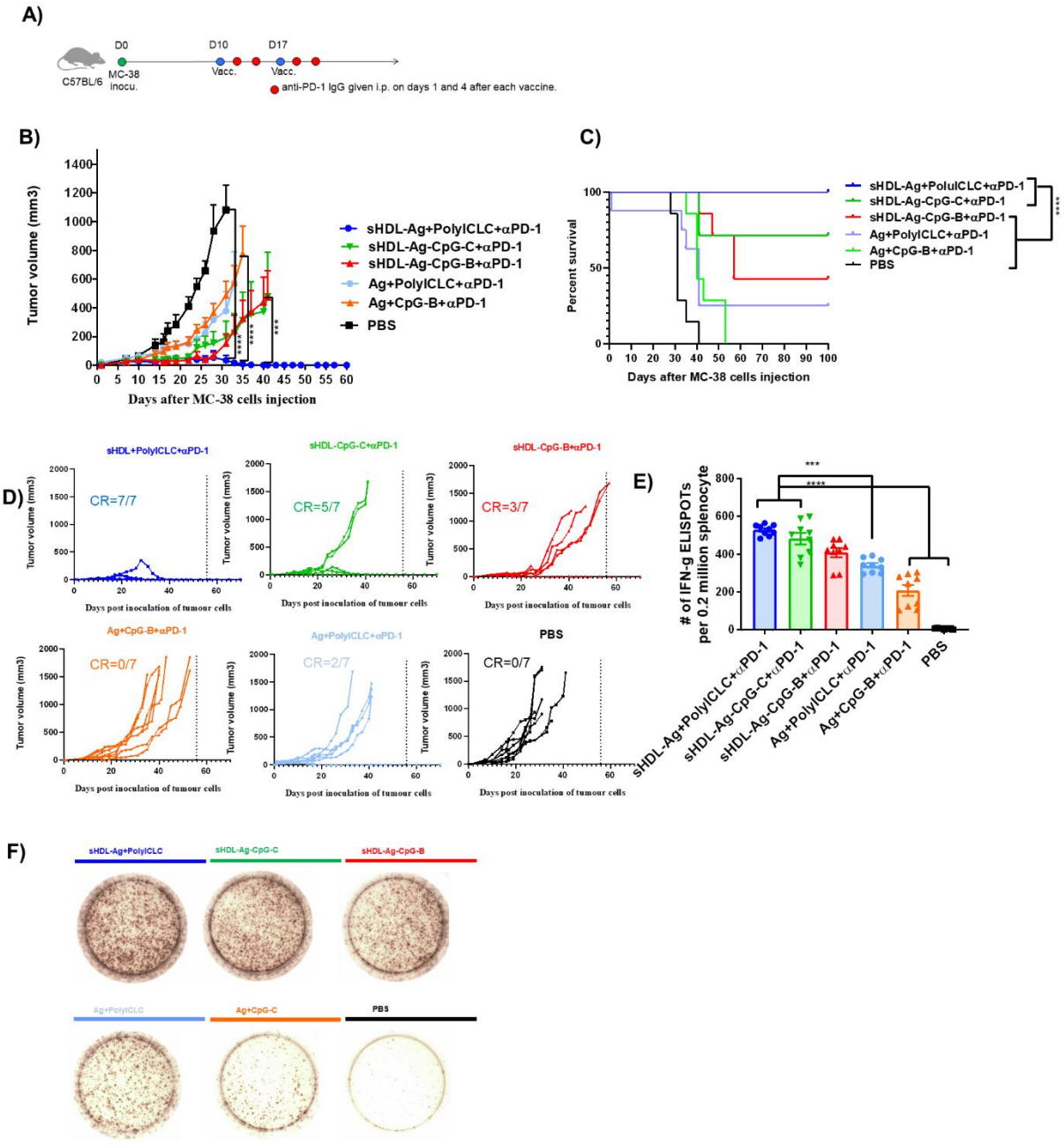

Figure 3-7. sHDL vaccine nanodiscs for vaccination against mutated tumor-specific neo-antigen. A. C57BL/6 mice were inoculated subcutaneously with 1x106 Mc-38 tumor cells and immunized with nanodiscs formulations (15.5 nmol Ag peptide, 2.3 nmol CpG, or 60 ug polyIC) on days 10 and 17. In addition, αPD-1 (100μg per dose) was administered on day 1 and 4 after each vaccination. B. Average tumor growth. C. Animal survival. D. Individual tumor growth of MC-38 tumor masses. Data represent mean ± SEM, n = 7. E and F. IFN-γ ELISPOT (enzyme-linked immunospot) assay were

performed by ex vivo restimulation of splenocytes with Adpgk peptides (10 µg/mL) on day 35.

3.4.5 sHDL vaccine nanodiscs elicit robust T cell responses in NHPs

We examined immunogenicity of sHDL formulated with polyICLC vs. CpG-type B vs. CpG-type C in rhesus macaques. CM9-nanodiscs admixed with polyICLC produced robust antigen-specific, polyfunctional T-cell responses in BAL tissues (Figure 3-8). CM9-nanodiscs co-loaded with either cholesterol CpG type B or type C generated detectable but weaker T-cell responses (Figure 3-8). After rAd boost was administered, we observed even stronger expansion of CM9-specific CD8+ T cells for the sHDL + polyICLC group. Taken together, these results suggest that sHDL + polyICLC is a potent vaccine system for induction of antigen-specific CD8 T-cell responses in NHPs.

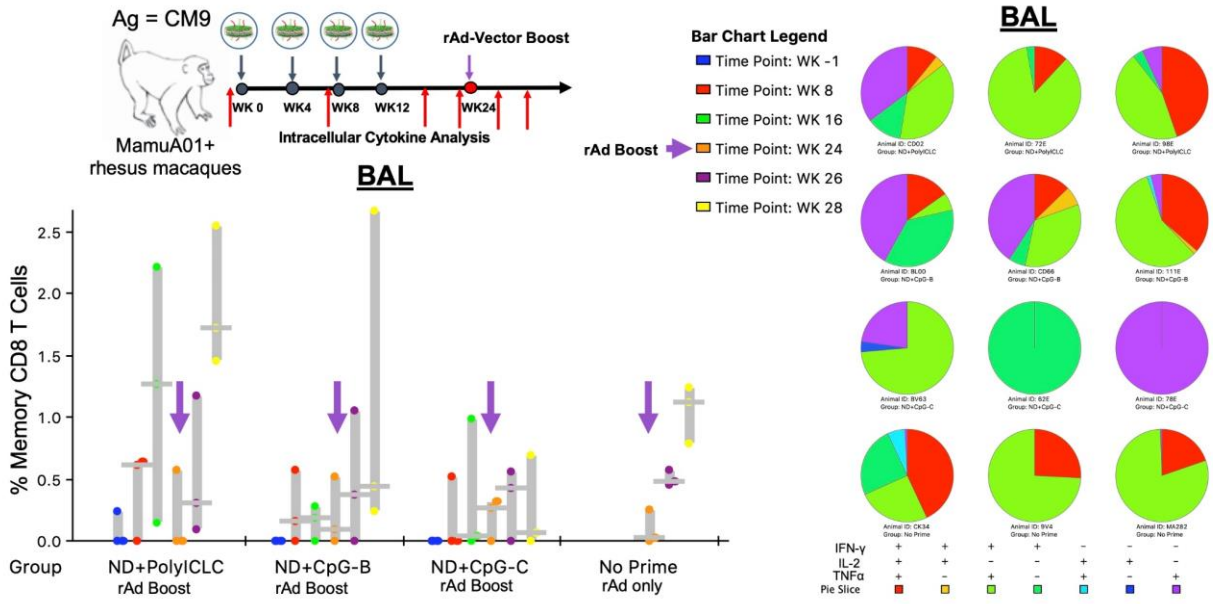

Figure 3-8. MamuA01+ rhesus macaques were immunized with sHDL formulated with polyICLC vs. CpG-type B vs. CpG-type C, followed by rAd-Gag vector boost vaccination. CM9-specific T-cell responses were analyzed by intracellular cytokine staining in BAL tissues.

3.5 Conclusions

Here we have examined immunogenicity of sHDL formulated with two different adjuvants, namely CpG ODNs (a TLR9 agonist) and polyICLC (a TLR3 agonist). First, we confirmed that sHDL and polyICLC could be admixed together, forming a potent adjuvant system (sHDL+polyICLC) that could be readily combined with an antigen. sHDL+polyICLC significantly enhanced activation of DCs, compared with free adjuvants or nanodiscs with CpG. Importantly, mice immunized with the mixtures of sHDL+polyICLC generated strong cellular immune responses with strong anti-tumor efficacy in the MC-38 colon cancer model. Compared with free adjuvants, sHDL+polyICLC markedly improved antigen-specific CD8+ T-cell responses by 8-fold and promoted regression of MC-38 colon cancer ($P < 0.0001$). We also observed that sHDL+polyICLC elicited robust CD8+ T cell responses in NHPs, thus demonstrating the promise of nanodisc vaccination for clinical translation. Taken together, this work highlights the simplicity, versatility, and potency of the sHDL+polyICLC system for applications in vaccines and cancer immunotherapy.

3.6 References

[1] R.L. Siegel, L.A. Torre, I. Soerjomataram, R.B. Hayes, F. Bray, T.K. Weber, A. Jemal, Global patterns and trends in colorectal cancer incidence in young adults, Gut 68(12) (2019) 2179-2185.

[2] P. Ragnhammar, L. Hafström, P. Nygren, B. Glimelius, A systematic overview of chemotherapy effects in colorectal cancer, Acta oncologica 40(2-3) (2001) 282-308.
[3] T. Seya, Y. Takeda, K. Takashima, S. Yoshida, M. Azuma, M. Matsumoto, Adjuvant immunotherapy for cancer: both dendritic cell-priming and check-point inhibitor blockade are required for immunotherapy, Proceedings of the Japan Academy, Series B 94(3) (2018) 153-160.
[4] M. Singh, M. Ugozzoli, J. Kazzaz, J. Chesko, E. Soenawan, D. Mannucci, F. Titta, M. Contorni, G. Volpini, G. Del Guidice, A preliminary evaluation of alternative adjuvants to alum using a range of established and new generation vaccine antigens, Vaccine 24(10) (2006) 1680-1686.
[5] A. Iwasaki, R. Medzhitov, Toll-like receptor control of the adaptive immune responses, Nature immunology 5(10) (2004) 987.
[6] D.E. Speiser, D. Liénard, N. Rufer, V. Rubio-Godoy, D. Rimoldi, F. Lejeune, A.M. Krieg, J.-C. Cerottini, P. Romero, Rapid and strong human CD8+ T cell responses to vaccination with peptide, IFA, and CpG oligodeoxynucleotide 7909, Journal of Clinical Investigation 115(3) (2005) 739.
[7] A.C. Carrington, C.J. Secombes, A review of CpGs and their relevance to aquaculture, Veterinary immunology and immunopathology 112(3-4) (2006) 87-101.
[8] Z.K. Ballas, W.L. Rasmussen, A.M. Krieg, Induction of NK activity in murine and human cells by CpG motifs in oligodeoxynucleotides and bacterial DNA, The Journal of Immunology 157(5) (1996) 1840-1845.
[9] G. Hartmann, A.M. Krieg, Mechanism and function of a newly identified CpG DNA motif in human primary B cells, The Journal of Immunology 164(2) (2000) 944-953.

[10] J. Vollmer, R. Weeratna, P. Payette, M. Jurk, C. Schetter, M. Laucht, T. Wader, S. Tluk, M. Liu, H.L. Davis, Characterization of three CpG oligodeoxynucleotide classes with distinct immunostimulatory activities, European journal of immunology 34(1) (2004) 251-262.

[11] D. Valmori, N.E. Souleimanian, V. Tosello, N. Bhardwaj, S. Adams, D. O'Neill, A. Pavlick, J.B. Escalon, C.M. Cruz, A. Angiulli, Vaccination with NY-ESO-1 protein and CpG in Montanide induces integrated antibody/Th1 responses and CD8 T cells through cross-priming, Proceedings of the National Academy of Sciences 104(21) (2007) 8947-8952.

[12] J. Karbach, S. Gnjatic, A. Bender, A. Neumann, E. Weidmann, J. Yuan, C.A. Ferrara, E. Hoffmann, L.J. Old, N.K. Altorki, Tumor-reactive CD8+ T-cell responses after vaccination with NY-ESO-1 peptide, CpG 7909 and Montanide® ISA-51: association with survival, International journal of cancer 126(4) (2010) 909-918.

[13] W.N. Haining, J. Davies, H. Kanzler, L. Drury, T. Brenn, J. Evans, J. Angelosanto, S. Rivoli, K. Russell, S. George, CpG oligodeoxynucleotides alter lymphocyte and dendritic cell trafficking in humans, Clinical cancer research 14(17) (2008) 5626-5634.

[14] D.E. Speiser, D. Liénard, N. Rufer, V. Rubio-Godoy, D. Rimoldi, F. Lejeune, A.M. Krieg, J.-C. Cerottini, P. Romero, Rapid and strong human CD8+ T cell responses to vaccination with peptide, IFA, and CpG oligodeoxynucleotide 7909, The Journal of clinical investigation 115(3) (2005) 739-746.

[15] O. Schulz, S.S. Diebold, M. Chen, T.I. Näslund, M.A. Nolte, L. Alexopoulou, Y.-T. Azuma, R.A. Flavell, P. Liljeström, C.R. e Sousa, Toll-like receptor 3 promotes cross-priming to virus-infected cells, Nature 433(7028) (2005) 887-892.

[16] K. Hoebe, E.M. Janssen, S.O. Kim, L. Alexopoulou, R.A. Flavell, J. Han, B. Beutler, Upregulation of costimulatory molecules induced by lipopolysaccharide and double-stranded RNA occurs by Trif-dependent and Trif-independent pathways, Nature immunology 4(12) (2003) 1223-1229.

[17] T. Matsumiya, D.M. Stafforini, Function and regulation of retinoic acid-inducible gene-I, Critical Reviews™ in Immunology 30(6) (2010).

[18] C. Yu, M. An, M. Li, H. Liu, Immunostimulatory properties of lipid modified CpG oligonucleotides, Molecular pharmaceutics 14(8) (2017) 2815-2823.

[19] C. Bourquin, D. Anz, K. Zwiorek, A.-L. Lanz, S. Fuchs, S. Weigel, C. Wurzenberger, P. von der Borch, M. Golic, S. Moder, Targeting CpG oligonucleotides to the lymph node by nanoparticles elicits efficient antitumoral immunity, The Journal of Immunology 181(5) (2008) 2990-2998.

[20] G.G. Zom, S. Khan, C.M. Britten, V. Sommandas, M.G. Camps, N.M. Loof, C.F. Budden, N.J. Meeuwenoord, D.V. Filippov, G.A. van der Marel, Efficient induction of antitumor immunity by synthetic toll-like receptor ligand–peptide conjugates, Cancer immunology research 2(8) (2014) 756-764.

[21] H. Huang, W. Cruz, J. Chen, G. Zheng, Learning from biology: synthetic lipoproteins for drug delivery, Wiley Interdisciplinary Reviews: Nanomedicine and Nanobiotechnology 7(3) (2015) 298-314.

[22] R. Kuai, L.J. Ochyl, K.S. Bahjat, A. Schwendeman, J.J. Moon, Designer vaccine nanodiscs for personalized cancer immunotherapy, Nature materials 16(4) (2017) 489-496.

[23] L.A. Torre, F. Bray, R.L. Siegel, J. Ferlay, J. Lortet-Tieulent, A. Jemal, Global cancer statistics, 2012, CA: a cancer journal for clinicians 65(2) (2015) 87-108.
[24] R. Kuai, X. Sun, W. Yuan, L.J. Ochyl, Y. Xu, A.H. Najafabadi, L. Scheetz, M.-Z. Yu, I. Balwani, A. Schwendeman, Dual TLR agonist nanodiscs as a strong adjuvant system for vaccines and immunotherapy, Journal of controlled release 282 (2018) 131-139.

Chapter 4 Development of sHDL Nanodiscs for Induction of Antigen-Specific Immune Tolerance

4.1 Abstract

Multiple sclerosis (MS) is an autoimmune disease caused by the autoimmune response against axons and myelin sheaths of the central nervous system (CNS), leading to axonal loss and demyelination. Current treatments for MS are mainly based on immunosuppressive therapies that have unintended side effects on global immune responses and cause significant toxicity. Antigen-specific approaches for induction of immune tolerance is a new method to treat autoimmune disease based on the use of antigenic peptides or proteins, and aims to inhibit autoimmune responses by inducing tolerogenic antigen-specific T-cell response. However, current approaches for inducing antigen-specific immune tolerance generally require prolonged treatments with high doses of tolerogenic antigen and have failed to deliver desired therapeutic results in clinical trials. Recently, nanotechnology has introduced novel technical advances capable of modulating immune responses. Here, we report the development of synthetic high-density lipoproteins (HDL) designed for the delivery of tolerogenic MS antigens, and we present initial in vivo efficacy studies in a murine model of experimental autoimmune encephalomyelitis (EAE), a widely accepted pre-clinical model of MS. Our results from in vivo experiments in murine model of EAE indicated that HDL-MOG effectively inhibited the symptoms of EAE, whereas treatments with blank HDL or free MOG peptide had no significant impact. Moreover, mice treated with HDL-MOG in the therapeutic model of

EAE exhibited significantly lower for EAE disease score, compared with those treated with HDL free peptide or even FTY720 (i.e. Fingolimod, an FDA-approved drug widely used for the treatment of MS). Mechanistically, HDL-MOG decreased production of IFN-ɣ and IL-17 in lymphocytes and increased the level of regulatory T cells (Treg), compared with free peptide, suggesting that our HDL-based strategy inhibited the autoantigen-specific Th1 and Th17 responses and upregulated the level of anti-inflammatory T cells, thereby ameliorating symptoms of EAE.

4.2 Introduction

Multiple sclerosis (MS) is the one of the most common progressive neurological disease in young adults, affecting one million people in the United States and nearly 2.5 million people globally [1, 2]. The majority of patients primary present with relapsing and remitting neurological symptoms, and MS diagnosis is confirmed by the presence of multiple inflammatory lesions with temporospatial dissemination in the brain, spinal cord, and/or optic nerve [3, 4]. These lesions are comprised of a variety of inflammatory infiltrates, including myeloid cells, which contribute to disease pathogenesis by presenting antigen and releasing cytotoxic factors that damage myelin and myelin-producing oligodendrocytes, and CD4+ T cells, which are believed to orchestrate these aberrant immune responses [5, 6].

Studies analyzing the immune infiltrates in the CNS lesions of MS patients as well as studies in murine models of MS have shown that CD4+ T helper cells (Th) cells polarized to Th1 (IFN-γ-producing) and/or Th17 (IL-17-producting) phenotypes are the main drivers of CNS autoimmunity [6-8]. Supporting this theory, the genetic variance of

molecules involved in the activation and function of CD4+ T cells can confer susceptibility for MS [9]. CD4+ T cells drive pathogenesis in the CNS by releasing pro-inflammatory cytokines and chemokines that recruit and activate peripheral myeloid cells and brain-resident glial cells. These cells then release more pro-inflammatory cytokines and chemokines, resulting in an inflammatory cascade and demyelination. Tolerizing CD4+ T cells to myelin antigens represent a potential therapeutic approach that could specifically target myelin-reactive T cells without affecting the immune response to pathogens (**Figure 4-1.**).

Systemic treatment with auto-antigen has been shown to be effective in experimental autoimmune encephalomyelitis (EAE), a common murine model of MS. Oral delivery of myelin-oligodendrocyte glycoprotein 35-55 (MOG_{35-55}) peptide showed a reduction in disease severity in MOG_{35-55}-induced EAE in C57Bl/6 mice [10]. Similarly, intravenous delivery of auto-antigens, such as myelin basic protein and alpha B-crystlin, can suppress ongoing autoimmunity [11, 12]. Mechanisms that underlie these treatments include suppression and deletion of autoreactive T cells, induction of tolerogenic dendritic cells, and stimulation of regulatory T cells [13-20]. However, soluble peptides as a treatment for MS pose the risk of an anaphylactic reaction, as reported in mice with EAE [20, 21]. Furthermore, soluble peptide delivery typically requires prolonged treatments with high doses of tolerogenic peptides and has failed to deliver desired therapeutic results in prior clinical trials [22]. Therefore, for successful application of auto-antigens as a disease-modifying therapy, a targeted delivery approach should be investigated.

Recent studies have indicated that nanoparticles hold considerable promise to fulfill the need for targeted therapeutics in autoimmune disease [22]. Nanoparticle-based

strategies for immune tolerance aim to alter the antigen-presentation pathways or deliver auto-antigens to anatomical regions for enhancing regulatory T-cell formation [23]. Other approaches seek to target and modulate antigen-specific, T-cell intrinsic signaling pathways capable of re-programming pathogenic auto-reactivity into disease-suppressing auto-regulation [24-26]. However, only a few nanoparticle systems have entered the clinical stage for immune tolerance, in part due to toxicity and low therapeutic outcomes.

HDL, known as good cholesterol, is a lipid-based nanoparticle involved in the transport and metabolism of cholesterol and triglyceride. HDL with a small hydrodynamic size, safety, long circulation half-life, and targeting ability to different recipient cells is a promising nanocarrier for the delivery of antigen to activate the immune system [27]. Here, we report the development of synthetic HDL designed for the delivery of tolerogenic MS antigens and initial in vivo efficacy studies in a murine model of EAE, a widely accepted pre-clinical model of MS.

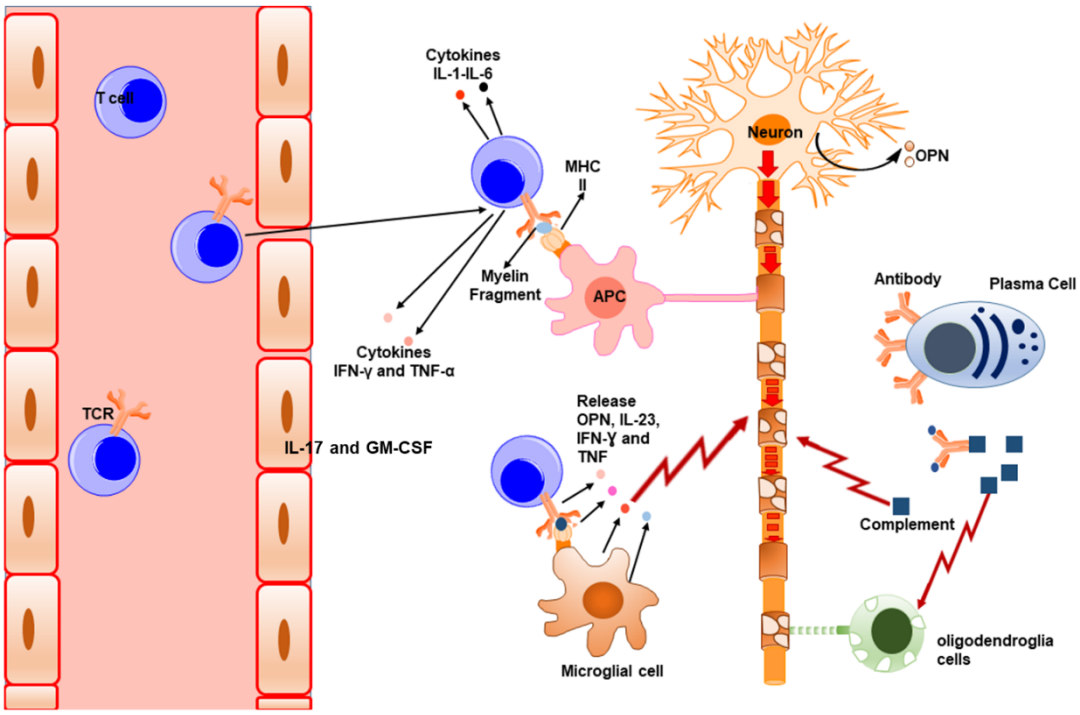

Figure 4-1. Cellular mechanism of multiple sclerosis (MS).

4.3 Experimental section

4.3.1 Materials and methods

CSS-MOG (CSSGWYRSPFSRVVHL), CSS-OVA-II (CSSISQAVHAAHAEINEAGR), CSS-MOG-FITC(CSSGWYRSPFSRVVHLK-FITC), CSS-Eα (CSSASFEAQGALANIAVDKA), CSS-M30 (CSSVDWENVSPELNSTDQ), MOG (GWYRSPFSRVVHL), OVA-II (ISQAVHAAHAEINEAGR) M30 (VDWENVSPELNSTDQ), and Eα (ASFEAQGALANIAVDKA) antigen peptides were synthesized by Genemed Synthesis Inc. (San Antonio, TX). 1, 2-dimyristoyl-sn-glycerol-3-phosphocholine (DMPC) and N-(3-Maleimide-1-oxopropyl)-L-α-phosphatidylethanolamine, Dioleoyl] (DOPE-MAL) were purchased from NOF America (White Plains, NY). 22A apolipoprotein-A1 mimetic

peptide was synthesized by GenScript (Piscataway, NJ). Interferon-γ (IFN-γ), IL-17, and IL-10 ELISPOT kits were purchased from Fisher Scientific (Hampton, NH). Cell media, ACK buffer were purchased from Invitrogen (Carlsbad, CA). The following antibodies for flow cytometry were purchased from BioLegend: anti-mouse CD8a-APC; anti-mouse CD45R (B220)-PE/Cy7; rat anti-mouse CD4-Brilliant Violet 605; anti-mouse CD3-FITC; rat anti-mouse F4/80-APC-CY7; anti-mouse CD11c-FITC; anti-mouse -B7-DC (PD-L2)-PE (clone: TY25), aPD-L1-PerCP (clone 10F.9G2); aCD80-FITC (clone16-10A1); aCD86-PE/Cy7 (clone GL-1); and aCD40-BV421. Tetramer (GWYRSPFSRVVHL) was kindly provided by the NIH Tetramer Core Facility (Atlanta, GA). aI-Ab-Ea52-68-FITC (clone eBioY-Ae) FITC was purchased from eBioscience. TMR-NHS and FITC-NHS was purchased from Thermo Fisher Scientific (Waltham, MA). Pertussis toxin was purchased from Merck.

4.3.2 Synthesis and characterization of HDL nanodiscs carrying tolerogenic MS antigen (MOG)

Lipid-peptide was prepared as previously reported [28]. Peptides (MOG, OVA-II, Eα, and M30) were synthesized with a cysteine-serine-serine (CSS) linker at the N-terminus, and antigen peptides were reacted with DOPE-MAL (antigen peptide: DOPE-MAL = 2:1, molar ratio) for 4 h on an orbital shaker in dimethylformamide (DMF) (Figure 4-1). The conjugation efficiency of the reaction was calculated based on the reduction in absorbance signal associated with DOPE-MAL as measured by HPLC/MS. As previously reported [28, 29], HDL was synthesized by dissolving 22A apo-A1 peptide and DMPC in acetic acid, followed by evaporation and rehydration in 10 mM phosphate buffer. Lipid-

peptide conjugates were incorporated into HDL by adding lipid-peptide dropwise in dimethylsulfoxide (DMSO) to HDL suspension. The mixture was incubated for 1 h at room temperature on an orbital shaker at 200 rpm to incorporate lipid-peptides into HDL. After incubation, unincorporated lipid-peptide was separated by ultracentrifuge filtration (MilliporeSigma™ Amicon™ Ultra Centrifugal Filter, 10KD). Incorporation of lipid-peptides into HDL was measured by reverse-phase HPLC/MS. The hydrodynamic size and zeta potential of HDL were measured by dynamic light scattering (DLS, Zetasizer Nano ZSP). Visualization by transmission electron microscopy (TEM) was performed after diluting HDL 10X with osmium tetroxide solution used as a negative staining. TEM images were obtained by JEM 1200EX electron microscope (JEOL USA) equipped with an AMT XR-60 digital camera (Advanced Microscopy Techniques).

4.3.3 Animal experiments

Animals were cared for following the federal, state, and local guidelines. The University of Michigan, Ann Arbor is an AAALAC international accredited institution, and all work conducted on animals was in accordance with and approved by the Institutional Animal Care and Use Committee (IACUC) with the protocol # PRO00008587. Female C57BL/6 mice (9-10 weeks old) were purchased from Jackson Laboratory (USA). Female 2D2 mice were also purchased from Jackson Laboratory.

4.3.4 Harvesting and culturing of APCs

Bone marrow-derived dendritic cells (BMDCs) were generated as previously described [30]. Briefly, bone marrow was flushed from femurs and tibia bone of 5 to 6 weeks old

C57BL/6 mice. Isolated bone marrow cells were plated at 1 × 10^6 cells per dish in RPMI 1640 supplemented with 10% FBS, 55 μM β-mercaptoethanol, 5 ng/ml of GM-CSF, and 100 U/ml penicillin (BMDC media). On day three and five, one half of the culture media was replaced with fresh media. After 8 days, BMDCs were harvested and plated at 1 × 10^6 cells per well in 12-well plates. After 24 h, BMDC incubated with 100 μg of antigen peptide antigen (Ag), Mal-antigen peptide (MPB-Ag), blank HDL, blank HDL mixture with antigen peptide, or HDL-Ag peptide in various formulations and cultured with or without lipopolysaccharide (LPS, 1 μg/mL) for 48 h at 37 °C with 5% CO2.

Mixed glial cell cultures were harvested from the cerebral cortex of newborn (P0–2) C57BL6/J mice as described previously. Cortices and brain stem were separated, and the blood vessels and meninges were carefully isolated. Then, the tissues were digested by enzymatic dissociation (0.05% trypsin-EDTA and 25 mg/ml DNase I), washed two times with 1% BSA in PBS. Cells were resuspended in DMEM (10% FBS, 1% penicillin/streptomycin, 0.5 mM 2-mercaptoethanol). Mixed glial cells were cultured in poly-D-lysine–coated flasks and grown at 37°C and 5% CO2. After 10 days, microglia cells were isolated from the underlying astrocytic layer by shaking of the flask. The cell culture contained more than 95% microglial (CD11b+, CD45+) cells, as analyzed by flow cytometry. Microglia cells were plated at 1 × 10^6 cells per well in 12-well plates. After 48 h, microglial cells were incubated with 100 μg of antigen peptide, blank HDL, blank HDL mixture with antigen peptide, or HDL-Ag peptide in various formulations and culture with lipopolysaccharide (LPS, 1 μg/mL) in Microglia media for 48 h at 37 °C with 5% CO2.

After 48 h, the supernatant was collected, and the level of different inflammatory and anti-inflammatory cytokines was measured by ELISA (Enzyme-linked

immunosorbent assay). Afterward, BMDCs and microglia were washed two times with FACS buffer (1% BSA in PBS), incubated with anti-CD16/32 at room temperature. They were stained on ice with fluorophore-labeled antibodies against fixable viability dye (Efluor 450) or antibodies against CD11b, CD11c, aI-Ab-Ea52-68-FITC (clone eBioY-Ae), CD40, CD80, CD86, PD-L1, or PDL-2. Cells were then washed twice, resuspended in FACS buffer, and analyzed by flow cytometry.

Internalization of fluorescent HDL-MOG by BMDCs or Microglia cells was visualized using confocal microscopy. BMDCs or Microglias cells were seeded at 1×10^6 cells on 35 mm Petri dishes (MatTek) and incubated with the mixture of free MOG-K(FITC), or HDL-CSS-MOG-K(FITC) with LPS (1 μg/ml) for 24 h. Cells were then washed three times with PBS, fixed with 4% paraformaldehyde, washed, and permeabilized with 0.1% Triton-X solution. Actin filaments were stained with AlexaFluor 647-Phalloidin, and the nuclei were stained with DAPI. The samples were imaged using a 63X oil-immersion lens on a Nikon A-1 spectral confocal microscope.

4.3.5 Biodistribution experiments

Tetramethylrhodamine (TMR, excitation/emission ~540/560 nm) modified MOG peptide (CSSGWYRSPFSRVVHLK-TMR, MOG-TMR) was prepared by reacting TMR-NHS and MOG peptide according to the manufacturer instruction. MOG-TMR was purified using HPLC and reacted with DOPE-MAL in DMF to produce DOPE-Mal-MOG-TMR (MOG-TMR). Next, the DMF solution was diluted with water, freeze-dried, dissolved in DMSO, and added to previously made HDL to produce HDL-MOG-TMR. Conjugation of MOG-TMR to DOPE-MAL and incorporation of MOG-TMR in HDL were measured by

HPLC/MS, as indicated above. For the lymph node draining studies, naive female C57BL/6 mice or EAE-induced mice were administered *subcutaneously* at the tail base with HDL-MOG-TMR or free MOG-TMR containing antigen peptide (100 µg per mouse) in 100 µl volume. After 24, 96, and 196 h, animals were euthanized, organs were harvested, and TMR signal was measured with an IVIS optical imaging system (Caliper Life Sciences). Inguinal lymph nodes and spinal cord were cut into small pieces and passed through a 70-µm cell strainer, washed two times, and stained with the indicated antibodies, followed by flow cytometry analysis.Copper-64 (64Cu) was synthesized with an onsite cyclotron (GE PETtrace) method. ^{64}CuCl2 (74 MBq) was diluted in 0.3 mL of 0.1 M sodium acetate buffer (pH 5.0) and mixed with 0.5 mg of nanodisc-MOG. The mixing was conducted at 37 °C for 30 min with constant shaking. Subsequently, 5 µL 0.1 M EDTA (ethylenediaminetetraacetic acid) was added into the solution and shaken for 5 min to remove non-specifically bound ^{64}Cu. The resulting ^{64}Cu-NOTA–nanodisc was purified by centrifugation filtration (10 kDa). The radioactive fractions were collected for further in vivo studies. C57BL/6 mice were administered *subcutaneously* with 5–8 MBq of ^{64}Cu-NOTA–nanodisc and PET imaging was performed over time using a microPET/microCT Inveon rodent model scanner (Siemens Medical Solutions USA, Inc.). Quantitative PET data for the major organs were presented as the percentage injected dose per gram of tissue (%ID g−1).

4.3.6 EAE induction and nanodisc vaccination

EAE was initiated as described previously [31]. Briefly, female C57BL/6 mice were injected subcutaneously with an emulsion of $MOG_{35–55}$ in complete Freund's adjuvant

(CFA) and intraperitoneal (i.p.) injection of pertussis toxin (120 ng/dose on days 0 and 2). Harsher EAE was induced in female C57BL/6 mice by inoculation with MOG_{1-125} in Complete Freund's Adjuvant on day 0, followed by the administration of pertussis toxin on days 0 and 2. Mice were then injected subcutaneously at the tail base with HDL-MOG, MOG, HDL-M30, M30, or PBS on indicated time points. In some studies, mice were orally gavaged daily with FTY720 (1 or 0.3 mg/kg) or water starting day 15 or 30 after the EAE induction. After one month of the treatment, all treatments were stopped, and mice were monitored for EAE scores.

Mice were scored daily and assigned an EAE clinical score from 0 to 5: No obvious changes in motor function compared to non-immunized mice (score 0); the tip of the tail is limp (score 0.5), limp tail (score 1.0); limp tail and hind leg inhibition (score 1.5); limp tail and weakness of hind legs (score 2.0); limp tail and dragging of hind legs (score 2.5); limp tail and complete paralysis of hind legs (score 3.0); limp tail and complete paralysis of hind legs and partial front leg paralysis (score 3.5); and mouse is minimally moving around the cage and is minimally alert (score 4.0); and mouse is spontaneously rolling in the cage or mouse is found dead due to paralysis (score 5.0).

4.3.7 Examination of inflammatory and anti-inflammatory T cells in CNS and spleen

On the indicated time point, various tissues were harvested from mice after intracardiac perfusion with PBS. The spinal cord was harvested, homogenized in 10 ml of PBS containing 1% BSA, and pelleted at 800xg for 5 min. Supernatants were collected and quantified by ELISA. Cell pellets were resuspended in 3 ml of collagenase A (1 mg/ml)

and DNase I (1 mg/ml) in HBSS and incubated in a 37˚C water bath for 30 min. Samples were pelleted at 800xg, resuspended in 27% Percoll, and centrifuged for 10 min at 800xg. The myelin/debris layer and Percoll were removed, and the cell pellet was stained and analyzed by flow cytometric analysis. Splenic immune cells were isolated by homogenization through a 70 μm strainer. RBCs were lysed using ACK lysis buffer. Cells were washed with 25 ml of PBS, centrifuged at 800xg, resuspended in FACS buffer, and stained with antibodies. For the cellular surface staining, cells were resuspended in PBS with a fixable viability dye (BV510) for 30 min. Then, cells were washed two times with FACs buffer and resuspended in Fc Block (anti–CD16/32; 100 ng/ml). For *ex vivo* re-stimulation, cells were incubated for 96 hr with $MOG_{35–55}$ before brefeldin A (BFA) (3 μg/ml) was added for 4 h. For intracellular staining, cells were stained for surface markers, as mentioned previously, fixed/permeabilized, and stained with antibody for 30 min on the ice. After 2× washing, cells were resuspended in FACS buffer and analyzed by flow cytometric analysis. Data were collected with a Cytek Aurora flow cytometer using FCS express software (V7).

4.3.8 Statistical analysis

Sample sizes were selected according to pilot experiments and previously published results in the literature. All animal studies were performed after randomization. Data were analyzed by one-way or two-way ANOVA, followed by Tukey's multiple comparisons post-test or log-rank (Mantel-Cox) test with Prism 8.0 (GraphPad Software). Statistical significance was indicated as *P < 0.05, **P < 0.01, ***P < 0.001 and ****P < 0.0001. All values are reported as means ± SEM.

4.4 Results and discussion

4.4.1 Synthesis of HDL nanodiscs incorporated with MOG epitope

Figure 4-2.A-B show the synthesis procedure for antigen-loaded HDL nanodiscs. Briefly, HDL was made by mixing 1, 2-dimyristoyl-sn-glycerol-3-phosphocholine (DMPC) and 22A Apo-A1 mimetic peptide in acetic acid, followed by lyophilization, rehydration in 10 mM phosphate buffer, and three heating and cooling cycles. Cysteine pre-modified antigen peptides were reacted with N-(3-maleimide-1-oxopropyl)-L-α-phosphatidylethanolamine, dioleoyl (DOPE-MAL) in DMF (**Figure 4-2.A-B**). Next, the peptide-lipid conjugate was dissolved in DMSO and added dropwise to HDL to produce HDL-MOG or HDL-M30 (**Figure 4-2.C**). HPLC/MS analysis showed efficient conjugation of antigen peptide to DOPE-MAL with > 90% conjugation efficiency (**Figure 4-2.C**). We also observed efficient incorporation of lipid-peptide into HDL with > 90% efficiency (**Figure 4-2.C**). Blank HDL, HDL-MOG, and HDL-M30 had comparable particle size ranging from 9-13 nm, a polydispersity index of 0.20 ± 0.02, and slightly negative surface charge of 3.4 ±.3 mV. TEM images showed that HDL, HDL-MOG, and HDL-M30 have uniform size and nanodisc-like morphology (10 ± 3 nm, **Figure 4-2.D and F**), which was consistent with the DLS results.

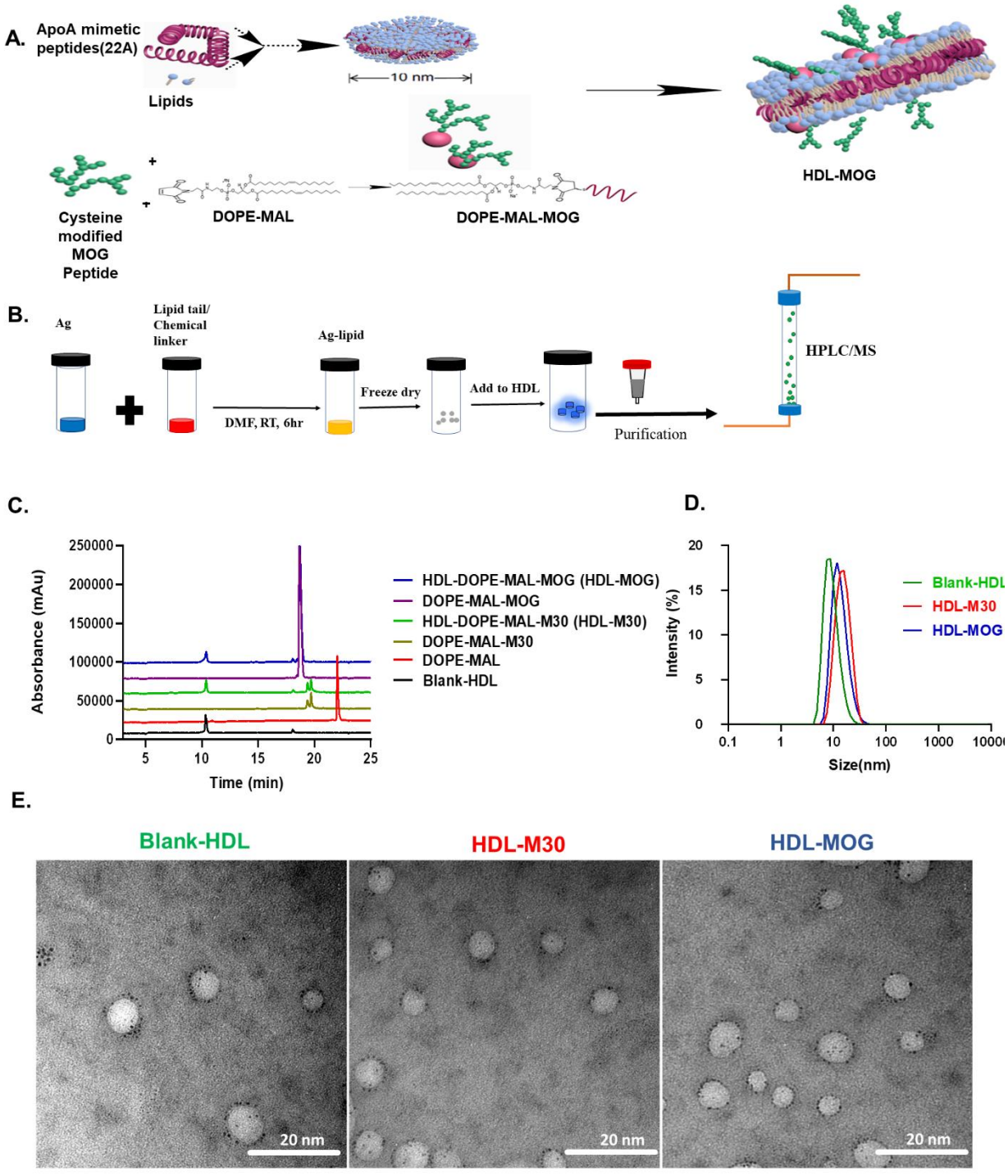

Figure 4-2. Schematic illustration of preparation, purification, and characterization of nanodiscs. A. HDL was formed by mixing DMPC and 22A apo-A1 mimetic peptide in acetic acid, followed by evaporation and rehydration in 10 mM phosphate buffers. B. Cysteine-modified antigen peptides were reacted with DOPE-MAL in DMF to produce peptide-lipid conjugates, which were then added dropwise to HDL to produce HDL-Ag.

The extent of peptide conjugation and incorporation into HDL were quantified by HPLC/MS. C. Characterization of HDL, HDL-MOG, and (HDL-M30 using HPLC. HPLC showed the efficient incorporation of D. DLS analyses of blank HDL, HDL-M30, and HDL-MOG. E. TEM images of Blank-HDL, HDL-M30, and HDL-MOG.

4.4.2 HDL-MOG is avidly taken up by APCs

We studied the internalization of fluorescent HDL-MOG by BMDCs or microglia by using confocal microscopy to visualize Ag internalization. As shown in **Figure 4-3**, BMDCs and microglia avidly internalized HDL-MOG-FITC. In contrast, we observed minimal signal of free MOG-FITC peptide in BMDCs and microglia. This suggests that APCs, such as DCs and microglia, phagocytose HDL-MOG with high efficiency. Next, we studied the impact of nanodiscs on Ag presentation. Bone marrow-derived dendritic cells (BMDCs) pulsed for 24 h with HDL-Eα presented Eα52-68 with a significant increase in peptide-MHC-II complex than BMDCs treated with free Eα52-68 peptides admixed with or HDL, as quantified by staining DCs with the aI-Ab- Eα52-68 monoclonal antibody directed against Eα52-68 complexed with MHC-II (**Figure 4-4.A-F**). Furthermore, HDL nanodiscs also significantly reduced the expression levels of co-stimulatory ligands (CD40, CD80, CD86) on BMDCs (**Figure 4-4. B-D**), compared with soluble peptides or HDL admixed with soluble peptides. In addition, HDL nanodiscs promoted DCs to increase the expression levels of PD-L1 and PD-L2 (**Figure 4-4. E-F**), which are ligands known to engage activated T cells, leading to inhibition of T cell proliferation and increase in apoptosis of activated T cells [32]. Collectively, these observations have indicated that APCs that phagocytose antigen-loaded HDL reduced the expression levels of positive co-stimulatory molecules (CD40, CD80, and CD86) involved in activating T cell effector

responses, while inducing inhibitory ligands (PD-L1/2) known to put “brakes” on activated T cells.

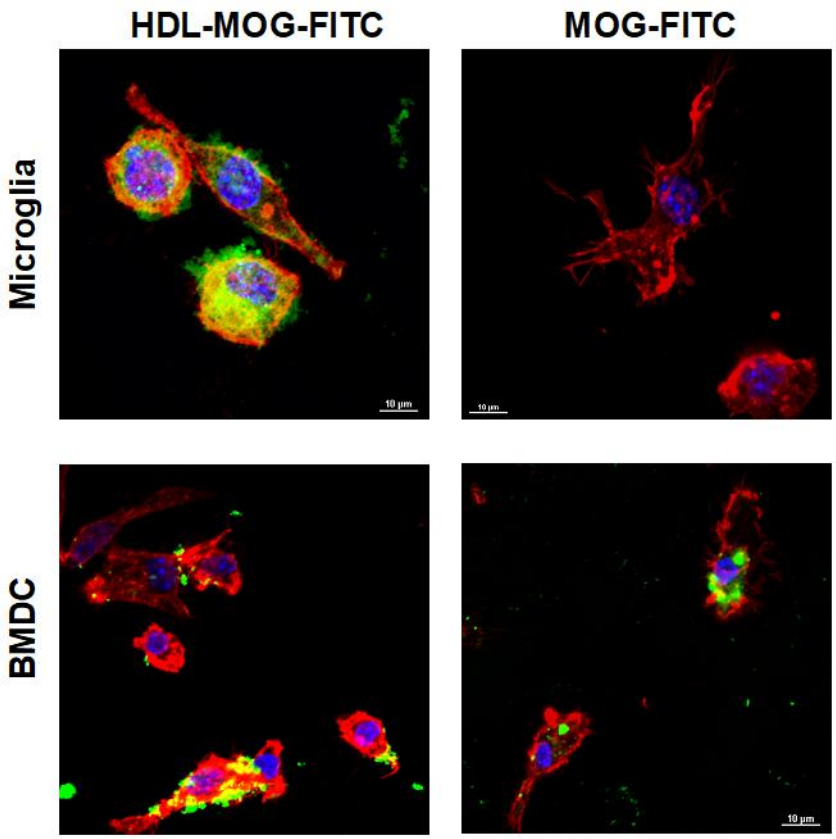

Figure 4-3. Uptake of HDL by BMDCs and microglia. BMDCs and microglia were incubated for overnight with HDL-MOG-FITC or MOG-FITC peptide and visualized for antigen uptake by confocal microscopy. Actin filaments were stained with AlexaFluor 647-Phalloidin, and nuclei were stained with DAPI.

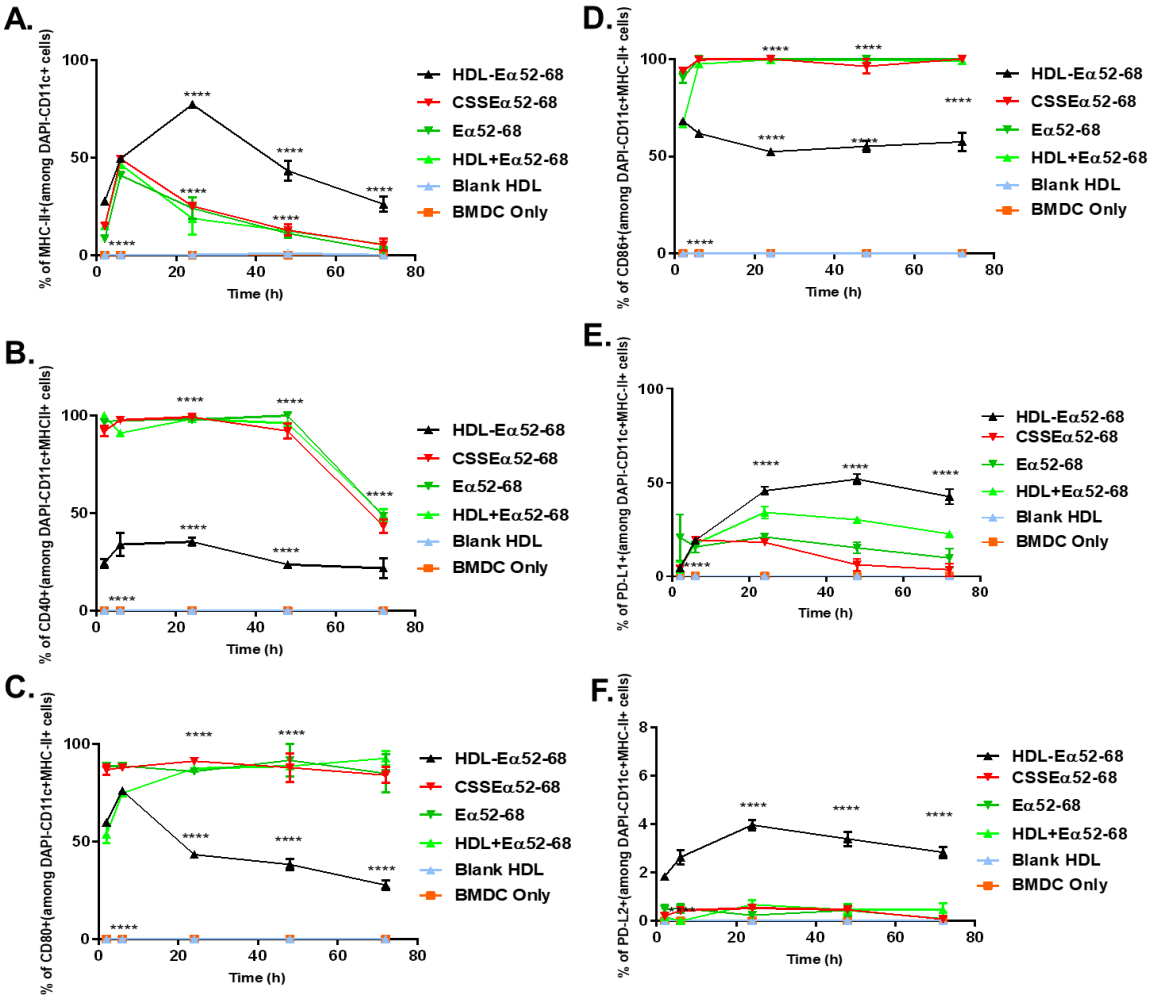

Figure 4-4. Effects of peptide-loaded HDL on the activation status of DCs. BMDCs were incubated with vaccine formulations for the indicated length of time, and Ag presentation was quantified by flow-cytometry analysis of DCs stained with aI-Ab-Ea52-68 monoclonal antibody that recognizes the Ea52-68 complexed with MHC-II. Shown are the percentage of BMDCs displaying A. peptide-MHC-II. B. CD40. C. CD80. D. CD86. E. PD-L1. And F. PD-L2. The data show mean ± SEM. (n = 3).

4.4.3 Biodistribution of HDL-MOG

To study biodistribution of nanodiscs *in vivo*, C57BL/6 naive and EAE mice were immunized s.c at the tail base with 100 ug/dose free MOG-TMR or HDL-MOG-TMR (**Figure 4-5.A**). As expected, MOG-TMR had minimal TMR signal in inguinal dLNs after

one day (**Figure 4-5.B**). The low signal intensity can be attributed to the systemic dissemination of small-molecular-weight peptides or direct antigen binding to non-APCs at the injection site. In contrast, HDL-MOG-TMR showed significantly increased TMR signal in dLNs ($p < 0.01$, **Figure 4-5.B-C**), indicating the ability of nanodiscs to enhance the delivery of Ag to draining inguinal lymph nodes. Next, we investigated the cellular uptake of HDL-MOG-TMR and MOG-TMR by flow cytometry. Consistent with the above results, HLD-MOG-TMR significantly increased cellular uptake of Ag, improving the mean fluorescence intensity (MFI) of TMR among CD11c+ DCs, B220+ B cells, and F4/80+ macrophages, compared with free MOG-TMR (**Figure 4-5.D-F**). Collectively, these results showed that compared with soluble Ag, nanodisc can efficiently deliver Ag to LNs, resulting in enhanced Ag uptake by APCs *in vivo*.

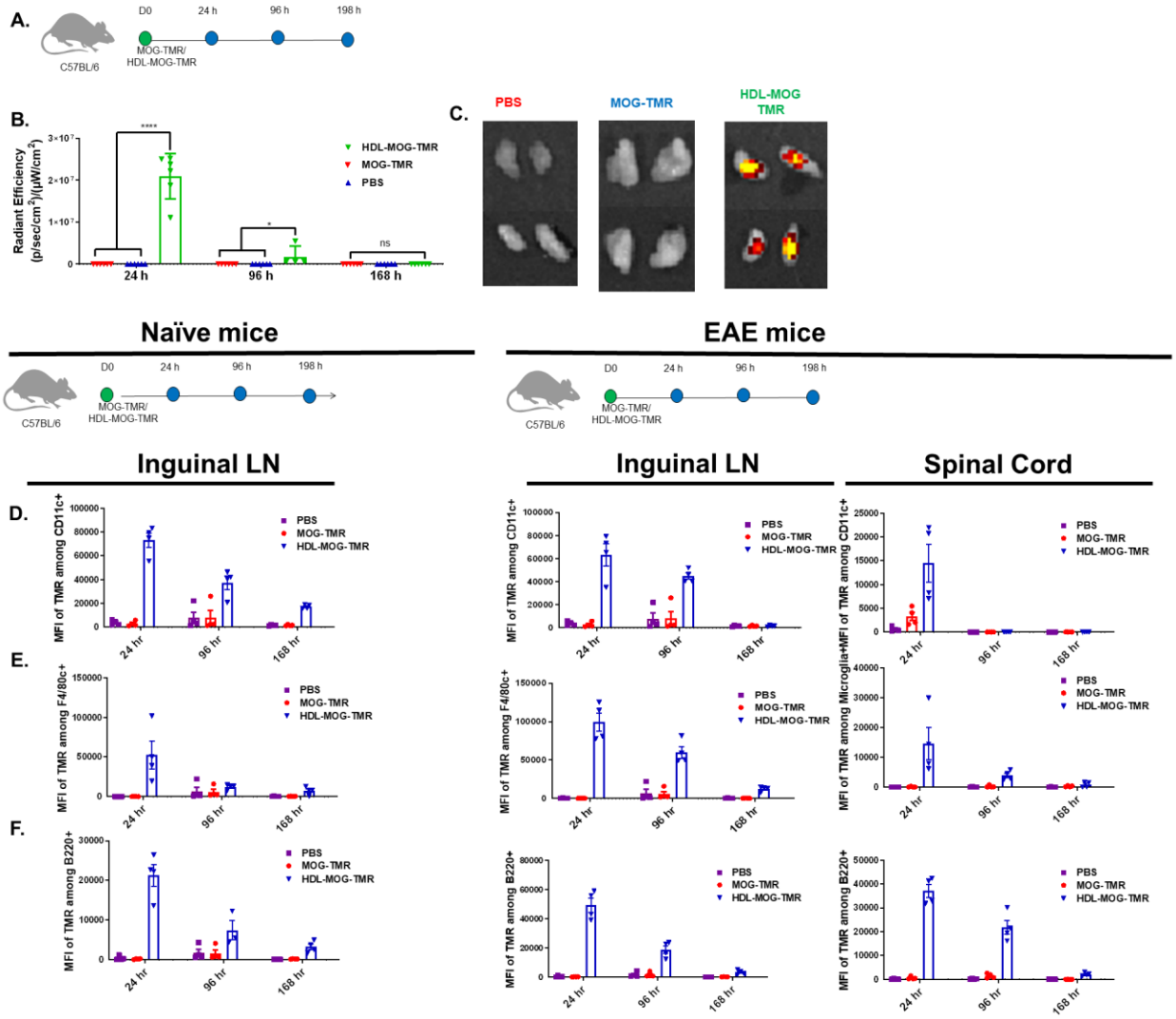

Figure 4-5. Biodistribution of HDL-MOG studied by IVIS. A. EAE-induced mice were administered subcutaneously at the tail base with 100 μg/dose of HDL-MOG-TMR. B. fluorescence signals in the draining inguinal LNs were quantified with IVIS. C. fluorescence signals in the draining inguinal LNs were monitored over time using IVIS. Naïve or EAE-induced mice were administered subcutaneously at the tail base with PBS, free MOG-TMR, or HDL-MOG-TMR. At the indicated time points, D. DCs. E. macrophages. and F. B cells were isolated from draining inguinal lymph nodes or spinal cord and analyzed for the TMR fluorescence signal.

Next, we examined the biodistribution of nanodiscs with PET imaging. Nanodisc vaccination administered s.c. at the tail base resulted in a significant amount of ^{64}Cu-

tagged MOG antigen accumulating in multiple draining LNs even within 1 hr of injection (**Figure 4-6**). After 50 hr, we detected ~20% injection dose per gram of tissue in proximal inguinal LNs as well as in distal axillary LNs (**Figure 4-6.B and C**). On the other hand, free MOG peptide administered s.c. at the tail base resulted in rapid systemic dissemination of Ag with the minimal signal in dLNs (~4% and ~11% ID/g for axillary and inguinal dLNs, respectively) (**Figure 4-6.C**).

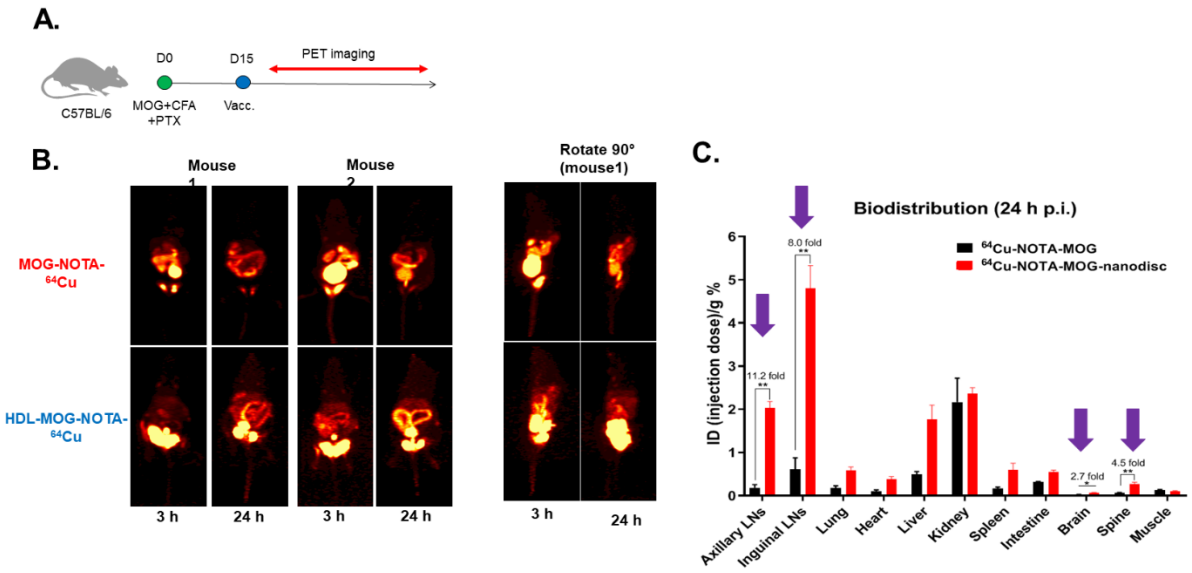

Figure 4-6.Biodistribution of HDL-MOG. A. EAE-induced mice were administered with HDL-MOG-NOTA-64Cu or MOG-NOTA-64Cu for the biodistribution study. B. PET imaging over 24 hr. C. Quantification of 64Cu signal in the major organs at 24 h post-injection.

4.4.4 HDL-MOG for the treatment of EAE

To demonstrate the utility of platform technology for the treatment of MS, we first induced EAE in naïve mice on day 0 by administering MOG_{35-55} in CFA and treated animals with HDL-MOG via subcutaneously at the tail base on days 2, 9, and 16 (**Figure 4-7**). Our

results indicated that SC administration of HDL-MOG significantly inhibited the symptoms of EAE, with the average pathological scores remaining below 1 for 100 ug dose of HDL-MOG (**Figure 4-7.B**), whereas 50 ug MOG-nanodisc group exhibited increases in EAE score beyond day 45. On the other hand, mice administered with PBS or free MOG peptide or to HDL conjugated with an irrelevant peptide were moribund within 35 days (**Figure 4-7.B**). We also repeated the same study by inducing harsher EAE via the use of MOG_{1-125}, which encompass both T-cell and B-cell epitopes for inducing EAE. MOG-nanodiscs exerted potent efficacy with most of the animals remaining at or below the EAE score of 1 (**Figure 4-7.C**). In contrast, mice treated with free MOG or PBS succumbed to EAE within 20 days (**Figure 4-7.C**).

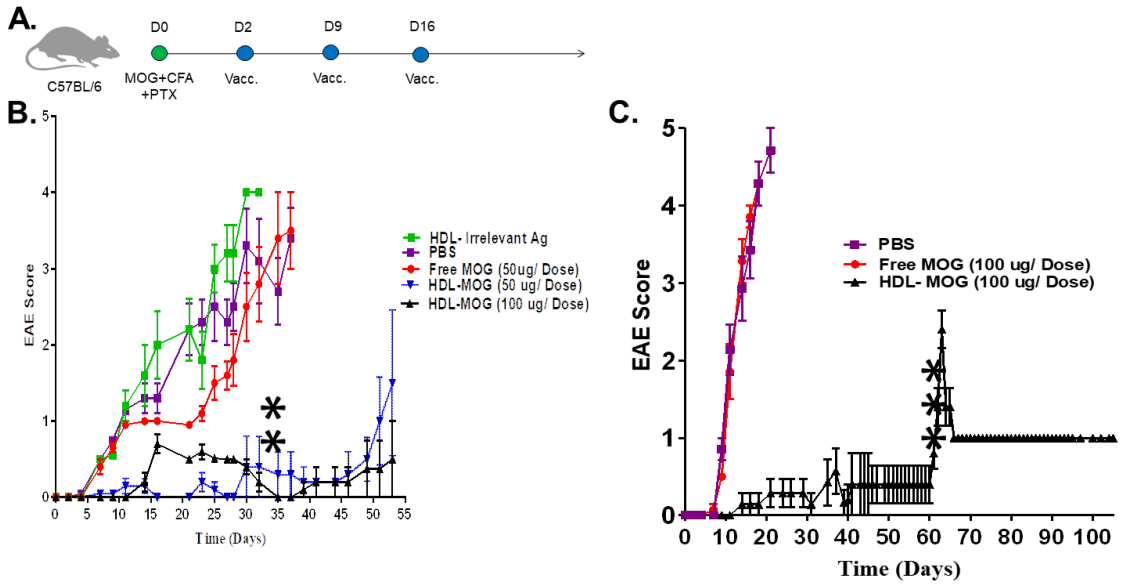

Figure 4-7. A. HDL-MOG nanodiscs administered starting day 2 exhibit potent efficacy against EAE. A. Treatment regimen. B. Pathological scores for EAE induced with MOG35-55. C. Pathological scores for EAE induced with MOG1-125.

Next, we sought to examine the potency of nanodiscs in a delayed treatment setting. We induced EAE in naïve mice on day 0 by administering MOG35-55 and vaccinated MOG-nanodiscs subcutaneously at the tail base on days 15, 22, and 29 (**Figure 4-8.A**). By day 15, animals exhibited severe signs of EAE with pathological scores of 2.5-3.5. On the other hand, HDL-MOG treatment resulted in a rapid reversal of EAE, with the pathological scores decreasing down to 0.5 by day 50 (**Figure 4-8.B**). In contrast, animals treated with free MOG did not exhibit any signs of improvement (**Figure 4-8.B**). We also examined the same treatments in the harsher EAE condition induced with MOG1-125. After 3 weekly administrations of HDL-MOG, the pathological EAE scores decreased from 4 on day 15 to score of 1 by day 30 and remained at 1 for the duration of the study (**Figure 4-8.C**). In contrast, animals treated with free MOG did not exhibit any signs of improvement and had to be euthanized by day 25 (**Figure 4-8.C**).

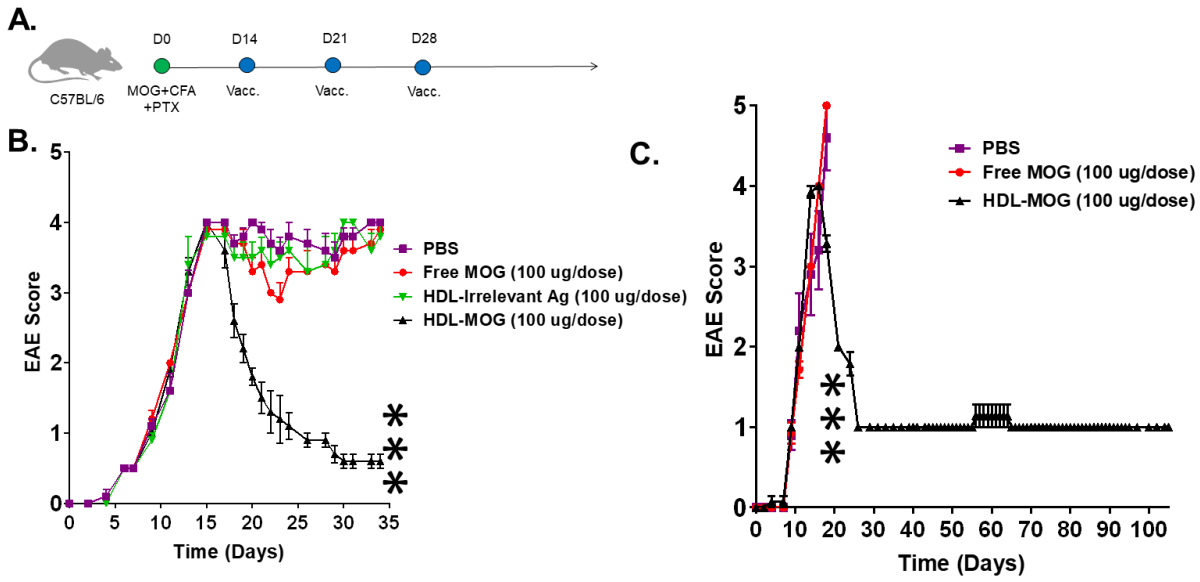

Figure 4-8. HDL-MOG nanodiscs administered starting day 15 exhibit potent efficacy against EAE. A. Treatment regimen. B. Pathological scores for EAE induced with MOG35-55. C. Pathological scores for EAE induced with MOG1-125.

Furthermore, we compared the therapeutic efficacy of HDL-MOG to FTY720 (i.e., Fingolimod), an FDA-approved drug widely used for the treatment of MS. In the first study, EAE was induced in mice, and the animals were treated with either HDL-MOG by 3 weekly subcutaneous administrations or daily oral gavage with FTY720 for 30 days starting day 15 of inducing EAE (**Figure 4-9.A**). Mice treated with HDL-MOG exhibited reversal of EAE score from 4 to 1 by day 20, and the pathological scores remained at 1 throughout 85 days (**Figure 4-9.A**). In contrast, animals treated daily with FTY720 either at 0.3 or 1 mg/kg dose showed decreased EAE score of 2, and within a few days of stopping FTY720 treatment, the pathological scores increased, and animals had to be euthanized day 60 (**Figure 4-9.A**). We also confirmed these results in a delayed treatment condition (**Fig. 9B**). EAE was induced in mice, and the animals were treated with either MOG-nanodiscs or FTY720 starting day 30 (**Figure 4-9.B**). Mice treated with HDL-MOG on days 30, 37, and 44 exhibited reversal of EAE score from 4 to 1 by day 45, and the pathological scores remained at 1 throughout 90 days (**Figure 4-9.B**). In stark contrast, animals treated daily with FTY720 at 0.3 mg/kg dose starting day 30 showed a decreased EAE score of 2.5, and within a few days of stopping FTY720 treatment, the pathological scores increased, and animals had to be euthanized day 90 (**Figure 4-9.B**). Animals treated daily with FTY720 at 1 mg/kg dose starting day 30 showed a decreased EAE score of 1, and within a few days of stopping FTY720 treatment, the pathological scores increased, and animals had to be euthanized day 90 (**Figure 4-9.A**).

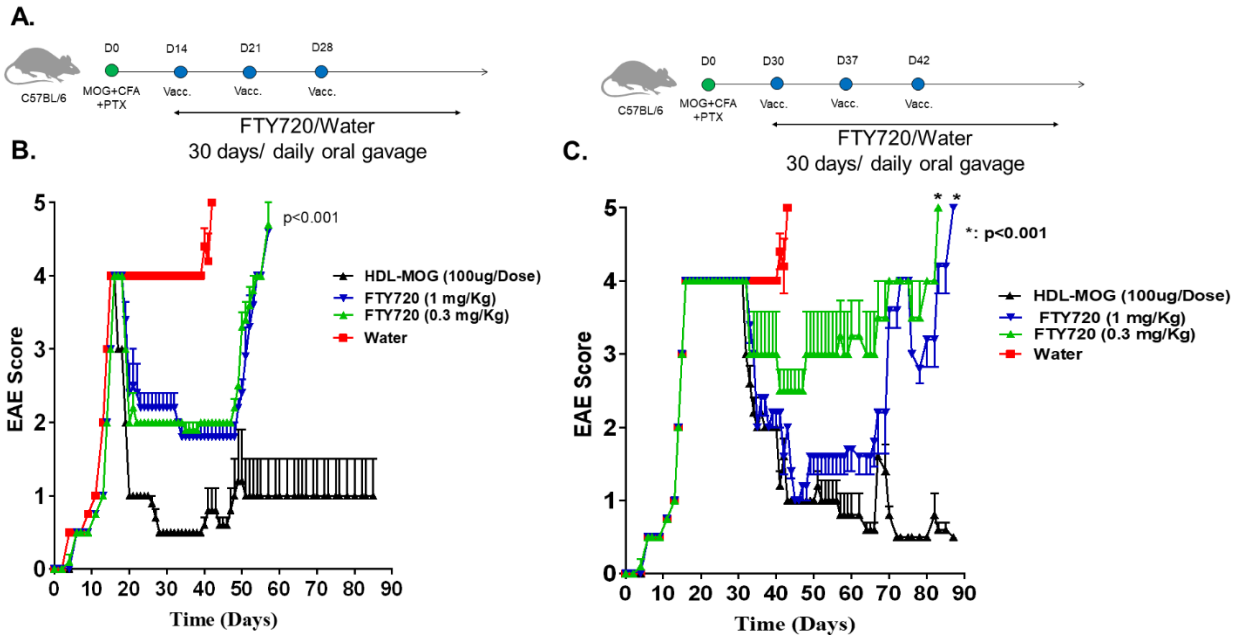

Figure 4-9. HDL-MOG nanodiscs exert more potent efficacy than FTY720 against EAE. A. Comparison of MOG-nanodiscs against FTY720 treatment after initiating the treatment on B. day 15 or C. day 35.

4.4.5 Immune profiling in CNS and spleen

To understand how HDL-MOG exerted potent efficacy against EAE, we examined CNS for inflammatory cytokines. On day 40, CNS tissues were isolated and pulsed ex vivo with MOG35-55 peptide, followed by measurement of IL-17, IFN-gamma, and GM-CSF by ELISA (**Figure 4-10.A**). Animals treated with PBS, free MOG peptide, or HDL-M30 had high levels of IL-17, IFN-gamma, and GM-CSF in CNS (**Figure 4-10.B**), indicating strong inflammation. In stark contrast, HDL-MOG treated animals had significantly reduced levels of IL-17, IFN-gamma, and GM-CSF in CNS (**Figure 4-10.B**), suggesting antigen-specific immune tolerance induced by HDL-MOG treatments. In parallel, we performed intracellular cytokine staining on CD4+ T cells from CNS cells (**Figure 4-10.C**) or

splenocytes (**Figure 4-10.D**) ex vivo stimulated with or without free MOG peptide. As in **Figure 4-10.B**, treatments with PBS, free MOG peptide, or HDL-M30 resulted in high frequencies of CD4+ T cells producing IL-17, IFN-gamma, and GM-CSF in both CNS and spleen. In stark contrast, HDL-MOG treated mice had significantly reduced the frequency of CD4+ T cells producing IL-17, IFN-gamma, and GM-CSF in both CNS and spleen (**Figure 4-10. C, and D**).

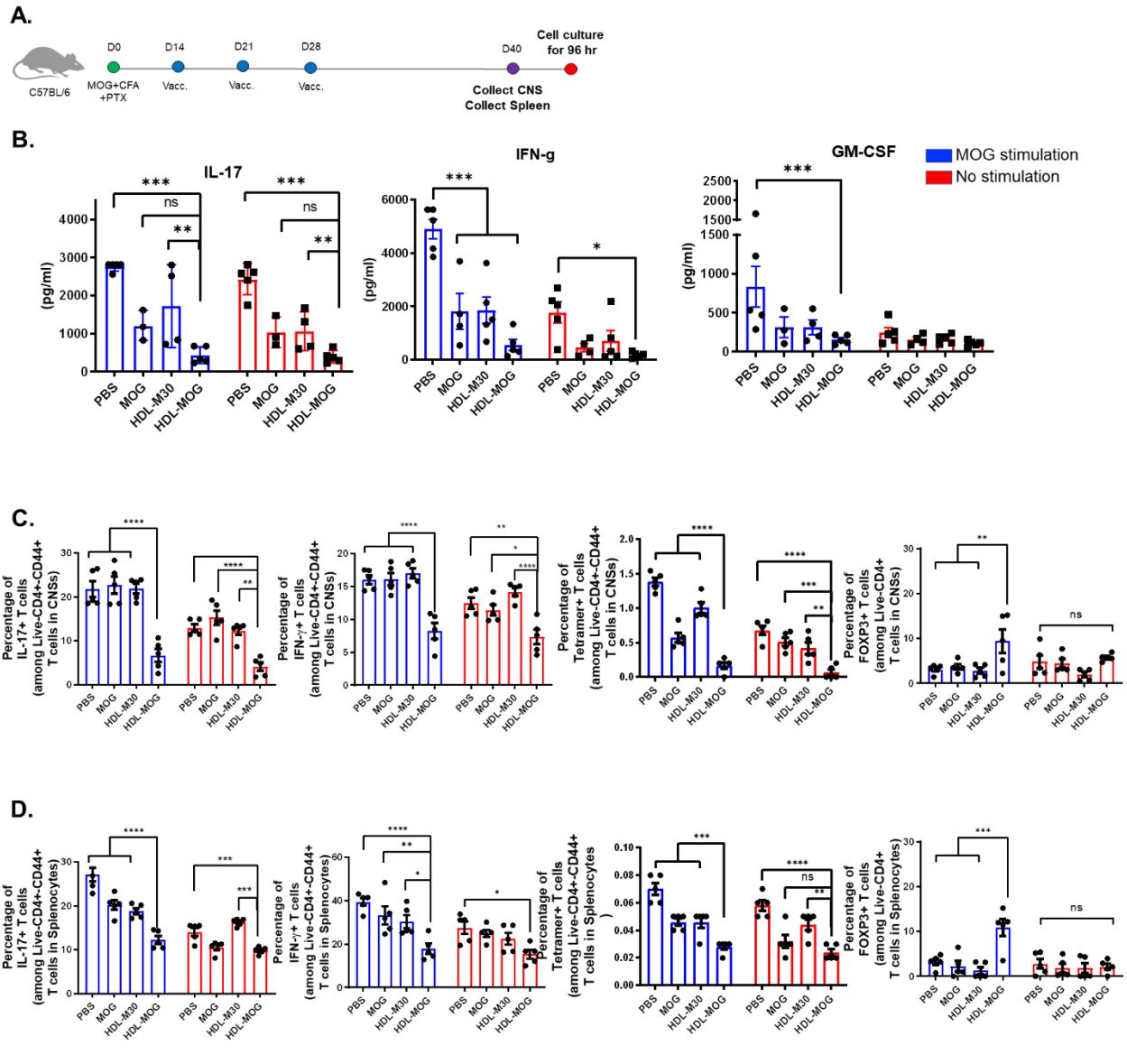

Figure 4-10. EAE-induced mice were treated with PBS, free MOG, HDL-M30, or HDL-MOG as shown. A. Vaccination timing, B. CNS collected on day 40 was processed into individual cells, restimulated ex vivo with MOG peptide, and quantified for the levels of IL-17, IFN-gamma, and GM-CFS. C. CNS cells and D. splenocytes were examined for the frequency of CD4 T cells secreting IL-17, IFN-gamma, and GM-CFS upon ex vivo restimulation with or without MOG peptide.

We next studied the impact of HDL-MOG treatment on regulatory T cells (Tregs), and the number of CD4+, CD8+ T cells in EAE mice. EAE-induced mice were treated as shown in **Figure 4-11.A**, and the frequency of Tregs, CD4+, CD8+ T cells were quantified in the CNS. Cells from CNS were stained by anti-CD25, anti-CD4 anti-CD8+, and MOG-tetramer, followed by fixation/permeabilization and intracellular staining with anti-Foxp3. Stained cells were then analyzed by flow cytometry. HDL-MOG treated mice have significantly lowered the number of CD4+ and CD8+ T cells in the CNS (**Figure 4-11.B and C**). Conversely, HDL-MOG treatments significantly increased the frequency of CD25+Foxp3+ Tregs in the CNS (**Figure 4-11.D**), and we also validated this using MOG-tetramer (**Figure 4-11.E**), indicating that HDL-MOG induced MOG-specific Tregs in CNS. On the other hand, mice treated with free MOG peptide or HDL-M30 had a basal level of Tregs as in PBS-treated EAE mice (**Figure 4-11.D, and E**).

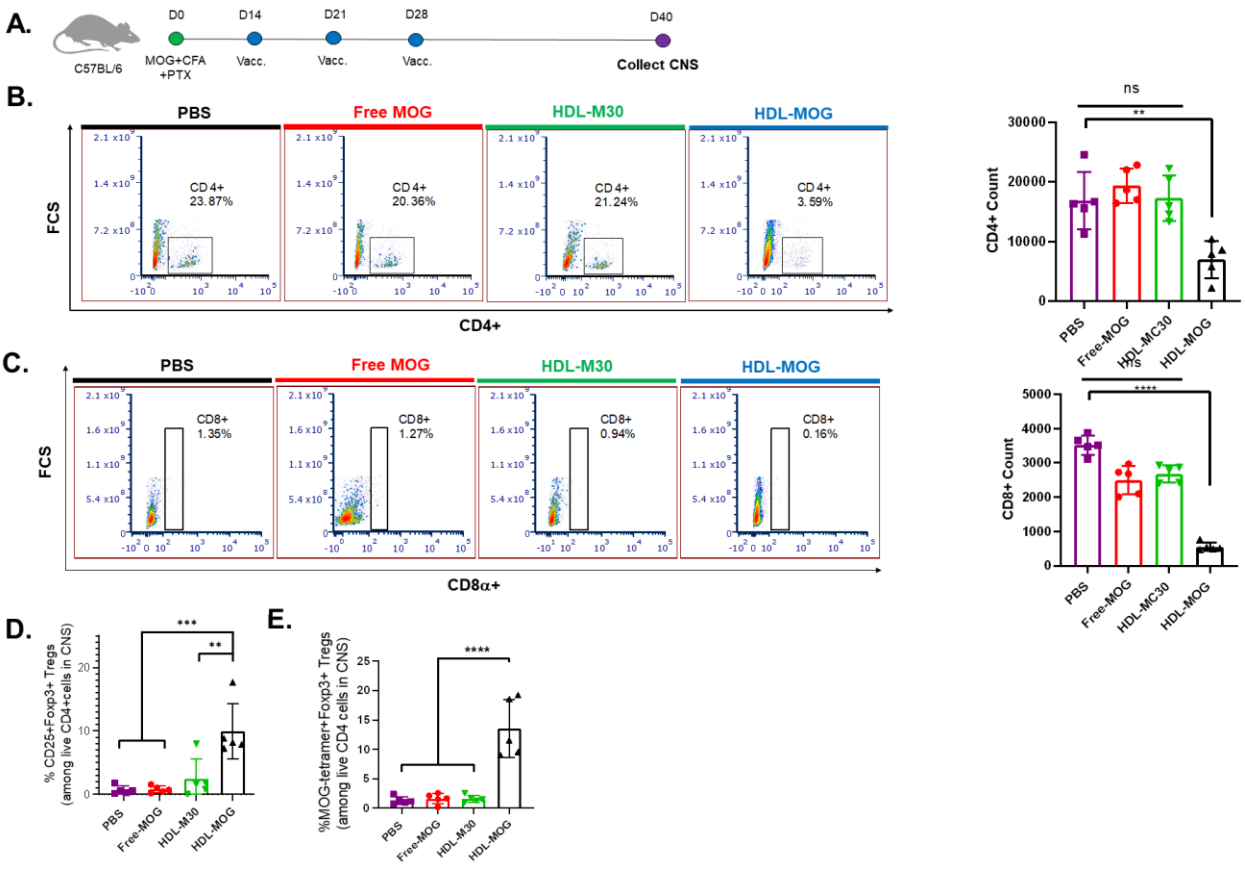

Figure 4-11. EAE-induced mice were treated with PBS, free MOG, HDL-M30, or HDL-MOG, as shown. CNS tissues collected on day 40 were examined for the frequency of Tregs, CD4+, CD8+ T cells. A. vaccination timing. Shown are the frequencies of B. CD4+ T cells, C. CD8+ T cells, D. CD25+Foxp3+ Tregs, and E. MOG-tetramer+Foxp3+ Tregs in CNS.

We next studied the impact of regulatory T cells (Tregs) on the treatment outcomes of HDL-MOG. EAE-induced mice were administered subcutaneously with PBS or HDL-MOG on days 15, 22, and 29, and a subset of animals also received i.p. administration of anti-CD25 IgG to deplete Tregs at the specified time points (**Figure 4-12.**). EAE-mice treated with HDL-MOG exhibited drastic improvement in the EAE symptoms (**Figure 4-12.**) as demonstrated before. When anti-CD25 was administered on days 35 and 37, mice quickly relapsed and exhibited EAE > 3 score by day 50 (**Figure 4-12.**), indicating that

anti-CD25-mediated depletion of Tregs triggered the relapse. Interestingly, the administration of anti-CD25 on days 21, 23, 35, and 37 resulted in similar outcomes as in mice given anti-CD25 only on days 35 and 37. These results suggest that Tregs play crucial roles in HDL-MOG-mediated immune tolerance and that Tregs are critical for the long-term control of the disease.

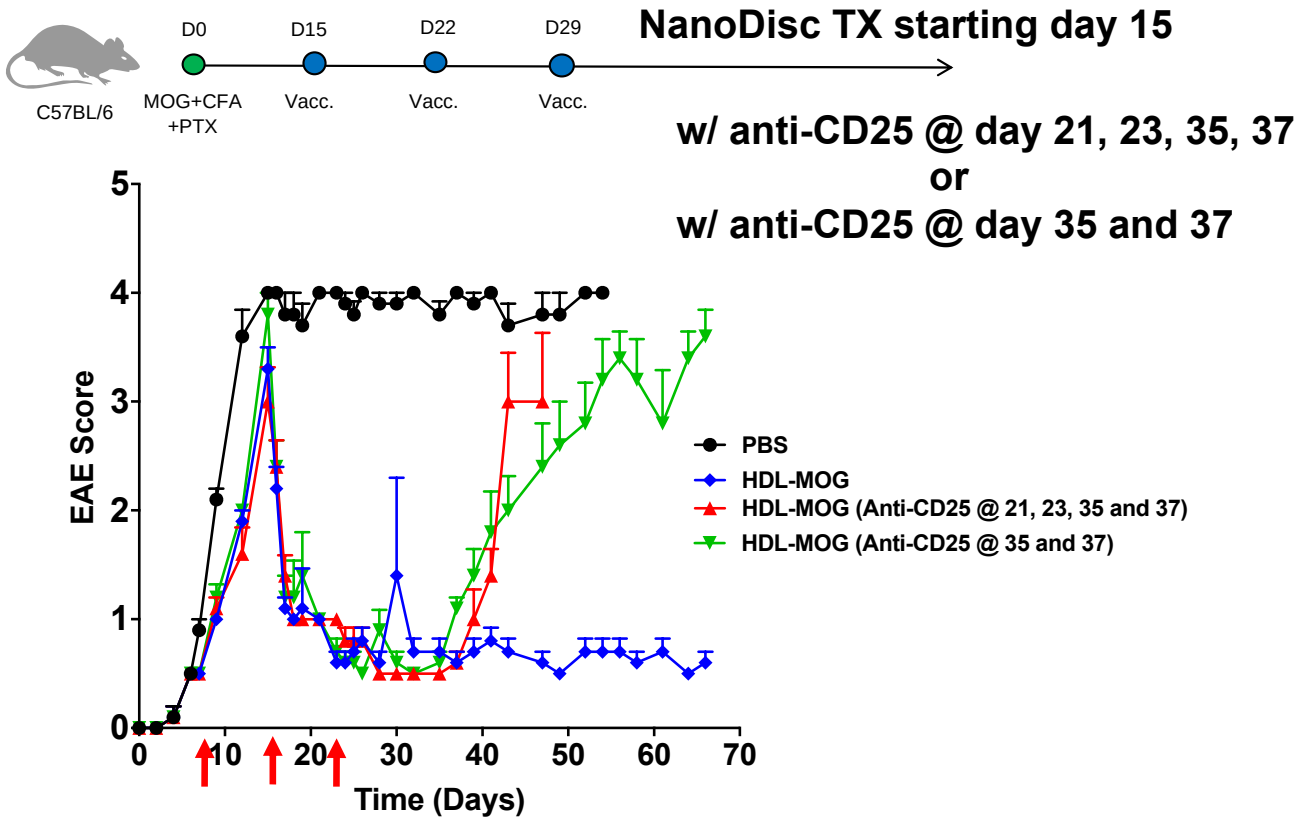

Figure 4-12. EAE-induced mice were treated with PBS or HDL-MOG as shown. Red arrows indicate the days of treatment. Some mice were administered with anti-CD25 IgG on the indicated time points. Mice were monitored over time for the EAE scores.

4.5 Conclusions

In this study, we have developed synthetic HDL designed for the delivery of tolerogenic MS antigens and tested them in a murine model of EAE, a widely accepted pre-clinical model of MS. This tolerogenic antigen-specific vaccine approach can elicit strong Treg responses, resulting in protection and reduce the inflammation in CNS. Our work shows that inverse vaccination with HDL carrying tolerogenic peptide antigens is a promising strategy for the treatment of MS. Overall, HDL-based inverse vaccination with its simplicity, scalability, and low-cost warrants further research as the basis for immunotherapy against MS and other autoimmune diseases.

4.6 References

[1] M.T. Wallin, W.J. Culpepper, J.D. Campbell, L.M. Nelson, A. Langer-Gould, R.A. Marrie, G.R. Cutter, W.E. Kaye, L. Wagner, H. Tremlett, The prevalence of MS in the United States: a population-based estimate using health claims data, Neurology 92(10) (2019) e1029-e1040.

[2] M.T. Wallin, W.J. Culpepper, E. Nichols, Z.A. Bhutta, T.T. Gebrehiwot, S.I. Hay, I.A. Khalil, K.J. Krohn, X. Liang, M. Naghavi, Global, regional, and national burden of multiple sclerosis 1990–2016: a systematic analysis for the Global Burden of Disease Study 2016, The Lancet Neurology 18(3) (2019) 269-285.

[3] D. Karussis, The diagnosis of multiple sclerosis and the various related demyelinating syndromes: a critical review, Journal of autoimmunity 48 (2014) 134-142.

[4] J. Oh, A. Vidal-Jordana, X. Montalban, Multiple sclerosis: clinical aspects, Current Opinion in Neurology 31(6) (2018) 752-759.

[5] W. Brück, N. Sommermeier, M. Bergmann, U. Zettl, H.H. Goebel, H.A. Kretzschmar, H. Lassmann, Macrophages in multiple sclerosis, Immunobiology 195(4-5) (1996) 588-600.

[6] R. Sobel, B. Blanchette, A. Bhan, R. Colvin, The immunopathology of experimental allergic encephalomyelitis. I. Quantitative analysis of inflammatory cells in situ, The Journal of Immunology 132(5) (1984) 2393-2401.

[7] J.M. Fletcher, S. Lalor, C. Sweeney, N. Tubridy, K. Mills, T cells in multiple sclerosis and experimental autoimmune encephalomyelitis, Clinical & Experimental Immunology 162(1) (2010) 1-11.

[8] A. Compston, A. Coles, Multiple sclerosis. Lancet (Lond, Engl) 372: 1502–1517, 2008.

[9] J.A. Hollenbach, J.R. Oksenberg, The immunogenetics of multiple sclerosis: A comprehensive review, Journal of autoimmunity 64 (2015) 13-25.

[10] J.P.S. Peron, K. Yang, M.-L. Chen, W.N. Brandao, A.S. Basso, A.G. Commodaro, H.L. Weiner, L.V. Rizzo, Oral tolerance reduces Th17 cells as well as the overall inflammation in the central nervous system of EAE mice, Journal of neuroimmunology 227(1-2) (2010) 10-17.

[11] R. Verbeek, K. Van Der Mark, E.F. Wawrousek, A.C. Plomp, J.M. Van Noort, Tolerization of an established αB-crystallin-reactive T-cell response by intravenous antigen, Immunology 121(3) (2007) 416-426.

[12] B. Hilliard, E.S. Ventura, A. Rostami, Effect of timing of intravenous administration of myelin basic protein on the induction of tolerance in experimental allergic encephalomyelitis, Multiple Sclerosis Journal 5(1) (1999) 2.

[13] H. Li, G.-X. Zhang, Y. Chen, H. Xu, D.C. Fitzgerald, Z. Zhao, A. Rostami, CD11c+ CD11b+ dendritic cells play an important role in intravenous tolerance and the suppression of experimental autoimmune encephalomyelitis, The Journal of Immunology 181(4) (2008) 2483-2493.

[14] H. Li, B. Ciric, J. Yang, H. Xu, D.C. Fitzgerald, M. Elbehi, Z. Fonseca-Kelly, S. Yu, G.-X. Zhang, A. Rostami, Intravenous tolerance modulates macrophage classical activation and antigen presentation in experimental autoimmune encephalomyelitis, Journal of neuroimmunology 208(1-2) (2009) 54-60.

[15] A. Rostami, MOG intravenous tolerance modulates macrophage classical activation and antigen presentation in experimental autoimmune encephalomyelitis (EAE)(99.2), Am Assoc Immnol, 2009.

[16] J.M. Critchfield, M.K. Racke, J.C. Zuniga-Pflucker, B. Cannella, C.S. Raine, J. Goverman, M.J. Lenardo, T cell deletion in high antigen dose therapy of autoimmune encephalomyelitis, Science 263(5150) (1994) 1139-1143.

[17] S.Y. Min, K.S. Park, M.L. Cho, J.W. Kang, Y.G. Cho, S.Y. Hwang, M.J. Park, C.H. Yoon, J.K. Min, S.H. Lee, Antigen-induced, tolerogenic CD11c+, CD11b+ dendritic cells are abundant in Peyer's patches during the induction of oral tolerance to type II collagen and suppress experimental collagen-induced arthritis, Arthritis & Rheumatism 54(3) (2006) 887-898.

[18] D.C. Fitzgerald, G.-X. Zhang, S. Yu, M.L. Cullimore, Z. Zhao, A. Rostami, Intravenous tolerance effectively overcomes enhanced pro-inflammatory responses and experimental autoimmune encephalomyelitis severity in the absence of IL-12 receptor signaling, Journal of neuroimmunology 247(1-2) (2012) 32-37.

[19] Z. Jiang, H. Li, D.C. Fitzgerald, G.X. Zhang, A. Rostami, MOG35–55 iv suppresses experimental autoimmune encephalomyelitis partially through modulation of Th17 and JAK/STAT pathways, European journal of immunology 39(3) (2009) 789-799.

[20] K.M. Thorstenson, A. Khoruts, Generation of anergic and potentially immunoregulatory CD25+ CD4 T cells in vivo after induction of peripheral tolerance with intravenous or oral antigen, The Journal of Immunology 167(1) (2001) 188-195.

[21] C.E. Smith, T.N. Eagar, J.L. Strominger, S.D. Miller, Differential induction of IgE-mediated anaphylaxis after soluble vs. cell-bound tolerogenic peptide therapy of autoimmune encephalomyelitis, Proceedings of the National Academy of Sciences 102(27) (2005) 9595-9600.

[22] P. Serra, P. Santamaria, Nanoparticle-based approaches to immune tolerance for the treatment of autoimmune diseases, European journal of immunology 48(5) (2018) 751-756.

[23] P. Serra, P. Santamaria, Nanoparticle-based autoimmune disease therapy, Clinical Immunology 160(1) (2015) 3-13.

[24] X. Clemente-Casares, J. Blanco, P. Ambalavanan, J. Yamanouchi, S. Singha, C. Fandos, S. Tsai, J. Wang, N. Garabatos, C. Izquierdo, Expanding antigen-specific regulatory networks to treat autoimmunity, Nature 530(7591) (2016) 434-440.

[25] S. Tsai, A. Shameli, J. Yamanouchi, X. Clemente-Casares, J. Wang, P. Serra, Y. Yang, Z. Medarova, A. Moore, P. Santamaria, Reversal of autoimmunity by boosting memory-like autoregulatory T cells, Immunity 32(4) (2010) 568-580.

[26] S. Singha, K. Shao, Y. Yang, X. Clemente-Casares, P. Solé, A. Clemente, J. Blanco, Q. Dai, F. Song, S.W. Liu, Peptide–MHC-based nanomedicines for autoimmunity function as T-cell receptor microclustering devices, Nature Nanotechnology 12(7) (2017) 701-710.

[27] R. Kuai, D. Li, Y.E. Chen, J.J. Moon, A. Schwendeman, High-density lipoproteins: nature's multifunctional nanoparticles, ACS nano 10(3) (2016) 3015-3041.

[28] R. Kuai, X. Sun, W. Yuan, L.J. Ochyl, Y. Xu, A.H. Najafabadi, L. Scheetz, M.-Z. Yu, I. Balwani, A. Schwendeman, Dual TLR agonist nanodiscs as a strong adjuvant system for vaccines and immunotherapy, Journal of controlled release 282 (2018) 131-139.

[29] R. Kuai, L.J. Ochyl, K.S. Bahjat, A. Schwendeman, J.J. Moon, Designer vaccine nanodiscs for personalized cancer immunotherapy, Nature materials 16(4) (2017) 489-496.

[30] C. Yu, M. An, M. Li, H. Liu, Immunostimulatory properties of lipid modified CpG oligonucleotides, Molecular pharmaceutics 14(8) (2017) 2815-2823.

[31] S.D. Miller, W.J. Karpus, T.S. Davidson, Experimental autoimmune encephalomyelitis in the mouse, Current protocols in immunology 88(1) (2010) 15.1. 1-15.1. 20.

[32] Y. Latchman, C.R. Wood, T. Chernova, D. Chaudhary, M. Borde, I. Chernova, Y. Iwai, A.J. Long, J.A. Brown, R. Nunes, PD-L2 is a second ligand for PD-1 and inhibits T cell activation, Nature immunology 2(3) (2001) 261-268.

Chapter 5 Conclusions & Perspectives

Over the course my dissertation projects, I have developed sHDL incorporated with a CSC antigen as a model antigen for cancer immunotherapy, investigated the role of different adjuvants to activate the immune system, and finally, applied the sHDL technology to induce antigen-specific immune tolerance as a new form of immunotherapy against autoimmune diseases. The overall goal of Chapter 2 and Chapter 3 of my dissertation was to develop a clinically translatable and scalable platform for the delivery of antigen and adjuvants to APCs for increasing the efficacy of cancer vaccines and reducing off-target side effects. To achieve this goal, in Chapter 2, I have developed sHDL nanodiscs co-loaded with CSC antigen and adjuvant to generate strong antigen-specific CD8+ T response against CSCs. In Chapter 3, I have studied the role of adjuvants in the sHDL vaccine formulations to further augment anti-tumor T cell immune responses. Finally, in Chapter 4, I have studied autoimmune disorders as a new application for our sHDL nanodiscs. I have evaluated the therapeutic and preventive applications of tolerogenic antigen delivery by sHDL nanodiscs. I have assessed the sHDL formulation in the murine EAE model of MS.

The vaccine composition is one of the essential factors that can affect the strength of the immunity provides by the vaccine. Thus, in this thesis, I have focused on two critical vaccine compositions, namely, antigen and adjuvant, in order to improve the efficacy of

the vaccine. In Chapter 2, I have developed sHDL for delivery of ALDH (aldehyde dehydrogenase) peptide antigens, ALDH-A1 and ALDH-A3, and have demonstrated their potency to elicit CD8+ T cell responses against CSCs. In particular, sHDL significantly enhanced the delivery of ALDH peptides to APCs in LNs, increased antigen uptake among APCs, and triggered robust induction of T cell responses against CSCs. sHDL vaccination combined with αPD-L1 IgG therapy exerted strong anti-tumor efficacy in D5 and 4T1 tumor models, leading to inhibition of tumor growth and extension of animal survival. Although our sHDL vaccine showed promising results, it may be limited due to its sole targeting of the ALDH antigen. Therefore, future studies should be directed to examine other genes involved in reprogramming adult cells to pluripotent stem cells, such as Sox2, Oct4, and SSEA2 and employ them as peptide antigens in CSC vaccines. Furthermore, as I have only studied one ICB antibody (αPD-L1) combined with sHDL vaccination, future studies should test other ICBs or combinations of multiple ICBs as a part of optimization processes for developing an effective cancer immunotherapy against CSC.

Another crucial factor that is essential for inducing robust T cell responses using vaccines is the choice of adjuvant. In Chapter 3, I have examined two different types of adjuvants: CpG ODNs, a TLR9 agonist, and polyICLC, a TLR3 agonist, and confirmed that sHDL and polyICLC could be admixed together, forming a potent adjuvant system (sHDL+polyICLC) that could be readily combined with an antigen. Previous studies on TLR7/8 adjuvant showed that conjugation of TLR7/8 agonist or co-delivery of antigen and TLR7/8 elicited robust adaptive immune responses in NHPs. Thus, future studies on this work could utilize TLR7/8 agonists in a preventative or therapeutic vaccine against

cancer. Mechanistic studies will be required to clarify the processes involved in sHDL vaccine-induced T-cell responses in mice and in NHPs.

In tolerogenic vaccine development and characterization, I have examined the application of sHDL vaccines to control and suppress autoimmune disease. My study has demonstrated the superior tolerogenic efficacy of sHDL nanodiscs delivering autoantigen peptides in the EAE mice model. In vivo experiments in the EAE mouse model indicated that sHDL-MOG dramatically decreased the production of IFN-ɣ and IL-17 in lymphocytes and increased the level of Tregs, suggesting that the sHDL-based strategy inhibited the autoantigen-specific Th1 and Th17 responses and upregulated the level of anti-inflammatory T cells critical to the pathogenesis of EAE. The results have shown that sHDL vaccine promotes induction of Tregs. This increase in the number of Tregs and decrease in inflammatory T cells may be also applicable as a potential therapy against other autoimmune diseases, such as type 1 diabetes, celiac disease, Lupus, or rheumatoid arthritis. It would be also interesting to examine epitope-spreading induced by the sHDL technology to enhance our understanding of how sHDL mediates immune tolerance.

While the proposed studies provide an ambitious set of goals, the work shown in my dissertation has (1) demonstrated a highly efficacious nanodisc vaccine strategy against CSCs, which may lead to a new form of immunotherapy against cancer with a high frequency of CSCs; (2) improved our understanding of how adjuvant selects impacts the efficacy of nanoparticle-based vaccines; and lastly (3) demonstrated a novel approach for inducing antigen-specific immune tolerance for the potential treatment of MS and other autoimmune diseases. These studies have demonstrated that by carefully tuning the

biochemical and biophysical properties of nano-vaccines, one can control the immune system to either activate or suppress immune responses.